2D noncarbon materials-based nonlinear optical devices for ultrafast photonics [Invited]

Bo Guo (郭 波)*

Key Laboratory of In-Fiber Integrated Optics, Ministry of Education, Harbin Engineering University, Harbin 150001, China

**Corresponding author: guobo512@163.com*

Received December 7, 2017; accepted January 12, 2018; posted online February 24, 2018

Ultrafast lasers play an important role in a variety of applications ranging from optical communications to medical diagnostics and industrial materials processing. Graphene and other two-dimensional (2D) noncarbon materials, including topological insulators (TIs), transition metal dichalcogenides (TMDCs), phosphorene, bismuthene, and antimonene, have witnessed a very fast development of both fundamental and practical aspects in ultrafast photonics since 2009. Their unique nonlinear optical properties enable them to be used as excellent saturable absorbers (SAs) that have fast responses and broadband operation, and can be easily integrated into lasers. Here, we catalog and review recent progress in the exploitation of these 2D noncarbon materials in this emerging field. The fabrication techniques, nonlinear optical properties, and device integration strategies of 2D noncarbon materials are first introduced with a comprehensive view. Then, various mode-locked/*Q*-switched lasers (e.g., fiber, solid-state, disk, and waveguide lasers) based on 2D noncarbon materials are reviewed. In addition, versatile soliton pulses generated from the mode-locked fiber lasers based on 2D noncarbon materials are also summarized. Finally, future challenges and perspectives of 2D materials-based lasers are addressed.

OCIS codes: 140.3510, 140.4050, 140.3540, 190.7110.

doi: 10.3788/COL201816.020004.

1. INTRODUCTION

Over the past few decades, ultrafast lasers are becoming ubiquitous tools in a wide variety of applications, ranging from optical communications to biomedical imaging and industrial materials processing[1,2]. To achieve ultrashort pulse operation, the majority of lasers use a mode-locking technique, whereby a nonlinear optical element, called a saturable absorber (SA), turns the continuous-wave (CW) output into a train of optical pulses. To be a proper SA, the key requirements for materials are fast response time, broad wavelength range, strong nonlinearity, low optical loss, high power handling, low power consumption, low-cost, and ease of integration into a laser system[3]. So far, many SAs, including the organic dyes, color filter glasses, ion-doped crystals, semiconductor SA mirror (SESAM), and single-wall carbon nanotubes (SWCNTs), have been developed[4]. Currently, the dominant mode-locking technology is based on SESAMs. They are complex quantum well devices, typically fabricated by molecular beam epitaxy on distributed Bragg reflectors. Nevertheless, SESAMs suffer from several drawbacks, e.g., slow recovery from saturation (∼ps level), narrowband operation, complex fabrication and integration methods, and low damage threshold. A simple, cost-effective alternative SA material is SWCNTs, in which the diameter controls the energy gap and thus the operation wavelength. Broadband operation (1–2 μm) is also possible using SWCNTs with a wide diameter distribution. However, when operating at a particular wavelength, SWCNTs not in resonance are not used and contribute unwanted losses. These limitations motivate research on novel nonlinear optical materials for SAs.

Since the discovery of mechanically exfoliated graphene in 2004[5], research on two-dimensional (2D) materials has grown exponentially in the fields of condensed matter physics, material science, chemistry, and nanotechnology due to its extraordinary properties. Inspired by studies on graphene, other 2D nanomaterials that possess similar layered structure features but versatile properties[6–23], such as topological insulators (TIs)[8–15], hexagonal boron nitride (h-BN), transition metal dichalcogenides (TMDCs)[16], black phosphorus (BP), MXenes[17], graphitic carbon nitride (g-C_3N_4), metal-organic frameworks (MOFs), covalent organic frameworks (COFs), polymers, metals, silicene, layered metal oxides, and layered double hydroxides (LDHs), have also been explored in recent years, greatly enriching the family of 2D materials, as illustrated in Fig. 1(a). As an example, Fig. 1(b) provides the stability analysis and semiconducting properties of 44 different TMDs (e.g., MoS_2, WS_2, $MoSe_2$, and WSe_2).

Interestingly, 2D materials also have profoundly promoted the fields of ultrafast photonics due to their broadband saturable absorption and nonlinear optical property, which is undoubtedly a key advantage of 2D materials over SESAMs[24–32]. For example, study found that, BP possesses a thickness-dependent direct bandgap that could be widely tunable within a broad region from 0.3 to 1.5 eV, which can bridge the gap between its 2D counterparts graphene and TMDs (bandgap: 1.5–2.5 eV), while BP exhibits broadband third-order nonlinear optical responses ranging from the visible to mid-IR[29–31]. On a

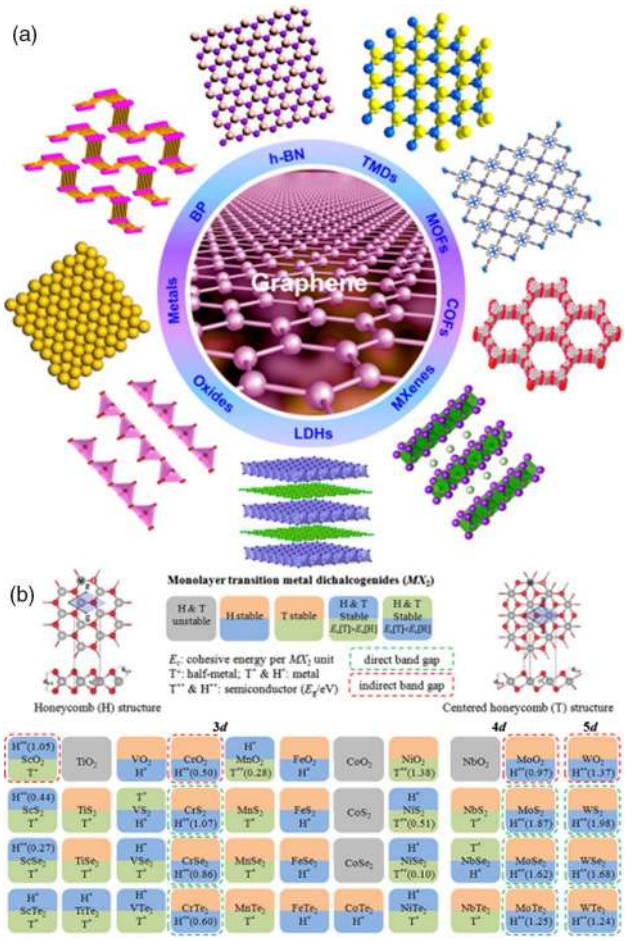

Fig. 1. (a) Schematic illustration of different kinds of typical 2D materials, such as graphene, h-BN, TMDs, MOFs, COFs, MXenes, LDHs, oxides, metals, and BP. Selected from Ref. [7]. (b) Summary of stability analysis and semiconducting properties of 44 different MX_2 compounds. Transition metal atoms indicated by M are divided into 3d, 4d, and 5d groups. MX_2 compounds shaded light gray form neither stable H (2H-MX_2) nor T (1T-MX_2) structure. In each box, the lower-lying structure (H or T) is the ground state. The resulting structures (T or H) can be half-metallic (+), metallic (∗), or semiconducting (∗∗) with direct or indirect band gaps. Selected from Ref. [21].

whole, 2D materials offer several key advantages, such as ultrafast response time, small size, low loss, the ability to operate both in transmission and reflection, and compatibility to optical fibers. Since the first demonstrations of a graphene SA in 2009, research into 2D materials has been progressing at a fast pace[33–35]. So far, various 2D materials-based SAs have been demonstrated for pulse generation in the lasers operating at 0.6 to 3 μm[36–44].

Here, we review the current state of 2D noncarbon materials-based ultrafast photonics with a particular focus on fabrication techniques, nonlinear optical properties, integration strategies, and laser applications. We catalog and review the nonlinear optical properties of 2D noncarbon materials and their application to ultrafast lasers. We believe that 2D noncarbon materials could play a significant role in future optoelectronic and photonic technologies, particularly as a kind of wideband SA for ultrafast lasers.

2. SYNTHESIS, CHARACTERIZATION, AND NONLINEAR OPTICAL PROPERTIES OF 2D NONCARTON MATERIALS

A. Synthesis and Characterization

Few-layer nanomaterials fabrication techniques can be broadly separated into two approaches: top-down exfoliation (including mechanical cleavage and solution-processing techniques) and bottom-up growth [such as chemical vapor deposition (CVD) and pulsed laser deposition (PLD)][45], as shown in Fig. 2. Mechanical exfoliation involves repeatedly cleaving layers from bulk layered crystal materials, often using adhesive tape, leaving few-layer and a small number of monolayer flakes. This technique can be used to produce high quality, single-crystal flakes. However, despite wide-spread usage of the mechanical cleavage technique for fundamental studies of 2D materials, poor scalability and low yield render it unsuitable for realistic large-scale applications. CVD offers a scalable method for the production of single- and few-layer 2D materials. The film growth is limited by the low nucleation rate on bare substrates, and pre-treatment of the substrate is often necessary to seed the 2D materials growth. Another growth technique is hydrothermal synthesis, where crystallization is achieved at a high vapor pressure reaction and elevated temperatures. However, the mechanism for the formation of the nanosheets from the reaction, which typically produces a one-dimensional (1D) structure, is not explained. PLD produces films of material following ablation from a target. The target is placed in a chamber (typically under vacuum) and irradiated, producing a plume of ejection, which can be deposited onto a substrate. In particular, the technique allows control over the ratio of different compounds in the film due to

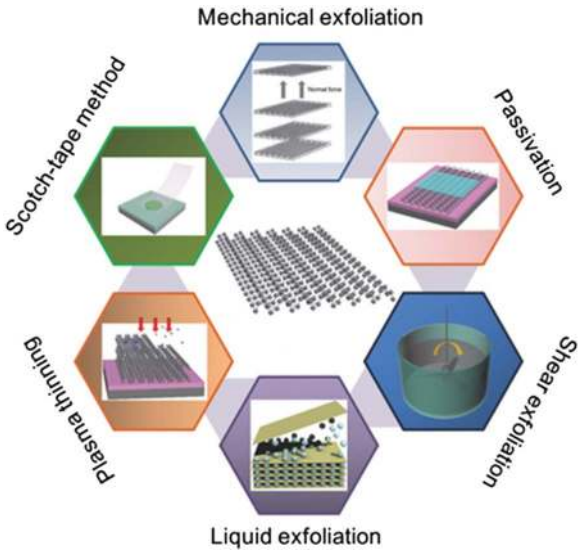

Fig. 2. Schematic of fabrication techniques of 2D materials. Selected from Ref. [45].

the different evaporation rates of the two ions. Solution processing of bulk layered-materials is a widely used technique that produces a high yield of mono- and few-layer flakes dispersed in liquid, carried out under ambient conditions with a high throughput.

Bulk layered-materials can either be chemically exfoliated (e.g., via lithium intercalation) or dispersed into select solvents via liquid phase exfoliation (LPE)[46], as shown in Fig. 3. Chemical exfoliation of bulk layered-materials is typically achieved via lithium intercalation followed by hydrothermal exfoliation. However, exfoliation of bulk layered-materials by this method can lead to structural alterations in the material, producing the other phase and requiring annealing. Ultra-centrifugation also enables sorting of 2D material flakes by thickness, providing a route to engineering 2D material dispersions with desired flake sizes. Finally, we note that other few-layer 2D materials fabrication techniques exist, such as physical vapor deposition and gas phase growth, which have been used to produce SA devices.

B. Nonlinear Optical Properties

Optical nonlinearity plays an important role in many photonic and optoelectronic applications[47–72]. In this part, we describe two well-known nonlinear effects in 2D materials: they are the Kerr effect and saturable absorption. A total polarization is used to model linear and nonlinear responses under electrical field, given by

$$\mathbf{P} = \varepsilon_0(\chi^{(1)} \cdot \mathbf{E} + \chi^{(2)} : \mathbf{E} + \chi^{(3)} \vdots \mathbf{E} + \ldots), \tag{1}$$

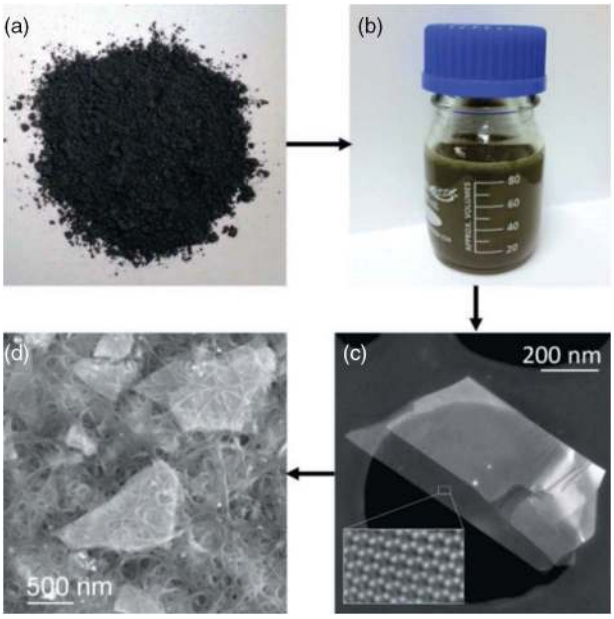

Fig. 3. Liquid exfoliation of layered crystals allows the production of suspensions of 2D nanosheets, which can be formed into a range of structures. (a) MoS_2 powder. (b) WS_2 dispersed in surfactant solution. (c) An exfoliated MoS_2 nanosheet. (d) A hybrid material consisting of WS_2 nanosheets embedded in a network of carbon nanotubes. Selected from Ref. [46].

where ε_0 is the vacuum permittivity. First-order susceptibility represents $\chi^{(1)}$, which is the linear response of the material. Second-order susceptibility $\chi^{(2)}$ represents two-frequency effects, such as second harmonic generation and sum-frequency generation. It is non-zero only when there is no inversion symmetry in the material molecules.

Third-order susceptibility $\chi^{(3)}$ represents three-frequency effects, such as four-wave mixing and third harmonic generation. The real part of third-order susceptibility $\chi^{(3)}$ represents the Kerr effect. In fiber optics, the refractive index n under high optical intensity I is given by

$$n = n_0 + n_2 I, \tag{2}$$

where n_0 is the linear refractive index. The nonlinear refractive index coefficient n_2 is related to the real part of $\chi^{(3)}$.

The imaginary part of $\chi^{(3)}$ represents the nonlinear absorption of the materials under the incident light field. Saturable absorption is one kind of nonlinear absorption and is related to the imaginary part of $\chi^{(3)}$. Two-photon absorption (TPA) is also a nonlinear absorption effect in the materials, which means that the electrons absorb two photons simultaneously to be excited to the conduction band. When the light intensity is very high, TPA becomes significant enough and should be taken into consideration. The saturable absorption expression including the TPA effect is given by

$$\alpha = \alpha_{\mathrm{ns}} + \frac{\alpha_S}{1 + I/I_{\mathrm{sat}}} + \beta I, \tag{3}$$

where β is the TPA coefficient, α_{ns} is the non-saturable absorption coefficient representing the intensity-independent loss, α_S is saturable absorption coefficient, I is the incident optical intensity, and I_{sat} is the saturation intensity. When the light intensity is low, the absorption is equal to $\alpha_{\mathrm{ns}} + \alpha_S$, and, when the intensity is high, the absorption is equal to α_{ns}. The maximum change of the absorption is α_S.

In addition, a modified model is also widely used[42],

$$T = T_0 - \Delta T \exp(-I/I_{\mathrm{sat}}) - T_0 \beta I, \tag{4}$$

where T is the transmission, α_S and βI are much smaller than 1 and low-intensity transmission $T_0 = \exp(-\alpha_{\mathrm{ns}})$.

For 2D materials, two measurement methods are generally used to characterize the Kerr effect and saturable absorption, and they are the Z-scan measurement and two-arm measurement[73–75]. For the Z-scan measurement, the sample is mounted on a Z direction translation stage, as shown in Fig. 4. The light from a pulsed source is first split into two paths. One path with low optical power is for reference and is measured by a slow detector. The other path with high optical power is for material characterization. The light beam in the measurement path is then focused to the sample by a lens. The transmitted light

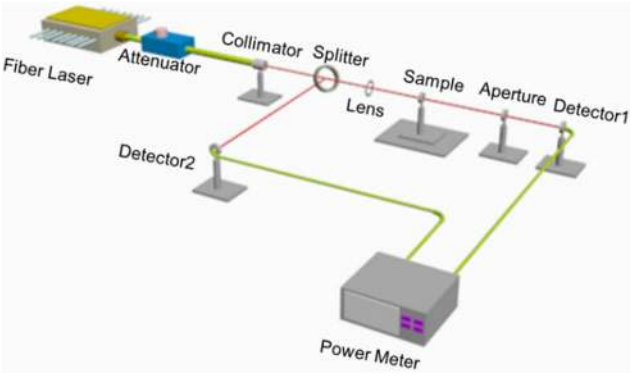

Fig. 4. Schematic of the Z-scan experimental setup.

beam after the sample is collected by a second detector. If there is an aperture before the second detector, the Z-scan measurement is called closed-aperture. Otherwise, it is called open-aperture. For open-aperture Z-scan measurement, the intensity-dependent transmission of the sample can be obtained by comparing the readings of two detectors. Open-aperture Z-scan measurement is therefore able to measure the saturable absorption of the sample. For closed-aperture Z-scan measurement, the reading from the second detector is not only dependent on the transmission of the sample but also the beam diameter after the sample. Because the beam diameter after the sample is related to the beam induced refractive index change of the sample, closed-aperture Z-scan measurement is able to investigate the Kerr effect of the sample and obtain the nonlinear index.

For the two-arm measurement, all of the light propagation is confined in an optical fiber. Different from the open-aperture Z-scan setup, the sample is incorporated to the fiber, and there is no translation stage. Because all of the light beams are confined in the fiber, no spatial information can be collected like in a closed-aperture Z-scan. Therefore, the two-arm measurement can only measure saturable absorption of the materials.

By using the Z-scan technology, we can provide the nonlinear optical parameters of 2D materials, as shown in Table 1. For 2D materials, the origin of saturable absorption is usually believed to be Pauli blocking[76–80]. As an example, we provide the optical and microwave saturable absorption in TI Bi_2Te_3, as shown in Fig. 5. Notably, the saturable absorption of 2D materials-based SAs beyond their direct bandgap belonging to sub-bandgap absorption can also happen, where the reason can be attributed to the defects, TPA[81–84], and absorption of edge mode[85,86]. In the experiment, chemical or physical exfoliated methods may not produce very complete nanosheets, and, thus, the absorption of defects should be weak; however, it is very difficult to obtain 2D nanosheets with a uniform shape and size. Therefore, there can be many edges in the 2D materials-based photonic device, leading to a relatively high absorption. Further investigation on the SA of 2D materials is still required in future work. Interestingly, third harmonic generation[87–90] and four-wave mixing[91] were also studied recently.

3. DEVICE FABRICATION

So far, various 2D materials-based SAs integration methods for fiber devices are developed[34]. For example, they can be sandwiched between two fiber connectors [Fig. 6(a)], injected into in-fiber microfluidic channels [Fig. 6(b)] and photonic-crystal fibers (PCFs) [Fig. 6(c)], and coated on the surfaces of D-shaped [Fig. 6(d)] or tapered fibers [Fig. 6(e)]. Specially, several common methods have been used to obtain the 2D

Table 1. Summary of the Nonlinear Optical Parameters of 2D Materials

2D Materials	Energy Gap (eV)	Source Laser Parameters	Nonlinear Process	Nonlinear Refractive Index ($cm^2 \cdot W^{-1}$)	Third-order Nonlinear Susceptibility (esu)	References
Graphene	0	1550 nm, 10 MHz, 3.8 ps	SA	$\sim 10^{-7}$	1.33×10^{-10}	[38]
Bi_2Se_3	~0.3	800 nm, 1 kHz, 100 fs	SA	2.26×10^{-10}	–	[48]
Bi_2Te_3	~0.06	1562 nm, 21 MHz, 1.5 ps	SA	8.6×10^{-9}	10^{-7}	[49]
Sb_2Te_3			SA			[53]
MoS_2	~1.87	488 nm, CW	SA	$(9.32 \pm 0.3) \times 10^{-7}$	$(3 \pm 0.1) \times 10^{-9}$	[55]
WS_2	~1.98	488 nm, CW	SA	$(6.09 \pm 0.14) \times 10^{-7}$	$(5.15 \pm 0.12) \times 10^{-9}$	[57]
$MoSe_2$	~1.62	488 nm, CW	SA	$(6.49 \pm 0.14) \times 10^{-7}$	$(7.75 \pm 0.24) \times 10^{-9}$	[61]
WSe_2		488 nm, CW	SA			[65]
BP	0.3–1.5	800 nm, 1 kHz, 100 fs	SA/TPA	$(6.5 \pm 0.6) \times 10^{-7}$	$(1.48 \pm 0.15) \times 10^{-9}$	[66]
h-BN	3.6–7.2	800 nm, 1 kHz, 100 fs	–	$(0.68–12) \times 10^{-9}$	$(1–17) \times 10^{-8}$	[69]
SiO_2	7.8	1500 nm	–	$(2.2–4.5) \times 10^{-14}$	–	[48]

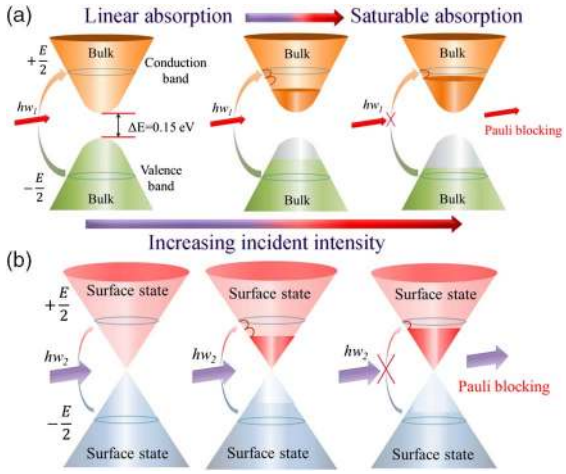

Fig. 5. Schematic of (a) optical and (b) microwave saturable absorption in TI:Bi_2Te_3. Selected from Ref. [49].

materials-based SAs, such as optical deposition, PLD, PCF filling, side-polished fiber or microfiber-based evanescent field interaction, and polymer film. In these methods, the fiber ferrule-type SAs are simple and low-cost but have an inherently short nonlinear interaction length; PCF-filled SAs show the strong light–matter interaction but exhibit relatively larger insertion loss and distorted guiding mode in the PCF region; the microfiber or side-polished fiber-based SAs are attractive for high power tolerance and long interaction length, but not easy to obtain uniform material profile; the 2D material polymer films could maintain the thermal stability of SAs, but they are vulnerable to destruction by high power operation; PLD shows many benefits, such as good security component, high deposition rate, and very uniform film. These strategies are particularly advantageous for lasers because they can be fully integrated into various fiber configurations while preserving an alignment-free, all-fiber format, which cannot be realized using SESAMs[33–44].

4. EXPERIMENTAL SCHEME AND THEORETICAL BASIS

A. Experimental Scheme

Generally, the linear and ring cavity is used to realize the mode-locking or Q-switching operation in the fiber lasers[85–91]. As an example, the experimental scheme of the ring cavity fiber laser is shown in Fig. 7. The pump source is a fiber-pigtailed laser diode (LD) and transferred the energy to a piece of gain fiber (DF) via a wavelength-division multiplexer (WDM). An optical coupler (OC) is used to extract the laser output. A polarization-independent isolator (ISO) is used for unidirectional operation of the fiber laser, and a polarization controller (PC) is used to adjust the polarization state in the cavity, respectively. The pulse information and laser power obtained are measured by an optical spectrum analyzer, a mixed oscilloscope combined with a high-speed photodetector, and an optical power meter, respectively.

B. Theoretical Basis

In order to fully understand the experiment, we adopt the propagation model of a passively mode-locked fiber laser. Numerical simulations are based on a Ginzburg–Landau equation (GLE), which considers the most important physical effects of group velocity dispersion (GVD), self-phase modulation, and saturation gain with a finite bandwidth.

The GLE can be given by

$$\frac{\partial U}{\partial z} + i\frac{\beta_2}{2}\frac{\partial^2 U}{\partial \tau^2} - \frac{\beta_3}{6}\frac{\partial^3 U}{\partial \tau^3} = \frac{g}{2}U + i\gamma|U|^2 U + i\gamma T_R \frac{\partial |U|^2}{\partial \tau}U. \tag{5}$$

Here, $U = U(z,\tau)$ is the slowly varying amplitude of the pulse envelope, z is the propagation coordinate, and τ is the time delay parameter. β_2 and β_3 are the second-order (GVD) and third-order dispersion (TOD) parameters, respectively. γ is the nonlinearity parameter given by

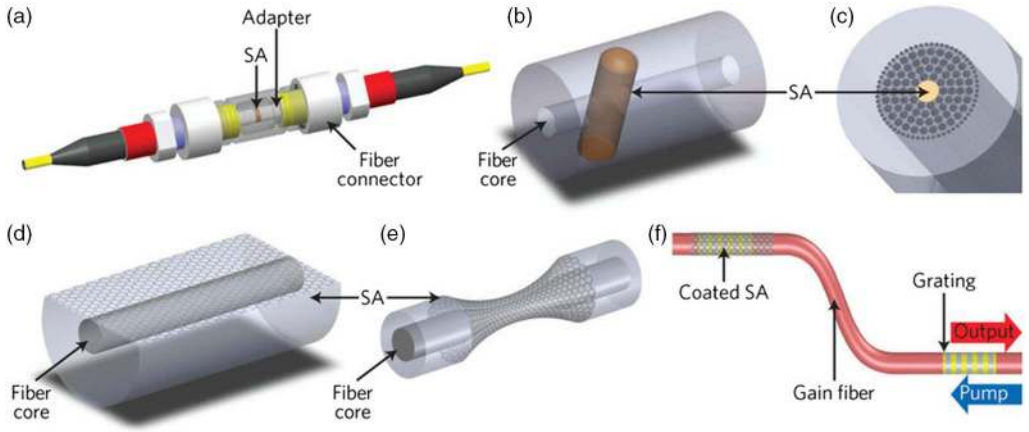

Fig. 6. Various integration methods of 2D materials for fiber devices: (a) Sandwiched device; (b) in-fiber microfluidic channels; (c) photonic-crystal fibers; (d) D-shaped and (e) tapered fibers. (f) Fully integrated monolithic fiber laser. The SAs represented in this figure could be 2D materials-based SAs. Selected from Ref. [34].

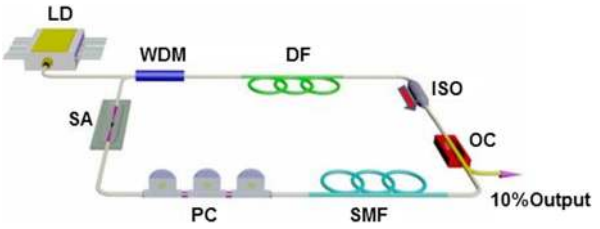

Fig. 7. Experimental setup.

$\gamma = n_2\omega_0/cA_{\text{eff}}$, where n_2 is the Kerr coefficient, ω_0 is the central angular frequency, c is the velocity of light in vacuum, and A_{eff} is the effective mode area. $T_R = 5$ fs is related to the slope of the Raman gain spectrum, which is assumed to vary linearly with frequency around the central frequency. The gain is given by

$$g = \frac{g_{SS}}{1 + W/W_0 + (\omega - \omega_0)^2/\Delta\omega^2}, \tag{6}$$

where g_{SS} is the small-signal gain, $\Delta\omega$ is the gain bandwidth, which is chosen to correspond to 50 nm, and $W(z) = \int |U|^2 \mathrm{d}\tau$ is the pulse energy. The gain is assumed to saturate over a large number of pulses with a response time much longer than the cavity roundtrip time. As such, the saturated values of the gain along the Er fiber are assumed to depend on average power only. W_0 presents an effective gain saturation energy corresponding to the saturation power (determined by pump power) for a given repetition rate. The SA is modeled by a transfer function that describes its transmittance as

$$T(\tau) = 1 - \frac{q_0}{1 + P(\tau)/P_0}, \tag{7}$$

where q_0 is the unsaturated loss, $P(z,\tau) = |U(z,\tau)|^2$ is the instantaneous pulse power, and P_0 is the saturation power. The specific shape of the transmittance function is found not to be important.

The numerical model can be solved with a standard split-step beam propagation algorithm, and the initial field is white noise. The stable solutions are reached from different initial noise fields.

5. DEMONSTRATION OF ULTRAFAST LASERS BASED ON 2D NONCARBON MATERIALS

A. Fiber Lasers

So far, various mode-locked lasers have been developed by using the 2D noncarbon materials. Then, we will briefly review these lasers as follows.

1. Mode-locking Operation

Since 2009, besides graphene and its derivatives[92–196], the 2D noncarbon materials have been used as excellent SAs to realize Q-switching[197–244] and mode-locking[245–321] in the fiber lasers. The performance of Q-switched fiber lasers based on 2D noncarbon materials is classified and summarized, as shown in Table 2. Among them, the maximum pulse energy of 1.525 μJ[204] and minimum pulse width of 154.9 ns[229] were demonstrated, respectively. As an example, Sun *et al.* obtained the stable Q-switched operation with pulse energy of 39.8 nJ and pulse repetition rate from 6.2 to 40.1 kHz in an Er-doped fiber laser (EDFL) based on a few-layer Bi_2Se_3 SA[200], as shown in Fig. 8. It can be seen that the tunable operation of these fiber lasers based on 2D noncarbon materials was also reported[198,204,210,212,214,217,221,240,241]. For the communication band, the widest tunable range of about 78.2 nm was achieved. For example, Chen *et al.* obtained the Q-switched pulses with per-pulse energy up to 1.5 μJ and tunable range from 1510.9 to 1589.1 nm in an EDFL Q-switched by a Bi_2Te_3 SA[204]. Meanwhhile, besides near-IR Q-switching, visible[202,225,226,239] and mid-IR operations were also demonstrated[199,209,213,238,241,243,244]. These results clearly show that 2D materials possess saturable

Table 2. Performance Summary of Q-switched Fiber Lasers Based on 2D Noncarbon Materials

2D Materials	Incorporation Method	Central Wavelength (nm)	Pulse Duration (μs)	Repetition Rate (kHz)	Max. Pulse Energy (nJ)	References
Bi_2Se_3	Deposited on fiber end	1060	Shortest, 1.95	8.3–29.1	17.9	[197]
Bi_2Se_3	Deposited on fiber end	Tunable, 1545.1–1565.1	13.4–36	4.5–12.88	13.3	[198]
Bi_2Se_3	Deposited on fiber end	1980	4.18–18.5	8.4–26.8	313	[199]
Bi_2Se_3	Deposited on fiber end	1530	4.9	6.2–40.1	39.8	[200]
Bi_2Se_3	Polyvinyl alcohol film	1565	1.9–7.76	459–940	23.8	[201]
Bi_2Se_3	Polyvinyl alcohol film	604	0.494–0.748	86.2–187.4	3.1	[202]
Bi_2Se_3	Deposited on tapered fiber	1562.27	1.6–17.7	12.3–52.7	0.08	[203]

(Table continued)

Table 2. Continued

2D Materials	Incorporation Method	Central Wavelength (nm)	Pulse Duration (μs)	Repetition Rate (kHz)	Max. Pulse Energy (nJ)	References
Bi_2Te_3	Deposited on fiber end	Tunable, 1510.9–1589.1	13–49	2.15–12.8	1525	[204]
Bi_2Te_3	Deposited on fiber end	1564.94	2.91	19.2	0.0042	[205]
Bi_2Te_3	Deposited on side-polished fiber	1562.9	2.81–9.36	7.5–42.8	12.7	[206]
Bi_2Te_3	Deposited on side-polished fiber	1559.5	4.88–8.46	8.74–21.24	3.8	[207]
Bi_2Te_3	Polyimide film	1557.5	3.71–5.15	31.54–49.4	3.3	[208]
Bi_2Te_3	Saturable absorber mirror	2979.9	1.37–4.83	46–81.96	3.99	[209]
Sb_2Te_3	Saturable absorber mirror	Tunable, 1530–1570	0.4	98–338	18.07	[210]
Sb_2Te_3	Deposited on side-polished fiber	1560	0.93–5.24	42–132	140	[211]
MoS_2	Polyvinyl alcohol film	Tunable, 1519.6–1567.7	5–9	10.6–34.5	160	[212]
MoS_2	Polyvinyl alcohol film	1066.5	5.8–17	6.4–28.9	32.6	[213]
		1560	5.4–23.3	6.5–27	63.2	
		2030	1.76–2.5	33.6–48.1	1000	
MoS_2	Polyvinyl alcohol film	Tunable, 1030–1070	2.68–4.4	65.3–89	1.1	[214]
MoS_2	Deposited on fiber end	1563	3.9–5.4	26.6–40.9	0.65	[215]
MoS_2	Saturable absorber mirror	1549.83	0.66–0.76	116–131	152	[216]
MoS_2	Deposited on fiber end	Tunable, 1550–1575	6–35	22	150	[217]
MoS_2	Polyvinyl alcohol film	1549.91	1.66–6.11	10.6–173.1	27.2	[218]
MoS_2	Polyvinyl alcohol film	1560.5	1.92–3.7	28.6–114.8	8.2	[219]
MoS_2	Polyvinyl alcohol film	1560	3.2–5.1	36.8–91.7	0.029	[220]
WS_2	Polyvinyl alcohol film	Tunable, 1027–1065	1.57–2.11	65.28–106.16	28.8	[221]
WS_2	Polyvinyl alcohol film	1030	3.2–6.4	24.9–36.7	13.6	[222]
		1558	1.1–3.4	79–97	179.6	
WS_2	Polyvinyl alcohol film	1547.5	1–3.1	80–120	0.05	[223]
WS_2	Polyvinyl alcohol film	1560	3.1–7.9	4.5–49.6	33.2	[224]
WS_2	Polyvinyl alcohol film	635.1	0.207	232.7–512.8	0.04	[225]
MoS_2		635.5	0.227	240.4–438.6	0.03	
$MoSe_2$		635.4	0.24	357.1–555.1	0.02	
WS_2	Polyvinyl alcohol film	604	0.435–1.101	67.3–127.9	6.4	[226]
MoS_2		602	0.602–1.955	50.8–118.4	5.5	
WS_2	Spin-coated on side-polished fiber	1567.8	0.92–2.82	82–134	19	[227]
WS_2	Deposited on tapered fiber	1530	0.78–2.3	174–250	23.5	[228]
WS_2	Saturable absorber mirror	1560	0.1549–1.269	29.5–367.8	68.5	[229]

(Table continued)

Table 2. Continued

2D Materials	Incorporation Method	Central Wavelength (nm)	Pulse Duration (μs)	Repetition Rate (kHz)	Max. Pulse Energy (nJ)	References
$MoSe_2$	Polyvinyl alcohol film	1060	2.8–4.6	60–74.9	116	[231]
		1566	4.8–7.9	26.5–35.4	825	
		1924	5.5–16	14–21.8	42	
MoS_2	Polyvinyl alcohol film	1560	9.92–13.534	7.758–41.452	184.7	[232]
$MoSe_2$			4.04–6.506	60.724–66.847	365.9	
WS_2			3.966–6.707	47.026–77.925	1179.4	
WSe_2			4.063–9.182	46.281–85.365	484.8	
WSe_2	Polyvinyl alcohol film	1550	0.8–1.5	92–140	29	[233]
BP	Deposited on fiber end	1562.87	10.32–39.84	6.983–15.78	94.3	[236]
BP	PMMA–BP–PMMA composites	1561.9	2.96–55	7.86–34.32	194	[237]
BP	Deposited on fiber end	1912	0.731–1.42	69.4–113	632.4	[238]
BP	Polyvinyl alcohol film	635.4	0.383–1.56	108.8–409.8	27.6	[239]
BP	Polyvinyl alcohol film	Tunable, 1563.3–1567.8	1.36–3.39	64.51–82.64	148.63	[240]
BP	Deposited on side-polished fiber	1550, tunable, 1832–1935	9.35–41	4.43–18	28.3	[241]
			4.9–5.7	20–42	114	
BP	Deposited on tapered fiber	1064.7	2–5.5	26–76	17.8	[242]
BP	Saturable absorber mirror	2411	0.189–0.4	98–176	205	[243]
BP	Saturable absorber mirror	2779	1.18–2.1	39–63	7.7	[244]

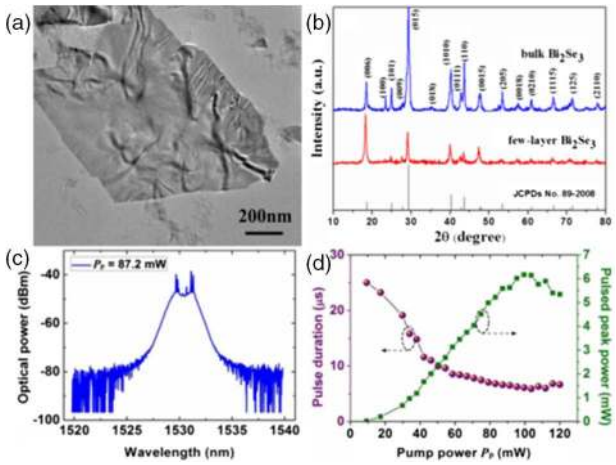

Fig. 8. Material characterization: (a) Transverse electromagnetic (TEM) image and (b) X-ray diffraction (XRD) patterns of Bi_2Se_3. *Q*-switching characteristics of an EDFL based on Bi_2Se_3 SA: (c) Optical spectrum and (d) the pulse duration and peak power as a function of the pump power. Selected from Ref. [200].

absorption, which can be exploited for the *Q*-switched fiber lasers applications.

Since 2009, the mode-locked fiber lasers have been developed by using the 2D materials, including graphene and its derivatives[92–168], Bi_2Se_3[245–249], Bi_2Te_3[250–261], Sb_2Te_3[262–267], MoS_2[279–288], WS_2[290–301], ReS_2[304], $MoSe_2$[305,306], SnS_2[307], and BP[313–319], as shown in Table 3. These results indicate that, after the characteristics of graphene, TIs, and TMDCs, BP is another highly potential 2D material for ultrafast lasers. Here, we review them as follows.

For the TI SAs, the maximum average power of 45.3 mW, maximum repetition rate of 2.95 GHz[253], and minimum pulse width of 70 fs[267], are achieved in the mode-locked fiber lasers, respectively. For example, Zhao *et al.* demonstrated the tunable soliton operation with a 1.57 ps pulse in an EDFL by inserting a TI Bi_2Se_3 SA[245]. They also obtained the mode-locked pulses with a pulse width of 1.21 ps in an EDFL with a Bi_2Te_3 SA[250], as shown in Fig. 9. The fundamental mode-locking pulse had the large full width at half-maximum of 2.33 nm with the repetition rate of ~1.11 MHz. Liu *et al.* also obtained the soliton pulse with ~660 fs in a fiber ring laser by using a polyvinyl alcohol (PVA)-based Bi_2Se_3 SA[246]. Gao *et al.* also demonstrated the conventional soliton with 908 fs duration and dissipative soliton (DS) with a 7.564 ps duration in an EDFL mode-locked by Bi_2Se_3 nanosheets interacting with a PCF[248]. In addition, Xu *et al.* obtained the mode-locking pulses in an EDFL with

Table 3. Performance Summary of Mode-locked Fiber Lasers Based on 2D Noncarbon Materials

2D Materials	Incorporation Method	Central Wavelength (nm)	Pulse Duration (ps)	Repetition Rate (MHz)	Output Power (mW)	References
Bi_2Se_3	Saturable absorber mirror	Tunable, 1557–1565	1.57	1.21	–	[245]
Bi_2Se_3	Polyvinyl alcohol film	1557.5	0.66	12.5	1.8	[246]
Bi_2Se_3	Polyvinyl alcohol film	1560	0.72	8.29	–	[247]
Bi_2Se_3	Filled into photonic crystal fiber	1554.56	0.908	20.27	0.8	[248]
Bi_2Se_3	Deposited on fiber end	1571	0.579	12.54	0.265	[249]
Bi_2Te_3	Saturable absorber mirror	Tunable, 1554–1564	1.21	1.21	–	[250]
Bi_2Te_3	Deposited on tapered fiber	1558.5	2.49	Harmonic, 2.04 GHz	5.02	[251]
Bi_2Te_3	Deposited on tapered fiber	1542.3	–	17.4	23	[252]
Bi_2Te_3	Deposited on tapered fiber	1564.1	0.92	Harmonic, 2.95 GHz	45.3	[253]
Bi_2Te_3	Deposited on tapered fiber	1564	1.34	232.14	5.3	[254]
Bi_2Te_3	Deposited on side-polished fiber	1547	0.543	15.11	–	[255]
Bi_2Te_3	Deposited on side-polished fiber	1555.9	0.63	Harmonic, 773.85	1.4	[256]
Bi_2Te_3	Filled into photonic crystal fiber	1065.4	575.8	Harmonic, 28.73	–	[257]
Bi_2Te_3	Filled into photonic crystal fiber	1064.47	0.96	1.11	–	[258]
Bi_2Te_3	Drop-casted membrane	1565.9	0.448	17.76	3.6	[259]
Bi_2Te_3	Polyvinyl alcohol film	1557	1.08	8.635	0.25	[260]
n-Bi_2Te_3	Deposited on fiber end	1572	0.4	–	–	[261]
p-Bi_2Te_3		1576	0.385	–	–	
Sb_2Te_3	Deposited on fiber end	1558.6	1.8	4.75	0.5	[262]
Sb_2Te_3	Deposited on fiber end	1558.2	2.2	Harmonic, 304	4.5	[263]
Sb_2Te_3	Deposited on side-polished fiber	1561	0.27	34.5	1	[264]
Sb_2Te_3	Deposited on side-polished fiber	1568.8	0.195	33.07	9	[265]
Sb_2Te_3	Deposited on side-polished fiber	1036.7	5.3	19.28	4	[266]
MoS_2	Deposited on fiber end	1054.3	800	6.58	9.3	[279]
MoS_2	Deposited on fiber end	1568.9	1.28	8.288	5.1	[280]
MoS_2	Deposited on tapered fiber	1042.6	656	6.74	2.37	[281]
MoS_2	Deposited on tapered fiber	1558	3	Harmonic, 2.5 GHz	5.39	[282]
MoS_2	Deposited on side-polished fiber	1560	0.2	14.53	3	[283]
MoS_2	Polyvinyl alcohol film	1569.5	0.71	12.09	1.78	[284]
MoS_2	Polyvinyl alcohol film	1556.3	0.935	Harmonic, 463	6	[285]

(Table continued)

Table 3. Continued

2D Materials	Incorporation Method	Central Wavelength (nm)	Pulse Duration (ps)	Repetition Rate (MHz)	Output Power (mW)	References
MoS_2	Polyvinyl alcohol film	Tunable, 1535–1565	0.96	12.99	–	[286]
MoS_2	Polyvinyl alcohol film	1567.7	1.4	5.78	–	[287]
MoS_2	Polyvinyl alcohol film	1598.94	0.83	17.1	1.26	[288]
G/MoS_2	Deposited on fiber end	1571.8	2.2	3.47	–	[60]
WS_2	Polyvinyl alcohol film	1572	0.595	25.25	4	[290]
WS_2	Deposited on tapered fiber	1558.5	0.675	19.58	0.625	[291]
WS_2	Deposited on tapered fiber	1561	0.369	24.93	1.93	[292]
WS_2	Deposited on tapered fiber	1565	0.332	31.11	0.43	[293]
WS_2	Deposited on tapered fiber	1561	0.246	101.4	18	[294]
WS_2 + NPE	Deposited on tapered fiber	1540	0.067	135	–	[295]
WS_2	Deposited on side-polished fiber	1557	1.32	8.86	110	[296]
WS_2	Filled into side-polished fiber	1557	0.66	10.2	–	[297]
WS_2	Filled into photonic crystal fiber	1563.8	0.808	19.57	2.64	[298]
WS_2	Saturable absorber mirror	1560	1.04	352	5.28	[299]
WS_2	Saturable absorber mirror	Tunable, 1530.5–1570.4	0.99	396	6	[300]
WS_2	Large area film	1568.3	1.49	0.487	62.5	[301]
ReS_2	Polyvinyl alcohol film	1558	1.6	5.48	0.4	[304]
$MoSe_2$	Polyvinyl alcohol film	1558.25	1.45	8.028	0.4	[305]
$MoSe_2$	Deposited on side-polished fiber	1557.3	0.688	Harmonic, 3.27 GHz	22.8	[306]
SnS_2	Deposited on side-polished fiber	1031	282	3.76	–	[307]
		1561	1.63	4.398	–	
BP	Deposited on tapered fiber	Tunable, 1532–1570	0.94	4.69	5.6	[313]
BP	Deposited on tapered fiber	Tunable, 1545–1579	0.28	60.5	–	[314]
BP	Deposited on fiber end	1558.7	0.786	14.7	–	[315]
BP	Deposited on fiber end	1560.5	0.242	28.2	0.5	[316]
BP	Deposited on fiber end	1568.19	117.6 ns	1.643	4.43	[317]
BP	Deposited on fiber end	1562	0.635	12.5	–	[318]
BP	Polyvinyl alcohol film	1085.5	7.54	13.5	80	[319]

pulse duration of 579 fs and a repetition rate of 12.54 MHz by using a bi-layer Bi_2Se_3 SA[249]. Duan *et al.* also demonstrated the passively harmonic mode-locking operation with a tunable repetition rate from 232 to 390 MHz and pulse duration of 1.32 ps in an EDFL with a microfiber-based Bi_2Te_3 SA[254]. Meanwhile, Lee *et al.* obtained the soliton pulses with a temporal width of ~600 fs in an EDFL by using a bulk-structured Bi_2Te_3 mode-locker[255]. Yan *et al.* also demonstrated that the mode-locking operation in an Yb-doped fiber laser employing the Bi_2Te_3 solution filled in PCF as an effective SA[258]. Recently, Wang *et al.* demonstrated passive mode-locking with pulse

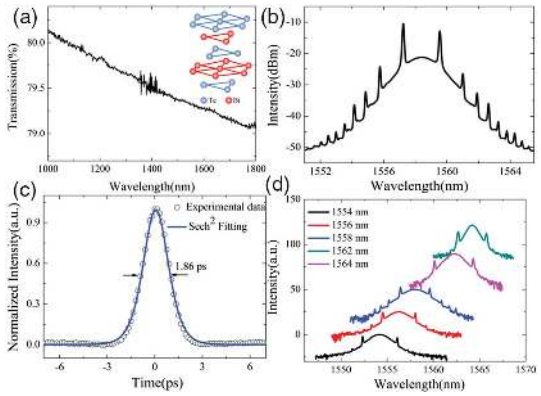

Fig. 9. Device characterization: (a) Linear absorption spectra of Bi_2Te_3 SA. Tunable mode-locking characteristics of an EDFL based on Bi_2Te_3 SA: (b) Output soliton spectrum, (c) its corresponding autocorrelation trace, (d) tunable wavelength spectra. Selected from Ref. [250].

duration of 448 fs in an EDFL by using a TI Bi_2Te_3 SA[259]. Mao *et al.* also proposed a soliton fiber laser passively mode-locked with two different types of film-like SAs, one of which is fabricated by mixing Bi_2Te_3 with deionized water, as well as PVA, and then evaporating them in a Petri dish, and the other of which is prepared by directly dropping Bi_2Te_3 solution on the PVA film[260]. Interestingly, Lin *et al.* demonstrated a soliton mode-locking operation with pulse widths of 400 and 385 fs in an EDFL employing n- and p-type Bi_2Te_3 nanosheets, respectively[261]. Sotor *et al.* also demonstrated the usage of a Sb_2Te_3 SA for efficient mode-locking of an EDFL, which was capable of generating soliton pulses with a pulse width of 1.8 ps and pulse energy of 105 pJ[262]. They also demonstrated the soliton operation with a pulse width of 270 fs in the EDFL incorporating Sb_2Te_3 SA[264]. From the point of view, TI SAs can act as promising modulators for ultrafast lasers.

For the TMDC SAs, the minimum pulse width of 67 fs[295], maximum average power of 110 mW[296], and maximum repetition rate of 3.27 GHz[306] were demonstrated in the mode-locked fiber lasers, respectively. For example, Zhang *et al.* demonstrated the generation of a stable mode-locked laser pulse with a 3 dB spectral bandwidth of 2.7 nm and a pulse duration of 800 ps in an Yb-doped fiber laser with a few-layer MoS_2-based mode-locker[279]. Xia *et al.* also achieved an EDFL mode-locked by a multilayer MoS_2 SA. The soliton pulses have a central wavelength, spectral width, pulse duration, and repetition rate of 1568.9 nm, 2.6 nm, 1.28 ps, and 8.288 MHz, respectively[280]. In addition, Liu *et al.* obtained the femtosecond pulse in an EDFL by using a MoS_2 SA[282]. A 710 fs pulse centered at 1569.5 nm wavelength with a repetition rate of 12.09 MHz has been achieved with proper cavity dispersion. Meanwhile, Luo *et al.* demonstrated the mode-locking regime with pulse duration of 1.4 ps in an EDFL based on a few-layer MoS_2 SA[287]. Ahmed *et al.* also demonstrated the self-started soliton pulse from an Er-doped fiber ring laser incorporating MoS_2 SA[288]. The pulse energy, pulse width, and repetition rate of the laser were 74 nJ, 0.83 ps, and 17.1 MHz, respectively. These findings suggest that MoS_2 is a promising SA for ultrafast laser operation.

Besides the MoS_2 SA, WS_2 SAs were also developed. For example, Yan *et al.* demonstrated the fundamental mode-locking with pulse duration of 675 fs and harmonic mode-locking with pulse duration of 452 fs and 1 GHz repetition rate in an EDFL by incorporating a WS_2 film SA fabricated by PLD[291], as shown in Fig. 10. Wu *et al.* also demonstrated the mode-locking operation with a pulse width of 595 fs in a fiber laser incorporated with a WS_2 SA[290]. In addition, Khazaeinezhad *et al.* demonstrated an all-fiber mode-locked laser with pulse duration of 369 fs based on a tapered fiber SA enclosed in WS_2 nanosheets[292]. Liu *et al.* also demonstrated the soliton pulse with the 246 fs duration and 57 nm bandwidth in an EDFL with a fiber-taper WS_2 SA, which was fabricated by using the PLD method[294]. Meanwhile, Mao *et al.* achieved the soliton mode-locking operations in an EDFL using two types of WS_2-based SAs, one of which is fabricated by depositing WS_2 nanosheets on a D-shaped fiber, while the other is synthesized by mixing WS_2 solution with PVA and then evaporating it on a substrate[296]. Li *et al.* also demonstrated the femtosecond fundamental mode-locking with a repetition rate of 10.2 MHz and pulse duration of 660 fs and harmonic mode-locking with a repetition rate of 460.7 MHz and pulse duration of 710 fs in an EDFL with a D-shaped fiber-based WS_2 solution SA[297]. Interestingly, Chen *et al.* demonstrated the passive mode-locking with pulse duration of 395 fs and 1 ns in a ring-cavity EDFL based on the microfiber-based WS_2 SA device by utilizing the PLD method and fiber tip integrated WS_2 SA mirror (SAM) by utilizing the magnetron sputtering technique, respectively[299]. They also demonstrated the soliton pulses with a pulse duration of 1.49 ps and large average power of 62.5 mW in the EDFL

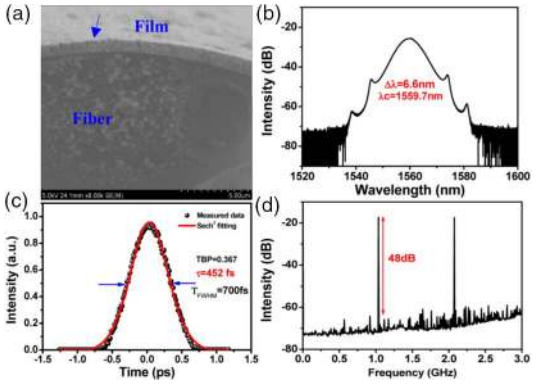

Fig. 10. Device characterization: (a) Scanning electron microscoped (SEM) image of the microfiber-based WS_2 SA. Harmonic mode-locking characteristics of an EDFL based on WS_2 SA: (b) Output optical spectrum, (c) measured pulse duration, and (d) the radio frequency (RF) spectrum in full range with a 10 kHz resolution bandwidth (RBW). Selected from Ref. [291].

by transferring a few-layered WS_2 with a large area on the facet of the pigtail, and it acted as an SA[301]. These works demonstrated that WS_2 was a competitive material as SAs in mode-locked fiber lasers.

Followed by these works, other TMDCs were developed. For example, Mao *et al.* demonstrated that few-layer ReS_2 displays saturable absorption properties at 1.55 μm and mode-locking of EDFLs by incorporating a film-type ReS_2-PVA SA[304]. Luo *et al.* also achieved the soliton mode-locking with pulse duration of 1.45 ps in an EDFL by exploiting a few-layer $MoSe_2$ SA[305]. By optimizing the polarization state, the soliton mode-locking was also obtained, emitting a train of pulses with the duration of 1.6 ps and a fundamental repetition rate of 5.48 MHz. In addition, Koo *et al.* demonstrated the use of a bulk-like, $MoSe_2$-based SA as a passive harmonic mode-locker for the production of femtosecond pulses from a fiber laser at a repetition rate of 3.27 GHz and pulse width of 737 fs[306]. Yang *et al.* also demonstrated the mode-locking operation at 1.03, 1.56, and 1.91 μm in Er-, Yb-, and Tm-doped fiber lasers by using SnS_2 covered on a D-shaped fiber[307]. Li *et al.* also achieved a passively mode-locked Yb-doped fiber laser based on the SnS_2-PVA film SA[308]. Its 3 dB bandwidth, pulse width, pulse repetition rate, and maximum average output power were 8.63 nm, 656 ps, 39.33 MHz, and 2.23 mW, respectively. These results suggest that TMDCs are promising 2D materials for ultrafast laser applications.

For the BP SAs, the maximum average power of 80 mW[296], maximum repetition rate of 60.5 MHz[314], and minimum pulse width of 242 fs[316] were demonstrated in the mode-locked fiber lasers, respectively. Considering the direct and flexible bandgap for different layers of BP, these works may provide a possible method for fabricating BP SAM to achieve ultrafast lasers. For example, by incorporating the BP-based SA device into the EDFLs, Chen *et al.* obtained either the passive *Q*-switching (with maximum pulse energy of 94.3 nJ) or the passive mode-locking operation (with pulse duration down to 946 fs). Sotor *et al.* also demonstrated the soliton pulse with the 272 fs duration in an EDFL by using a BP SA[316]. Li *et al.* also demonstrated the soliton pulse with the 786 fs duration in an EDFL by using a BP SA[315]. Other operation states, including bound-soliton pulses and noise-like states, have also been observed[317]. In addition, Xu *et al.* demonstrated the ultrashort pulse with pulse duration of ∼635 fs in an EDFL by using smaller sized BP as an SA[318]. These works reveal that BP is a class of promising and reliable SAs for ultrafast lasers.

Meanwhile, wavelength-tunable operation in the mode-locked lasers based on 2D materials also was developed rapidly. Although various approaches, including an unbalanced Mach–Zehnder interferometer, bandpass filter, or Sagnac fiber filter have been used as the wavelength selective element, the 2D materials-based SAs exhibit more advantages. The maximum tunable range of ∼40 nm was demonstrated[300]. For example, Zhang *et al.* obtained the picosecond pulses, tunable from 1535 to 1565 nm in a mode-locked fiber laser with a few-layer MoS_2 SA[286]. Yan *et al.* also demonstrated the self-starting mode-locking with a pulse width of 1 ns in a linear EDFL[300]. In addition, Luo *et al.* also demonstrated the mode-locked pulse with a duration of 940 fs and wavelength tunable from 1532 to 1570 nm in an EDFL by using a microfiber-based BP SA[313]. Chen *et al.* also demonstrated that the stable passive mode-locking operation and, eventually, a record 280 fs transmission limited soliton pulse in an all-anomalous dispersion fiber laser cavity could be ensured[314]. These findings suggest that 2D materials could be promising SAs for broadband wavelength-tunable applications.

As an important technique to increase the pulse repetition rate, the harmonic mode-locking lasers based on 2D materials have been developed. The maximum repetition rate of 3.27 GHz was demonstrated[306]. For example, Luo *et al.* demonstrated the passive harmonic mode-locking with a repetition rate of 2.04 GHz in an EDFL by using a microfiber-based Bi_2Te_3 SA[251]. Yan *et al.* also obtained the stable harmonic soliton pulse generation with repetition rate of 2.95 GHz and output power of 45.3 mW in an EDFL by using a microfiber-based Bi_2Te_3 SA, which was fabricated by the PLD method[253]. In addition, Lee *et al.* demonstrated femtosecond harmonic mode-locking with temporal widths of 630–700 fs and harmonic frequency of 773.85 MHz in an Er-doped fiber ring cavity using a bulk-structured Bi_2Te_3 deposited on a side-polished fiber as a mode-locker[256]. Sotor *et al.* also demonstrated the harmonic mode-locking with a repetition rate of 304 MHz and 2.2 ps duration in an EDFL by using a microfiber-based Sb_2Te_3 SA[262]. Meanwhile, Liu *et al.* obtained the generation of high-order harmonic mode-locking with a 2.5 GHz repetition rate in a fiber laser using a microfiber-based MoS_2 SA[282]. Wu *et al.* also demonstrated the passive-mode-locking operation of a fiber laser with a fundamental repetition rate of 463 MHz based on MoS_2 SA[285]. These works will open up promising optoelectronic applications of 2D materials for the HML lasers.

2. Dissipative Soliton Operation

High-energy optical pulses have attracted much interest due to their wide applications in optical sensing, optical frequency metrology, and data inquiring process. Among them, DSs in passively mode-locked lasers were extensively developed in recent years, because they allow for an increase in pulse energy of lasers by several orders of magnitude in comparison to the conventional soliton pulses. The study found that DSs are generated from the lasers in the normal dispersion regime through the mutual nonlinear interaction among the cavity dispersion, Kerr nonlinearity, spectral filtering effect, and cavity loss. Its dynamics is governed by the cubic–quintic GLE. Up to date, DSs were demonstrated in the lasers by using various schemes.

Since 2010, besides graphene and its derivatives[322–331], the DS fiber lasers have been demonstrated by using the 2D noncarbon materials, including Bi_2Se_3[332],

Table 4. Performance Summary of Dissipative Soliton Fiber Lasers Based on 2D Noncarbon Materials

2D Materials	Incorporation Method	Central Wavelength (nm)	Pulse Duration (ps)	Repetition Rate (MHz)	Pulse Energy (nJ)	References
Bi_2Se_3	Bi_2Se_3-SA film	1031.7	47	44.6	0.756	[332]
Bi_2Te_3	Self-assembly film	Tunable, 1548.2–1570.1	4.5	10.71	2.8	[333]
Bi_2Te_3	Deposited on side-polished fiber	1560	Tunable, 2.7–12.8 ns	1.7	22.4	[334]
Sb_2Te_3	Deposited on side-polished fiber	1565	0.128	22.32	44.8 pJ	[335]
Sb_2Te_3	Deposited on side-polished fiber	1558	0.167	25.38	0.21	[336]
Sb_2Te_3	Deposited on side-polished fiber	1065.3	5.9	19.28	0.81	[337]
MoS_2	Deposited on side-polished fiber	1568	4.98	26.02	0.08	[338]
$MoSe_2$	Polyvinyl alcohol film	1040	471	15.44	0.13	[339]
WS_2	Polyvinyl alcohol composite	1052.45	0.713	23.26	1.29	[340]
WS_2	Deposited on side-polished fiber	1063.6	630	5.57	13.6	[341]
		1565.5	21.1	8.05	2.2	

Bi_2Te_3[333,334], Sb_2Te_3[335–337], MoS_2[280,338], $MoSe_2$[339], WS_2[340,341], and BP[342], as shown in Table 4. Among them, the maximum pulse energy of 22.4 nJ[334] and minimum pulse width of 128 fs[335] were demonstrated, respectively. As an example, Dou *et al.* obtained an all-normal-dispersion Yb-doped fiber laser based on a few-layer Bi_2Se_3 SA delivering with pulse energy of 0.756 nJ, pulse width of 46 ps, and repetition rate of 44.6 MHz[322]. In addition, Wang *et al.* obtained the stable DS with a 3 dB spectral bandwidth of 51.62 nm, a pulse width of 6.2 ps, and tunable range of 21.9 nm in an EDFL incorporating a polymethylmethacrylate (PMMA)-TI-PMMA SA, respectively[333]. Boguslawski *et al.* also obtained the DSs with a 34 nm full width at half-maximum and a pulse width of 167 fs in an EDFL mode-locked by Sb_2Te_3 in the near-zero dispersion regime[336]. By using the few-layer WS_2, Mao *et al.* demonstrated the DS fiber lasers at 1.55 μm based on evanescent field interaction with WS_2 nanosheets[341]. In the EDFL, the pulse width and pulse energy of the DS is 21.1 ps and 2.2 nJ, respectively, as shown in Fig. 11. Notably, the rectangular pulse based on the DS resonance was also developed[343].

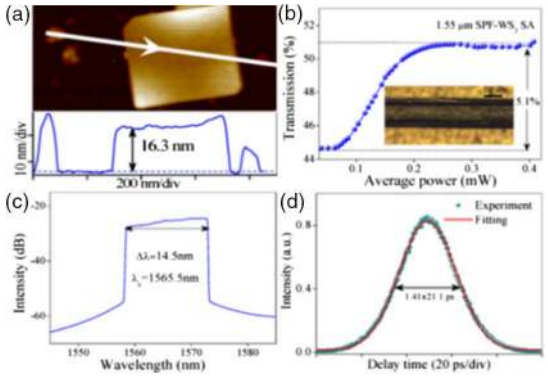

Fig. 11. Material and device characterization: (a) Atomic force microscope (AFM) image of WS_2 nanosheets; (b) nonlinear transmission of WS_2 SA at 1550 nm. Dissipative soliton characteristics of an EDFL based on WS_2 SA: (c) Output optical spectrum, (d) its corresponding autocorrelation trace. Selected from Ref. [341].

3. Mid-infrared Waveband Operation

In the past decade, ultrafast laser sources covering from 2 to 20 μm have received wide interest due to their potential applications in environmental monitoring, pollution control, food quality control, laser surgery, spectroscopy, nonlinear optics, and defense. Passive mode-locking, due to its simple configuration, has been a more preferred choice to obtain ultrashort mid-IR pulses. Although the SESAMs have been developed as a mode-locker or *Q*-switcher, they have some drawbacks, such as a complex design for improving damage threshold and narrow operation range. Fortunately, the rise of 2D materials including graphene, TIs, TMDCs, and BP provide an excellent opportunity for lasers in the mid-IR band due to their broadband saturable absorption, ultrafast carrier dynamics, and planar characteristic.

Since 2012, besides graphene and its derivatives[344–357], the mode-locked fiber lasers at 2 μm have been developed by using the 2D noncarbon materials, including Bi_2Te_3[358,359], MoS_2[360], WS_2[361], WTe_2[362], and BP[363,364], as shown in Table 5. Among them, the maximum pulse energy of 15.5 nJ[360], maximum repetition rate of 36.8 MHz, and minimum pulse width of 739 fs[363] were demonstrated, respectively. As an example, Sotor *et al.* demonstrated a mode-locked, Tm-doped fiber laser with

Table 5. Performance Summary of Mid-infrared Mode-locked Fiber Lasers Based on 2D Noncarbon Materials

2D Materials	Incorporation Method	Central Wavelength (nm)	Pulse Duration (ps)	Repetition Rate (MHz)	Pulse Energy (nJ)	References
Bi_2Te_3	Deposited on side-polished fiber	1935	0.795	27.9	0.72	[358]
Bi_2Te_3	Deposited on side-polished fiber	1909.5	1.26	21.5	–	[359]
MoS_2	Saturable absorber mirror	1905	843	9.67	15.5	[360]
WS_2	Deposited on side-polished fiber	1941	1.3	34.8	0.0172	[361]
WTe_2	Deposited on tapered fiber	1915.5	1.25	18.72	2.13	[362]
BP	Deposited on fiber end	1910	0.739	36.8	0.0407	[363]
BP	Deposited on fiber end	20	1.3	29.1	0.379	[364]
		94	1.6	290	0.231	
Bi_2Te_3	Saturable absorber mirror	2830	6	10.4	8.6	[365]
BP	Saturable absorber mirror	2783	42	24	25.5	[366]
BP	Saturable absorber mirror	2866.7	8.6	13.987	6.2	[367]
		2970.3, *Q*-switched	2.41-5.8 μs	12.43-62.5 kHz	84.93 μJ	
$Cu_{2-x}S$	Deposited on fiber end	2769, *Q*-switched	0.75 μs	66.4-90.7 kHz	2.36 μJ	[368]

a pulse width of ~739 fs by using a few-layer BP SA[363]. The SA was based on mechanically exfoliated BP deposited on a fiber connector tip, as shown in Fig. 12. Jung *et al.* also demonstrated a femtosecond mode-locked, Tm/Ho co-doped fiber laser with a pulse width of ~795 fs at 1935 nm by using a bulk-structured Bi_2Te_3 SA[358]. The SA was prepared by depositing a mechanically exfoliated, ~30-μm-thick Bi_2Te_3 layer on a side-polished fiber. Interestingly, they also demonstrated the Tm/Ho co-doped fiber laser mode-locked with a WS_2-deposited side-polished fiber[361]. Inserting the SA into the cavity, stable mode-locked pulses at 1941 nm with a temporal width of ~1.3 ps at a repetition rate of 34.8 MHz were obtained. In addition, Tian *et al.* demonstrated the linear-cavity Tm^{3+}-doped fiber laser mode-locked with a multilayer MoS_2 SAM[360]. The mode-locking operation at 1905 nm is realized with maximum output power of 150 mW, pulse width of 843 ps, and repetition rate of 9.67 MHz, respectively. These results indicate that 2D materials are potential SAs at the mid-IR band.

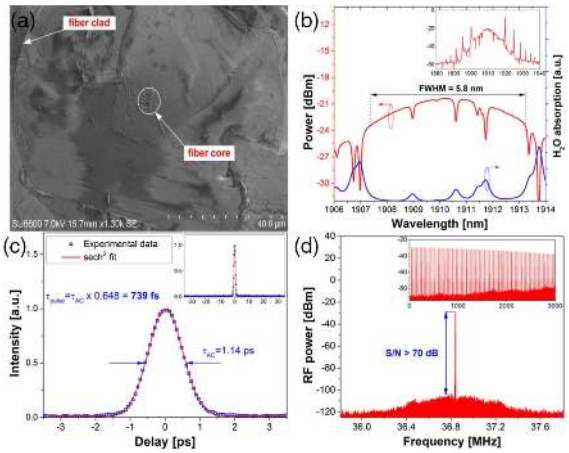

Fig. 12. Device characterization: (a) SEM image of the fiber connector end facet with marked fiber cladding and core with visible BP layer covering the core. Mode-locking characteristics of an EDFL at 2 μm based on BP SA: (b) Optical spectrum of the laser (red line) together with the water absorption lines taken from the high-resolution transmission (HITRAN) database (blue line). Inset: spectrum measured in wide 60 nm span. (c) Autocorrelation trace and (d) RF spectrum. Selected from Ref. [363].

Recently, the pulsed fiber lasers at 3 μm based on 2D materials, including graphene[369,370], Bi_2Te_3[365], BP[366,367], and $Cu_{2-x}S$ nanocrystal[368], were also developed. Among them, the minimum pulse width of 6 ps[365], maximum pulse energy of 25.5 nJ, and maximum repetition rate of 24 MHz[366] were demonstrated, respectively. For example, Yin *et al.* demonstrated the mode-locking operation of the mid-IR mode-locked HoPr-ZrF_4-BaF_2-LaF_3-AlF_3-NaF (ZBLAN) fiber laser at 2830 nm with a TI Bi_2Te_3 SA[361]. The mode-locking pulse has a pulse width of ~6 ps, maximum pulse energy of 8.6 nJ, and pulse repetition rate of 10.4 MHz. In addition, Qin *et al.* successfully fabricated a mid-IR SAM by transferring the mechanically exfoliated BP onto the gold-coated mirror[366]. With the as-prepared BP SAM, a passively mode-locked Er:ZBLAN fiber laser is demonstrated at 2783 nm, which delivers a maximum average output power of 613 mW, a repetition rate of 24 MHz, and a pulse

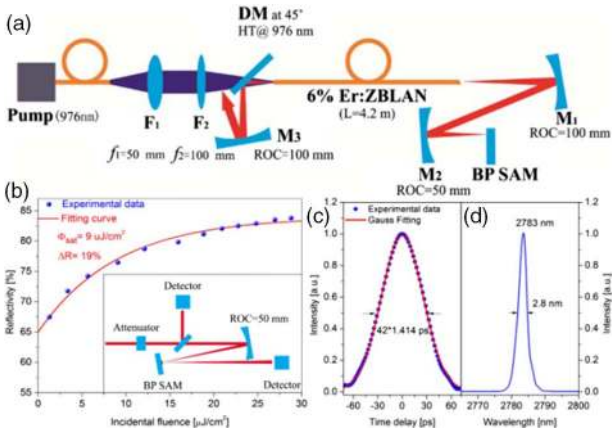

Fig. 13. Experimental setup: (a) Schematic of the mode-locked Er:ZBLAN fiber laser based on BP SAM; DM, dichroic mirror; ROC, radius of curvature. (b) Saturable absorption curve and its measurement setup. Mode-locking characteristics of an EDFL at 3 μm: (c) Autocorrelation trace; (d) the optical spectrum. Selected from Ref. [366].

duration of 42 ps, as shown in Fig. 13. Interestingly, Li *et al.* also demonstrated the *Q*-switched Ho^{3+}-doped and mode-locked Ho^{3+}/Pr^{3+}-doped ZBLAN fiber laser incorporating the same BP SAM[367]. The *Q*-switching pulses at ~2970.3 nm with the pulse energy of 4.93 μJ and mode-locking with the pulse duration of 8.6 ps at ~2866.7 nm were obtained, respectively. These results verify that BP is a novel kind of highly promising optical material for generating ultrafast lasers in the mid-IR region after the previous 2D SAs, such as graphene, TIs, and TMDCs.

4. Multiwavelength Mode-locking Operation

Multiwavelength pulsed lasers are of great importance due to their versatile applications in optical communication, biomedical research, and radar systems. So far, several actively/passively mode-locked techniques have been exploited for achieving multiwavelength mode-locked pulses in fiber lasers. Compared with active schemes, passive schemes share more benefits, such as very simple, compact, low-cost without a modulator required, and easily achieved mode-locked pulses with ultrahigh peak power.

To date, several passive schemes have been used to generate the multiwavelength mode-locked pulses, i.e., nonlinear polarization rotation (NPR), nonlinear optical loop mirror (NOLM), and real SAs (e.g., SESAM, carbon nanotubes). Interestingly, the multiwavelength mode-locked lasers based on 2D materials, including graphene[371–375], Bi_2Se_3[343,376–378], Bi_2Te_3[379], TMDCs[380–382], BP[383–385], and graphene nanocomposite[386], were also developed. Their performances are summarized in Table 6. Among them, the maximum wavelength number of 4[376], maximum repetition rate of 388 MHz[379], minimum pulse width of 585 fs[380], and maximum pulse energy of 6.64 nJ[381] were demonstrated, respectively. These results suggest that 2D materials are promising candidates for realizing multiwavelength pulsed lasers.

For example, Guo *et al.* demonstrated the four-wavelength mode-locked EDFL incorporating a Bi_2Se_3 SA, which can be both an excellent SA for mode-locking and a high-nonlinearity medium to induce a giant third-order optical nonlinear effect for mitigating the mode competition and stabilizing the multiwavelength oscillation[376]. For the four-wavelength operation, they obtained its pulse width of ~22 ps and pulse energy of 1.1 nJ at the pump power of 155 mW. The group also obtained the dual-wavelength soliton pulses in an EDFL with a WS_2-based fiber taper, which was fabricated by depositing the few-layer WS_2 onto a fiber taper under the femtosecond-level pulsed laser[380,381], as shown in Fig. 14. The pulse width is 585 and 605 fs for the dual-wavelength soliton, respectively[380]. The group also demonstrated the dual-wavelength rectangular pulse EDFL with a Bi_2Se_3 SA[377]. The rectangular pulse could be stably initiated with pulse width from 13.62 to 25.16 ns and fundamental repetition rate of 3.54 MHz. Interestingly, the group also demonstrated a switchable dual-wavelength soliton fiber laser based on a graphene ternary composite[386]. The dual-wavelength soliton is stably initiated with a minimum pulse width of 1.25 ps and pulse energy of 1.51 nJ. Further investigations in this respect are on the way.

Interestingly, Liu *et al.* demonstrated the dual-wavelength passively harmonic mode-locking operation with repetition rates of 388 and 239 MHz in an EDFL with a microfiber-based Bi_2Te_3 SA[379]. They also achieved the dual-wavelength pulse cluster phenomena in an EDFL, incorporating the microfiber-based BP quantum dot (QD) device[385]. In the case of the dual-wavelength pulse cluster, each wavelength corresponds to one sequence of the pulse cluster, which has different amplitudes and time intervals. Zhao *et al.* also obtained a picosecond-level BP mode-locked EDFL with a synchronous tri-wavelength of 1557.2, 1557.7, and 1558.2 nm[383]. Yun also reported the usage of few-layer BP as SAs to achieve dual-wavelength vector soliton mode-locking in an EDFL[384].

B. Solid/Disk/Waveguide Lasers

Solid-state lasers typically consist of a free-space cavity, which is formed by mirrors using doped glass or crystalline host materials as a solid-state gain media, and are the most commonly used in industry, research, and military applications. Since 2010, the *Q*-switched solid-state lasers based on 2D materials, including graphene and its derivatives[387–412] Bi_2Se_3[413–417], Bi_2Te_3[418–420], MoS_2[78,421–429], WS_2[430–438], WSe_2[439], ReS_2[440], BP[243,441–451], and g-C_3N_4[452,453], were developed. Their performance is summarized as shown in Table 7. Among them, a variety of gain media have been coupled with 2D materials SAs in pulsed solid-state lasers. These include Nd:$GdVO_4$[413,420,424,454], Nd:Lu_2O_3[414], Nd:YVO_4[415,427,434,450,455], Nd:$LiYF_4$[416], Yb:$GdAl_3(BO_3)_4$[418], Tm:LuAG[419,431], Tm:$YAlO_3$ (Tm:YAP)[420,442,443], Er:$Y_3Sc_2Ga_3O_{12}$ (Er:YSGG)[420,440],

Table 6. Performance Summary of Multiwavelength Mode-locked Fiber Lasers Based on 2D Noncarbon Materials

2D Materials	Incorporation Method	Central Wavelength (nm)	Pulse Duration (ps)	Repetition Rate (MHz)	Pulse Energy (nJ)	References
Bi_2Se_3	Polyvinyl alcohol film	1567.2/1568/ 1568.8/1569.2	22	8.83	1.1	[376]
Bi_2Se_3	Polyvinyl alcohol film	1561.6/1562.1	13.62–25.16 ns	3.54 Harmonic, 15	0.593–2.824	[377]
Bi_2Se_3	Deposited on fiber end	Tunable, 1527.6–1528.4	–	8.95	–	[343]
		1529.2–1530				
		1531.4–1532.2				
Bi_2Se_3	Deposited on fiber end	Tunable, 1547.6–1548.4	30	8.95	1.12	[378]
		1549.2–1550				
		1551.4-1552.2				
Bi_2Te_3	Deposited on tapered fiber	1559.4	1.3	239, 47th harmonic	–	[379]
		1557.4		388, 76th harmonic		
WS_2	Deposited on tapered fiber	1558.54	0.605	8.83	1.14	[380]
		1565.99	0.585			
WS_2	Deposited on tapered fiber	1568.55/1569	11	2.14	6.64	[381]
BP	Deposited on fiber end	1557.2/1557.7/ 1558.2	9.41	1.65	–	[383]
BP	Deposited on fiber end	1533/1558	–	20.8	–	[384]
BP QD	Deposited on tapered fiber	1532.02/1556.25	–	9.45	–	[385]
$G/SnO_2/PANI$	Ternary composite film	1532/1557.6	1.25	2.13	1.51	[386]

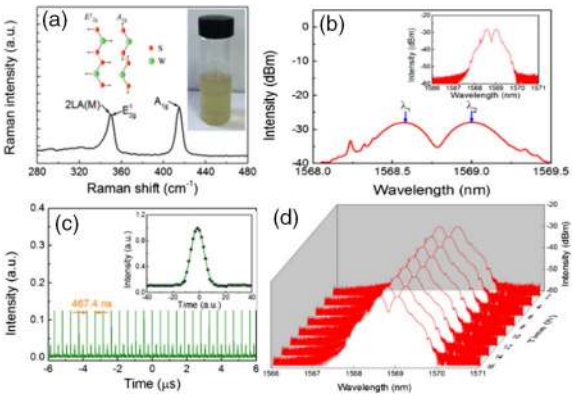

Fig. 14. Material characterization: (a) Raman spectrum of few-layer WS_2 (inset: the photograph of the solution sample). Dual-wavelength soliton characteristics of an EDFL based on WS_2 SA: (b) Optical spectrum, (c) the oscilloscope trace (inset: the auto-correlation trace), and (d) long-term optical spectra of dual-wavelength soliton operation. Selected from Ref. [381].

$Nd:Y_{2.8}Ga_5O_{12}$ (Nd:YGG)[78], Tm, Ho:YGG[78], $Nd:YAlO_3$[421], $Yb:(Lu_xGd_{1-x})_3Ga_5O_{12}(x = 0.062)$ (Yb:LGGG)[422], Tm-doped calcium lithium niobium gallium garnet (Tm:CLNGG)[423], $Tm:GdVO_4$[424], $Er:Lu_2O_3$[425,452], Tm:Ho:YAP[426], $Er:Y_3Al_5O_{12}$ (Er:YAG)[428,449], $Nd:Gd_{0.93}Y_{2.04}Sc_2Ga_3O_{12}$ (Nd:GYSGG)[430], $YVO_4/Nd:YVO_4$[432], Tm, $Ho:LuLiF_4$ (Tm, Ho:LLF)[433], $Nd:Lu_{0.15}Y_{0.85}VO_4$[435], Nd:YAG[436], $Er:SrF_2$[441], $Tm:CaYAlO_4$[444], $Er:Y_2O_3$[444], Tm:YAG[445], Cr:ZnSe[243], $Yb:ScBO_3$[446], $Ho/Pr:LiLuF_4$[447], $Yb:CaYAlO_4$ (Yb:CYA)[448], Nd:LLF[453], Yb:YAG[456,457], $Pr:GdLiF_4$[458], $Nd:GdTaO_4$[459], and Yb, Lu:$CaGdAlO_4$ (Yb, Lu:CALGO)[460]. The output spectra of these solid-state lasers have covered 0.6–3 μm. These results open a way to use the 2D materials in pulsed solid-state lasers.

For the TI SAs, the minimum pulse width of 850 ps[420] and maximum pulse energy of 21.7 μJ[436] are obtained in the *Q*-switched solid-state lasers, respectively. For example, Yu *et al.* demonstrated a bulk solid-state laser by

Table 7. Performance Summary of *Q*-switched Solid Lasers Based on 2D Noncarbon Materials

2D Materials	Gain Medium	Central Wavelength (nm)	Pulse Duration (μs)	Repetition Rate (kHz)	Pulse Energy (μJ)	References
Bi_2Se_3	Nd:$GdVO_4$	1063	0.666–1.3	100–547	0.0585	[413]
Bi_2Se_3	Nd:Lu_2O_3	1077, 1081	0.7–1.8	44.3–94.7	0.8342	[414]
Bi_2Se_3	c-cut Nd:YVO_4	1066.6, 1066.8	0.25–0.55	1–135	0.56	[415]
Bi_2Se_3	Nd:$LiYF_4$	1313.04	0.433–0.628	36.5–161.3	1.23	[416]
Bi_2Te_3	Yb^{3+}:$GdAl_3(BO_3)_4$	1043.7, 1045.3, 1046.2	0.37–2.5	30–110	0.5117	[418]
Bi_2Te_3	Tm:LuAG	2027	0.62–1.9	30–118	18.4	[419]
Bi_2Te_3/graphene	Tm:YAP	1980	0.238	108	1.25	[420]
	Er:YSGG	2796	0.243	88	1.25	
MoS_2	Nd:$GdVO_4$	1060	0.97	90–732	0.31	[78]
	Nd:YGG	1420	0.729	40–77	0.67	
	Tm:Ho:YGG	2100	0.41	110–149	1.38	
MoS_2	Nd:$YAlO_3$	1079.57	0.227–0.58	32–232.5	1.11	[421]
MoS_2	Yb:LGGG	1025.2, 1028.1	0.182	94–333	1.8	[422]
MoS_2	Tm:CLNGG	1979	4.84–6	80–110	0.72	[423]
MoS_2	Tm:$GdVO_4$	1902	0.8–2	25.58–48.09	2.08	[424]
MoS_2	Er:Lu2O3	2840	0.335–1	48–121	8.5	[425]
MoS_2	Tm, Ho:YAP	2129	0.435	55	–	[426]
MoS_2 + AOM	Nd:YVO_4	1064	0.00085	10	18.3	[427]
MoS_2	Er:YAG	1645	1.138	15–46.6	23.08	[428]
WS_2	Nd:GYSGG	1057, 1061	0.62, 0.591	35–67.35, 45–70.7	1.05	[430]
WS_2	Tm:LuAG	2012.9	0.66–1.6	10–63	17	[431]
WS_2	YVO_4/Nd:YVO_4	1064	0.056–0.24	100–1030	1.6	[432]
WS_2	Tm, Ho LLF	1895	4–6.8	11.29–16.89	5.21	[433]
WS_2	Nd:YVO_4	1064	2.3–4.94	55–135	0.145	[434]
WS_2 + EOM	Nd:$Lu_{0.15}Y_{0.85}VO_4$	1064	0.467	519–731	341.5	[435]
WSe_2 + EOM	Nd: YAG	946.3	0.0495	125	2630	[436]
ReS_2	Er:YSGG	2796	0.324–1.1	47–126	0.825	[440]
BP	Er:SrF_2	2790.1, 2790.9	0.702–1.5	61–77.03	2.34	[441]
BP	Tm:YAP	1969, 1979	0.181–0.72	41–81	39.5	[442]
BP	Tm:YAP	1988	1.78–4	11–19.25	7.84	[443]
BP	Yb:LuYAG	1030	1.73	63.9	0.09	[444]
	Tm:$CaYAlO_4$Er:Y_2O_3	1930	3.1	17.7	0.68	
		2720	4.47	12.6	0.48	
BP	Tm:YAG	2009	2.9–9	6–11.6	3.32	[445]
BP	Cr:ZnSe	2411	0.189–0.396	98–176	0.205	[243]
BP	Yb^{3+}:$ScBO_3$	1063.6	0.4955–1393	20–30	1.4	[446]
BP	Ho^{3+}, Pr^{3+}:$LiLuF_4$	2950	0.1943–0.58	55–158.7	2.4	[447]
BP	Yb:CYA	1046	0.62–1.2	87.7–113.6	0.3257	[448]

(Table continued)

Table 7. Continued

2D Materials	Gain Medium	Central Wavelength (nm)	Pulse Duration (μs)	Repetition Rate (kHz)	Pulse Energy (μJ)	References
BP	Er:YAG	1645, $LG_{0,-1}$ mode	3.2	40	2150	[449]
		$LG_{0,+1}$ mode	2.9		2400	
BP MoS_2WS_2	Nd:YVO_4	1064.4	0.00286	–	166	[450]
			0.00399		150	
			0.0054		365	
g-C_3N_4	Er:Lu_2O_3	2840	0.351–1.5	48–99	11.1	[452]
g-C_3N_4	Nd:LLF	1320.9	0.275–1.3	112–147	9.51	[453]

using few-layer Bi_2Se_3 as the pulse modulator[413]. Xu *et al.* also demonstrated a passively *Q*-switched Nd:$LiYF_4$ laser at 1.3 μm based on a Bi_2Se_3 SA[416]. The laser has a maximum average power of 0.2 W, corresponding to a pulse repetition rate of 161.3 kHz, shortest pulse width of 433 ns, and pulse energy of 1.23 μJ, respectively. In addition, Liu *et al.* demonstrated a *Q*-switched Tm:LuAG laser at 2027 nm using a Bi_2Te_3 SA[419]. *Q*-switched pulses with an average power of 2.03 W are generated, corresponding to the maximum pulse energy of 18.4 μJ and peak power of 23 W. The pulse duration and repetition rate of the laser is 620 ns and 118 kHz, respectively. These results indicate the promising potential of TIs as nonlinear optical switches for achieving efficient pulsed solid lasers.

For the TMDC SAs, the minimum pulse width of 850 ps[427] and maximum pulse energy of 2.63 mJ[436] are achieved in the *Q*-switched solid-state lasers, respectively. For example, Wang *et al.* demonstrated Nd:$GdVO_4$, Nd:YGG, Tm/Ho:YGG lasers at 1.06, 1.42, and 2.1 μm with a broadband MoS_2 SA, respectively[78]. Xu *et al.* also demonstrated an Nd:$YAlO_3$ laser at 1079.5 nm using a MoS_2 SA[421]. The laser has a maximum average power of 0.26 W corresponding to a pulse repetition rate of 232.5 kHz, pulse width of 227 ns, and pulse energy of 1.11 μJ. In addition, Tang *et al.* demonstrated a YVO_4/Nd:YVO_4 laser by using WS_2 as an SA[433]. Under the pump power of 6.28 W, a maximum output power of 1.36 W and pulse duration of 56 ns with a repetition rate of 1.03 MHz are obtained, resulting in a peak power as high as 23.6 W. Interestingly, Ling *et al.* demonstrated a Tm, Ho:$LuLiF_4$ laser by using a WS_2 SA[434]. The laser has a maximum power of 0.088 W, corresponding to a pulse repetition rate of 16.89 kHz, pulse width of 4 μs, and pulse energy of 5.21 μJ. Recently, Su *et al.* demonstrated an Er:YSGG laser at 2.8 μm by using a ReS_2 SA[440]. Under a pump power of 920 mW, an average power of 104 mW was obtained with a pulse width of 324 ns and a repetition rate of 126 kHz. These results indicate that TMDCs have a prosperous application future in solid-state lasers.

For the BP SAs, the minimum pulse width of 2.86 ns and maximum pulse energy of 2.4 mJ are demonstrated, respectively[450]. For example, Chu *et al.* demonstrated a Tm:YAP laser at 1988 nm by using a BP SA[443]. Under the pump power of 3.38 W, an average power of 151 mW was generated with a minimum pulse width of 1.78 μs and repetition rate of 19.25 kHz, corresponding to pulse energy of 7.84 μJ. Kong *et al.* also demonstrated the *Q*-switching operation of Yb:LuYAG, Tm:$CaYAlO_4$, and Er:Y_2O_3 lasers at 1.03, 1.93, and 2.72 μm by using a broadband BP SAM, respectively[444]. In addition, Wang *et al.* demonstrated the mid-IR pulse generation from a BP *Q*-switched Cr:ZnSe laser[243]. A pulse as short as 189 ns with an average power of 36 mW was realized at 2.4 μm, corresponding to a repetition rate of 176 kHz and single-pulse energy of 205 nJ, respectively. Nie *et al.* also demonstrated a Ho, Pr:LLF laser operating at 2.95 μm using a BP SAM[447]. Under the absorbed pump power of 7.36 W, the shortest pulse width of 194.3 ns was obtained. Ma *et al.* also obtained the stable *Q*-switched pulses with a pulse width of 620 ns at 1046 nm in a Yb:$CaYAlO_4$ laser with the BP SAM[448]. The generated pulse train has a repetition rate of 113.6 kHz and an average power of 37 mW. Interestingly, Liu *et al.* demonstrated the vortex pulses at 1645 nm from an Er:YAG laser based on the BP SA[449]. Laser guided ($LG_{0,-1}$) mode pulses with maximum pulse energy of 2.15 μJ and $LG_{0,+1}$ mode pulses with maximum 2.4 μJ pulse energy were obtained individually, as well as pulsed $LG_{0,\pm2}$ laser beams. Recently, Liu *et al.* demonstrated an Nd:YVO_4 laser by using BP, WS_2, and MoS_2 solutions as SAs[450]. The pulse durations of the lasers were 2.86, 3.99, and 5.40 ns with the pulse energy of 0.166, 0.150, and 0.365 mJ, respectively. Li *et al.* also demonstrated a *Q*-switched Yb^{3+}-doped $ScBO_3$ laser using a BP SA[451]. Its maximum output energy is 1.4 μJ. These results show that BP might be considered as a universal broadband SA that could compete with other 2D nanomaterials.

Besides single-wavelength operation, multiwavelength *Q*-switching was also reported. The minimum pulse width of 181 ns and maximum single-pulse energy of 39.5 μJ were demonstrated, respectively[442]. For example, Wang *et al.* first demonstrated a dual-wavelength *Q*-switched Nd:Lu_2O_3 laser at 1066.6 and 1066.8 nm with a TI:Bi_2Se_3 SA[414]. Jia *et al.* also demonstrated a

dual-wavelength *Q*-switched c-cut Nd:YVO_4 laser with a TI:Bi_2Se_3 SA[415]. Its repetition rate is tunable in a wide range of 1–135 kHz, where the pulse width is 250 ns, and maximum pulse energy is 0.56 μJ. In addition, Sun *et al.* demonstrated a triple-wavelength *Q*-switched Yb^{3+}:$GdAl_3(BO_3)_4$ laser at 1043.7, 1045.3, and 1046.2 nm based on a TI:Bi_2Te_3 SA[418]. The shortest pulse width was 370 ns with 110 kHz pulse repetition rate. The maximum average power was 57 mW with the pulse energy of 511.7 nJ. Lou *et al.* also obtained a dual-wavelength *Q*-switching at 1025.2 and 1028.1 nm in an Yb:LGGG laser based on the MoS_2 SAM[422]. The maximum average power of 0.6 W with a pulse width of 182 ns was obtained, corresponding to single-pulse energy of 1.8 μJ. Gao *et al.* also demonstrated the stable dual-wavelength *Q*-switched laser operation with a maximum average power of 367 mW, pulse repetition rate of 70.7 kHz, pulse width of 591 ns, and pulse energy of 1.05 μJ in an Nd:GYSGG laser using a WS_2 SAM[431]. Interestingly, multiwavelengh *Q*-switching in the mid-IR band was studied. For example, Liu *et al.* demonstrated a dual-wavelength *Q*-switched Er:SrF_2 laser at 2.79 μm by using a BP SA[441]. The maximum average output power of 180 mW with pulse duration of 702 ns and repetition rate of 77.03 kHz was achieved at a pump power of 2.47 W. Zhang *et al.* also achieved a dual-wavelength *Q*-switched Tm:YAP laser at 1969 and 1979 nm with a BP SAM[442]. The pulses with a duration of 181 ns, average power of 3.1 W, and pulse energy of 39.5 μJ were generated at a pulse repetition rate of 81 kHz. These results well prove that 2D materials are reliable optical modulators for multiwavelength solid-state lasers.

Notably, besides the single scheme, hybrid *Q*-switching was also demonstrated. For example, Qiao *et al.* proposed a diode-pumped passively *Q*-switched laser with a MoS_2 SA[427]. At an incident pump of 6.54 W, a maximum output power of 1.15 W with a pulse duration of 70.6 ns was obtained. Then, by using a hybrid *Q*-switched laser with a MoS_2 SA and an acousto-optic modulator (AOM) as a pumping fundamental laser, a sub-nanosecond $KTiOPO_4$ (KTP) -based intracavity optical parametric oscillation was realized. With an incident pump power of 10.2 W and AOM repetition rate of 10 kHz, the maximum output power of 183 mW with minimum pulse duration of 850 ps was obtained. In addition, Tang *et al.* demonstrated a dual-loss modulation *Q*-switched and mode-locked Nd:$Lu_{0.15}Y_{0.85}VO_4$ laser with the pulse duration of 467 ps and peak power of 731 kW by simultaneously employing the WS_2 and electro-optic modulator (EOM) as a modulator[437]. Sun *et al.* also demonstrated a passively *Q*-switched Nd:YAG laser at 946 nm by using a WSe_2 SA and an EOM[439]. The laser has an average power of 0.1 W, corresponding to a pulse repetition rate of 0.5 Hz, pulse width of 10.8 ns, and pulse energy of 2.63 mJ. These findings indicate that the hybrid *Q*-switched laser may exhibit more advantages and a need for further study.

Other 2D materials such as g-C_3N_4 were also proposed. For example, Fan *et al.* demonstrated a stable *Q*-switched Er:Lu_2O_3 laser at 2.84 μm by using a g-C_3N_4 SA, generating the pulse duration of 351 ns and an average output power of 1.09 W. For example, Fan *et al.* demonstrated a stable *Q*-switched Er:Lu_2O_3 repetition rate of 99 kHz, corresponding to the pulse energy of 11.1 μJ[452]. They also used the g-C_3N_4 nanosheets as an SA in a passively *Q*-switched Nd:LLF laser at 1.3 μm[453]. Under an incident pump power of 9.97 W, the pulse duration of 275 ns was acquired with output power of 0.96 W and pulse repetition rate of 154 kHz, resulting in the pulse energy of 6.2 μJ. These results indicate a great potential for g-C_3N_4 as a new SA in lasers.

The study found that, compared with the Kerr-lens mode-locking, 2D materials-based SAs share more advantages, such as self-starting and alignment-free. To make them convenient for application, 2D materials are normally coated on high reflectivity mirrors and then employed as cavity mirrors. Since 2010, the mode-locked solid-state lasers based on 2D materials, including graphene and its derivatives[461–492] WS_2[456], MoS_2[458,459], and BP[455,457,460], were developed. Their performances are summarized in Table 8. Among them, the minimum pulse width of 272 fs and maximum pulse energy of 6.48 nJ were demonstrated, respectively. For example, Su *et al.* demonstrated a femtosecond solid-state laser modulated by a BP SA[455]. Pulses as short as 272 fs were achieved with an average power of 0.82 W, corresponding to the pulse energy of 6.48 nJ and peak power of 23.8 MW. In addition, Hou *et al.* obtained excellent mode-locking performance by applying the samples into a solid-state Yb: YAG laser based on a few-layer WS_2 SAM[456]. The pulse repetition rate was 86.7 MHz with a pulse width of 736 fs. The maximum output power was 270 mW, and the peak power was 4.23 kW. Wang *et al.* also demonstrated the *Q*-switched mode-locking operation at 1066 nm of the Nd:$GdTaO_4$ laser by using the MoS_2 SAM[459]. The maximum average output power of 156 mW was obtained. Meanwhile, Zhang *et al.* demonstrated ultrafast pulse generation at 1064.1 nm from a bulk laser by employing the BP SAM[457], as shown in Fig. 15. Pulses as short as 6.1 ps with an average power of 460 mW were obtained.

Recent developments in nanooptics have made possible the manipulation of light at sub-wavelength scales. Due to its unique aspect ratio, thermal management, and high peak power, thin-disk lasers based on 2D materials, including graphene[454], perovskites[493], WS_2[494], and MoS_2[495,496], were developed. Their performance is summarized in Table 8. Among them, the minimum pulse width of 13.1 ps and maximum pulse energy of 18.3 nJ were demonstrated, respectively[493]. For example, Ye *et al.* demonstrated a 2D excitonic laser at the visible waveband by embedding monolayer WS_2 in a microdisk resonator[494], as shown in Fig. 16. In addition, Reed *et al.* demonstrated an integrated narrowband light source based on thin MoS_2 emissive material[495]. The active light-emitting material consists of chemically enhanced bi-layer MoS_2 flakes that

Table 8. Performance Summary of Mode-locked Solid/Disk Lasers Based on 2D Noncarbon Materials

2D Materials	Gain Medium	Central Wavelength (nm)	Pulse Duration (ps)	Repetition Rate (MHz)	Pulse Energy (nJ)	References
WS_2	Yb:YAG	1064	0.736	86.7	3.11	[456]
MoS_2	a-cut Pr^{3+}:$GdLiF_4$	522.4	46	101.4	0.1	[458]
		607.6	30	90.2	0.2	
		639.2	55	104.4	0.21	
		639	25	94.7	0.49	
MoS_2	Nd:$GdTaO_4$	1066	725	83	–	[459]
BP	Nd:YVO_4	1064.1	6.1	140	3.29	[457]
BP	Yb, Lu:CALGO	1053.4	0.272	63.3	6.48	[455]
BP	Nd:$GdVO_4$	1340.7	9.24	58.14	–	[460]
MoS_2	Yb:YAG, disk	1031	13.1	48.6	18.3	[493]

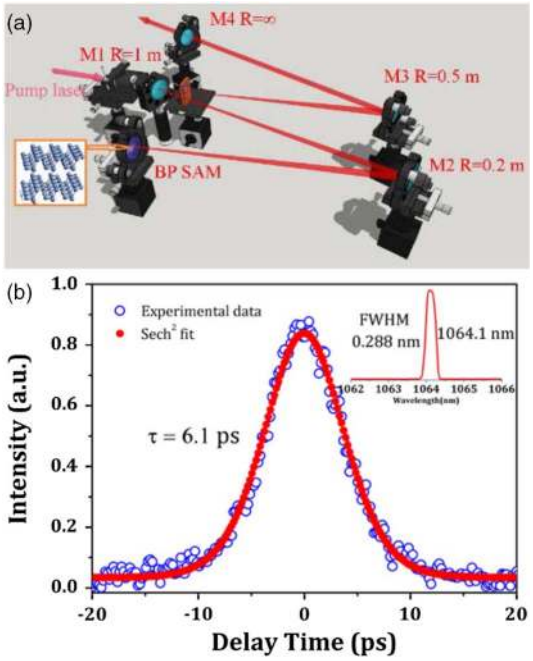

Fig. 15. Experimnetal setup: (a) Schematic of the mode-locked solid laser based on BP SAM, M1 is an input mirror, dichroic mirror coated for high transmission at the pump wavelength and high reflection in 1020–1100 nm range. Mode-locking characteristics of an EDFL: (b) The autocorrelation trace (inset: the optical spectrum). Selected from Ref. [457].

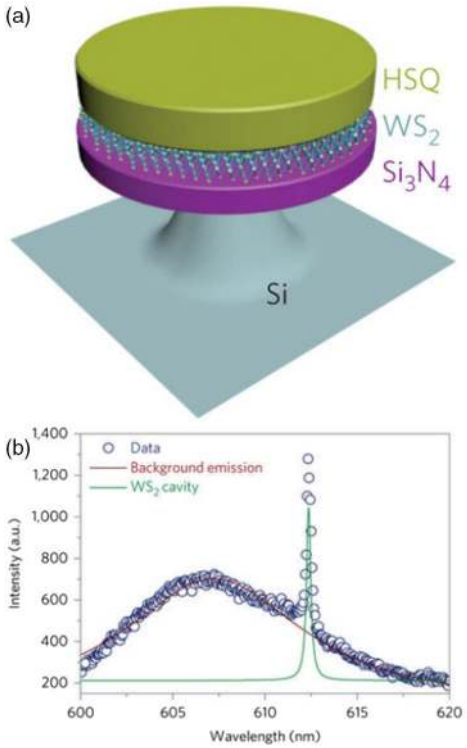

Fig. 16. Experimental setup: (a) Schematic image of a monolayer WS_2 microdisk laser. Output characteristics: (b) Photoluminescence spectrum, the brown line is a fit to the background emission, and the green line is a fit to the WS_2 cavity emission. Selected from Ref. [494].

yield 20 times brighter chemically enhanced photoluminescence compared to as-exfoliated monolayers. Quality factors ∼1000 are observed as well as a high degree of spatial coherence. Recently, Lu *et al.* demonstrated a picosecond Yb-doped thin-disk laser using a monolayer MoS_2 SA[496]. The maximum output power is ∼890 mW, while the corresponding repetition rate, pulse energy, and pulse duration are 48.6 MHz, 18.3 nJ, and 13.1 ps, respectively.

As a basic active device for the integrated photonic circuits, the waveguide laser has attracted continuous attention ever since its first proposal in 1961. It is defined as the miniature and integrated laser with the cavity resonant in the waveguide platform. The waveguide works as both the resonant cavity and the gain medium. Since the waveguide structure has a small volume, the intracavity intensity could be considerably high even at low pumping power. Hence, the waveguide lasers have superior laser performances, including low threshold and enhanced slope

efficiency, compared to bulk or fiber lasers in some cases. So far, several technologies have been applied to fabricating various waveguide structures in dielectrics, such as ion/proton exchange, femtosecond laser writing, epitaxial growth, and ion irradiation.

Waveguide lasers have been realized in both continuous-wave and pulsed operation regimes. Especially, *Q*-switched waveguide lasers based on 2D materials were developed[497–511]. Their performance is summarized in Table 9. Among them, the maximum pulse energy of 112 nJ[510] and minimum pulse width of 24 ns[511] were obtained, respectively. For example, Tan *et al.* demonstrated the stable *Q*-switched laser pulses in an Nd:YAG waveguide laser by using a Bi_2Se_3 SA[506], as shown in Fig. 17. The laser operation has a repetition rate ranging from 2.7 to 4.7 MHz. Its minimum pulse duration and maximum pulse energy were 46 ns and 31.3 nJ, respectively. In addition, Cheng *et al.* demonstrated the passively *Q*-switched Nd:YAG waveguide lasers based on few-layer $MoSe_2$ and WSe_2, respectively[507]. The repetition rate was tunable from 0.995 to 3.334 MHz ($MoSe_2$) and 0.781 to 2.938 MHz (WSe_2), and the obtained minimum pulse duration was 80 ns ($MoSe_2$) and 52 ns (WSe_2), respectively. Under an optical pump at 808 nm, the laser reaches a maximum average output power of 115 mW ($MoSe_2$) and 45 mW (WSe_2), which correspond to single-pulse energy of 36 and 19 nJ, respectively. Ma *et al.* also demonstrated the *Q*-switched waveguide laser based on the Yb:YSGG crystal and WS_2 SA[508]. The *Q*-switched laser emission was obtained with the pulse duration of 125 ns. Recently, Cheng *et al.* demonstrated the passively *Q*-switched Nd:YAG waveguide laser by employing the $SnSe_2$ SAM[509]. They also demonstrated the passively *Q*-switched waveguide laser based on the Nd:YAG crystal and MoS_2 SA[510]. The repetition rate of the laser system is tunable from 0.51 to 1.10 MHz, and the obtained minimum pulse duration is 203 ns. The laser reaches maximum average output power of 85.2 mW, corresponding to single-pulse energy of 112 nJ. Li *et al.* also demonstrated highly stable *Q*-switched laser pulses at 1064 nm in an Nd:YAG waveguide laser by using a WS_2 and BP SA,

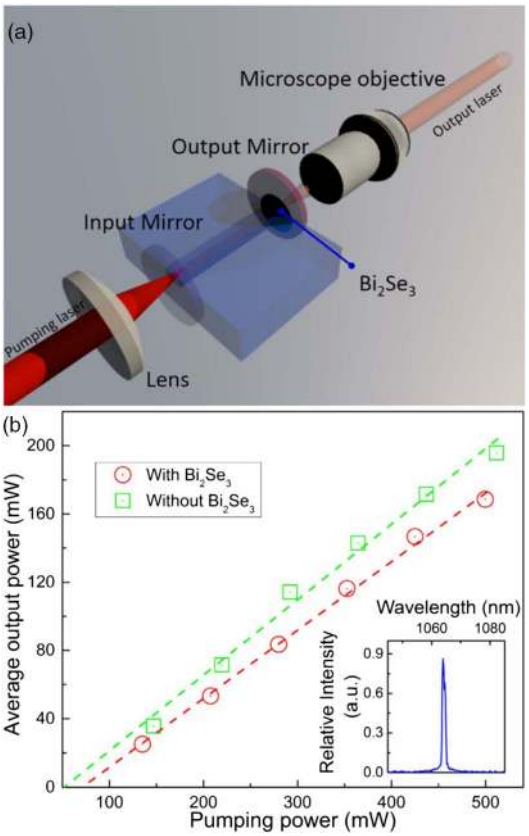

Fig. 17. Experimnetal setup: (a) Output testing of the *Q*-switched waveguide laser based on few-layer Bi_2Se_3 SA. *Q*-switching characteristics of waveguide laser: (b) The output power as a function of the pump power (inset: the optical spectrum). Selected from Ref. [506].

Table 9. Performance Summary of *Q*-switched Waveguide Lasers Based on 2D Noncarbon Materials

2D Materials	Gain Medium	Central Wavelength (nm)	Pulse Duration (ns)	Repetition Rate (MHz)	Pulse Energy (nJ)	References
Bi_2Se_3	Nd:YAG ceramic	1064	46	2.7–4.7	31.3	[506]
$MoSe_2WSe_2$	Nd:YAG crystal	1064	80	0.995–3.334	36	[507]
			52	0.781–2.938	19	
WSe_2	Yb:YSGG crystal	1024.8	125	0.36	21.7	[508]
$SnSe_2$	Nd:YAG crystal	1064	129	0.337–2.294 (TE)	6.7-44.5	[509]
			183	0.438–1.865 (TM)	6.5-43.1	
MoS_2	Nd:YAG crystal	1063.9	203	0.51–1.1	112	[510]
MoS_2 BP	Nd:YAG ceramic	1064	24	3.23–6.1	25	[511]
			55	4.3–5.6	23	
G/WS_2 heterostructure	Nd:YVO_4	1064	66	3.528–7.777	33.1	[512]

respectively[511]. The pulse durations was 55 ns (modulated by BP) and 24 ns (modulated by WS_2), respectively.

C. Pulsed Lasers Based on the 2D Materials Heterostructure and Quantum Dots

From the point of view of energy structure, zero or small bandgap materials are the most suitable candidates for broadband operation of laser applications, as they own a wavelength insensitive optical response. However, there are some optical limitations in terms of absorption strength, modulation depth, spectral range, and carrier dynamics if these 2D materials are used individually. Recent advances in producing 2D materials-based heterostructures with high-quality nanoplates and enhanced absorption strength, as well as broadened spectral range, provide new possibilities for optoelectronic devices that could operate from the visible to the near-IR range[512–518].

Since 2015, pulsed lasers with 2D nanomaterials-based heterostructures were developed[519–523]. Their performance is summarized in Table 10. Among them, the maximum pulse energy of 3 nJ[520] and minimum pulse width of 296 fs[522] were demonstrated, respectively. For example, Mu *et al.* demonstrated the *Q*-switching and mode-locking operation in an EDFL, incorporating a graphene-Bi_2Te_3 heterostructure[519], as shown in Fig. 18. The soliton mode-locking pulses have a pulse width of 837 fs. They found that the formation of a graphene-Bi_2Te_3 heterostructure gives a larger modulation depth than pure graphene and faster carrier dynamics than pure Bi_2Te_3. Wang *et al.* also demonstrated the ultrashort pulse in an Er-doped or Yb-doped fiber laser by incorporating a graphene-Bi_2Te_3 heterostructure SA[521]. The study found that, with the help of graphene, the surface states of Bi_2Te_3 in the graphene-Bi_2Te_3 heterostructure remain intact because of the few defects in the process of preparation and are well protected from environmental contamination. Thus, the graphene-Bi_2Te_3 heterostructure not only exhibits the wavelength-independent saturable absorption, but also exhibits stronger nonlinear optical properties than that of individual graphene or Bi_2Te_3. Chen *et al.* also obtained the stable soliton pulses with durations as short as 296 fs and average power as high as 25 mW in an EDFL based on the WS_2-MoS_2-WS_2 heterostructure SA, respectively[522]. Liu *et al.* also fabricated a graphene/phosphorene nanoheterojunction-based optical SA, and integrated it into an EDFL to demonstrate the generation of a stable ultrashort pulse down to 148 fs[523]. In addition, You *et al.* demonstrated a *Q*-switched Tm:YAP and Er:YSGG solid laser with a Bi_2Te_3/graphene heterostructure, respectively[420]. One is a Tm:YAP laser with an average power of 2.34 W and a pulse width of 238 ns. The other one is an Er:YSGG laser producing a pulse width of 243 ns. Li *et al.* also demonstrated a *Q*-switched Nd:YVO_4 waveguide laser based on the graphene/WS_2 heterostructure[512]. The waveguide laser has a maximum output power of 275 mW and slope efficiency of 37%. These results show that the 2D

Table 10. Performance Summary of Mode-locked Fiber Lasers Based on 2D Heterostructure/QD SAs

2D Materials	Incorporation Method	Central Wavelength (nm)	Pulse Duration (ps)	Repetition Rate (MHz)	Pulse Energy (nJ)	References
G-Bi_2Te_3 heterostructure	Deposited on fiber end	1568.07	0.837	17.3	0.178	[519]
G-Bi_2Te_3 heterostructure	Deposited on fiber end	1058.9	189.94	Harmonic, 79.13	3	[520]
G-Bi_2Te_3 heterostructure	Deposited on fiber end	1049.1	144.3	3.7	–	[521]
		1565.6	1.1	6.9	–	
WS_2-MoS_2-WS_2 heterostructure	Deposited on fiber end	1562.66	0.296	36.46	–	[522]
G-BP heterostructure	Deposited on D-shaped fiber	1529.92	0.82	7.43	–	[523]
BP QD	Polymethylmethacrylate film	1567.5	1.08	15.22	–	[524]
BP QD	Polyvinylidene fluoride film	1568.5 bound soliton	0.787	15.15	–	[525]
			0.813	15.1		
			0.748	15		
BP QD	Deposited on fiber end	1567.6	1.07	11.01	–	[526]
P QD	Deposited on tapered fiber	1561.7	0.88	5.47	0.0247	[527]
BP QD	Deposited on tapered fiber	1562.8	0.291	10.36	–	[528]

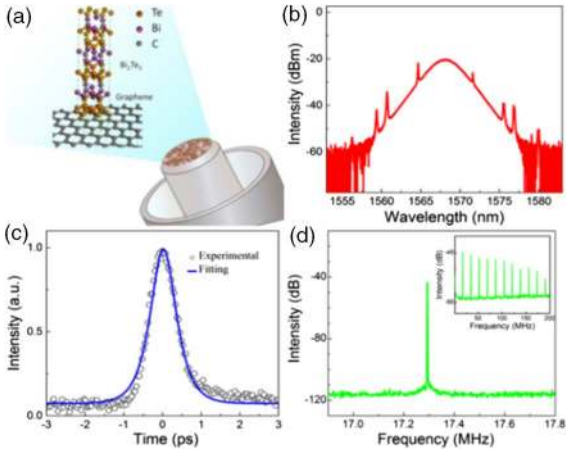

Fig. 18. Material and device characterization: (a) Schematic of a graphene-Bi_2Te_3 heterostructure on the end-facet of the fiber connector. Mode-locking characteristics of an EDFL based on a graphene-Bi_2Te_3 heterostructure SA: (b) Optical spectrum, (c) autocorrelation trace, and (d) RF spectrum (inset: wideband RF spectrum). Selected from Ref. [519].

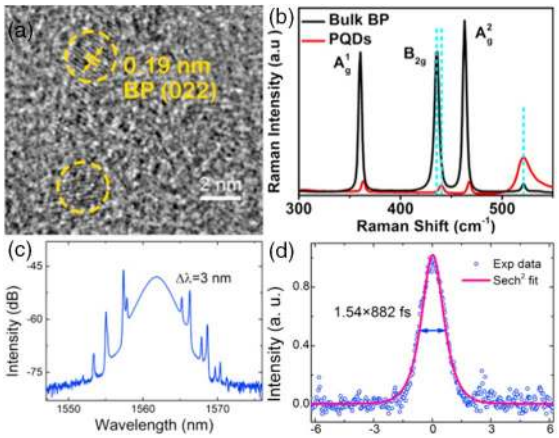

Fig. 19. Material characterization: (a) High-resolution TEM (HRTEM) image and (b) Raman spectra of phosphorene QDs (PQDs). Mode-locking characteristics of an EDFL based on a PQDs SA: (c) Optical spectrum and (d) autocorrelation trace. Selected from Ref. [527].

materials-based heterostructure can be a promising nonlinear optical material for ultrafast laser photonics.

The QD, which is another type of nanomaterial, exhibits its unique optoelectronic properties due to the quantum confinement and edge effects. Therefore, QDs may be developed as another kind of promising nanomaterial for ultrafast photonics. Since 2015, the pulsed lasers with 2D materials-based QDs were developed[524–532]. Their performances are summarized in Table 10. Among them, the maximum pulse energy of 0.02 nJ[527] and minimum pulse width of 291 fs[528] were demonstrated, respectively. For example, Du *et al.* demonstrated the soliton pulse with a pulse duration of 0.88 ps and repetition rate of 5.47 MHz in an EDFL by using the phosphorene QDs, which interacted with microfiber evanescent light field[527], as shown in Fig. 19. In addition, Xu *et al.* obtained the picosecond-level pulse in an EDFL by employing the BP QDs/PMMA composite nanofiber film as an optical SA[526]. Wang *et al.* also demonstrated the generation of bound soliton in an EDFL passively mode-locked based on a BP QD SA[525]. In the experiment, the three-pulse bound-soliton operation with pulse-to-pulse separation of 5.2 ps was obtained.

Other QDs may be developed as a kind of *Q*-switch for laser photonics. For example, Liu *et al.* demonstrated a *Q*-switched Nd:$GdVO_4$ laser with the shortest pulse width of 66.8 ns and a maximum repetition rate of 1.13 MHz by using high-quality carbon QDs as an SAM[530]. Lee *et al.* also demonstrated a passively *Q*-switched EDFL utilizing a colloidal PbS QD thin film as an SA. The laser generated 801 nJ pulses with a 24.2 kHz repetition rate[531]. Li *et al.* also demonstrated a passively *Q*-switched laser based on the $CsPbBr_3$ perovskite QDs acting as SAs[532]. For a 522 nm laser, a maximum average output of 9.11 mW was achieved with a corresponding shortest pulse width of 653 ns and pulse repetition rate of 96.2 kHz.

Very recently, other nanomaterials have also been developed as a kind of SAs for laser photonics[533–544]. For example, Jiang *et al.* demonstrated the mode-locked pulse generation in an EDFL by using the MoS_2/graphene nanocomposites[60]. Huang *et al.* also reported a passively *Q*-switched cylindrical vector beam with the shortest pulse width of 919 ns, pulse repetition rate of 36.4 kHz, and pulse energy of 0.77 μJ from a Yb-doped vectorial fiber laser based on hybrid organic–inorganic perovskites $CH_3NH_3PbI_3$[538]. In addition, Guo *et al.* obtained a femtosecond pulse train with temporal width as short as 593 fs in an EDFL with indium tin oxide (ITO) nanocrystals as an SA[540]. They also obtained the stable passively *Q*-switched pulses with the minimum pulse width of 1.15 μs and repetition rate of 81.28 kHz in an EDFL using the ITO SAs[541]. The maximum output power of 1722 μW and pulse energy of 21.19 nJ were realized when the pump power was 480 mW. Meanwhile, Lee *et al.* demonstrated a Tm–Ho co-doped fiber laser with the shortest pulse width of 2.2 μs and a maximum repetition rate of 44 kHz by using filled skutterudites of $InCo_4Sb_{12}$ and $In_{0.25}Co_4Sb_{12}$ as broadband SA that can cover 1.5–1.9 μm[542]. These results are promising for the development of robust, compact, and practical pulsed laser sources.

6. NONLINEAR OPTICAL PHENOMENON

A passively mode-locked laser as an effective tool to investigate soliton pulse dynamics and the related nonlinear phenomenon, has received much attention in recent years. Among all the cavity parameters of mode-locked lasers, the intracavity nonlinear effect is vital to the evolution of solitons. Thus, under the condition of high cavity nonlinearity, the conventional soliton in the lasers will be shaped into versatile multi-soliton patterns. Studies found that a 2D materials-based nonlinear optical device has

been demonstrated to be an excellent platform in fields of ultrafast nonlinear photonics. This is because, apart from the broadband saturable absorption effect, 2D materials also exhibit a giant nonlinear refractive index. Furthermore, if 2D materials are transferred onto a micro/nanofiber, this will greatly increase the interaction length between the light and the 2D materials, making it suitable for generating a versatile pulse.

Since 2012, versatile soliton fiber lasers based on 2D materials, including graphene and its derivatives[545–560] Bi_2Se_3[561–567], Bi_2Te_3[568,569], Sb_2Te_3[570], MoS_2[571,572], WS_2[573,574], and BP[314], were developed. For example, Liu *et al.* obtained versatile multi-soliton patterns, including soliton molecules, bound solitons, and soliton rains, in an EDFL with a microfiber-based Bi_2Se_3 device, which exhibits both the high third-order nonlinear susceptibility and excellent saturable absorption[561,562]. They also observed the dissipative rogue waves (DRWs) induced by long-range chaotic multi-pulse interactions in a fiber laser based on a TI-deposited microfiber photonic device[563], as shown in Fig. 20. By virtue of the simultaneous saturable absorption effect and high nonlinearity provided by the TI-deposited microfiber, a localized, chaotic multi-pulse wave packet with strong long-range nonlinear interactions could be obtained, which gives rise to the formation of DRWs. In addition, they also found that, apart from the conventional soliton, some soliton patterns, namely, multiple soliton molecules, localized chaotic multi-pulses, and double-scale soliton clusters, could be formed in an EDFL by taking advantage of the unique nonlinear optical properties of the microfiber-based MoS_2 device[571]. These findings deepen the understanding of nonlinear dynamics of multi-soliton patterns, and further demonstrate that the 2D materials-based microfiber may operate as a high-performance photonic device for studying nonlinear optics phenomena.

Interestingly, Guo *et al.* demonstrated three dual-wavelength pulse patterns, namely, bright pulse, bright–dark soliton pair, and hybrid step-like and dark pulse in an EDFL incorporating a Bi_2Se_3/PVA film[564,565]. The harmonic form of the bright–dark soliton pair was also obtained. Its highest repetition rate is ~433.8 MHz, which corresponds to the 280th harmonic of the fundamental repetition rate. They also demonstrated the direct generation of six kinds of dip sidebands, namely, dip–dip type, hybrid peak–dip and dip type (I, II), dual-peak–dip type (I, II), and nearly flat-top type from a passively mode-locked fiber laser with a WS_2-deposited fiber taper[573]. The maximum depth of ~16.8 and ~22 dB for dual-peak–dip type I and dual-peak–dip type II, and their second-order forms were also obtained, respectively, as shown in Fig. 21.

A bound-soliton pulse and its harmonic form were also observed in the lasers mode-locked by 2D materials. For example, Liu *et al.* achieved three types of bound states in an EDFL with a filmy Bi_2Se_3 SA by properly rotating the PCs at a higher pump power level[562]. It was found that the different widths and peak intensities of the constructed solitons within the bound state would result in different spectral modulations. Li *et al.* obtained the wavelength-switchable operation from 1532 to 1557 nm and the dual-wavelength soliton in an EDFL with three pieces of Bi_2Se_3-PVA film[569]. They found that the dual-wavelength pulses operate at different mode-locked states. One is the single-pulse mode-locking operation at 1532 nm, and the other one is the bound-soliton states at 1557 nm. The separations of bound pulses have small variations. Wang *et al.* presented a kind of harmonic mode-locking of bound-state solitons in an EDFL with a D-shaped fiber-based MoS_2 SA[572]. In the fiber laser, two solitons form the bound-state pulses with a temporal separation of 3.4 ps, and the bound-state pulses are equally distributed at a repetition rate of 125 MHz,

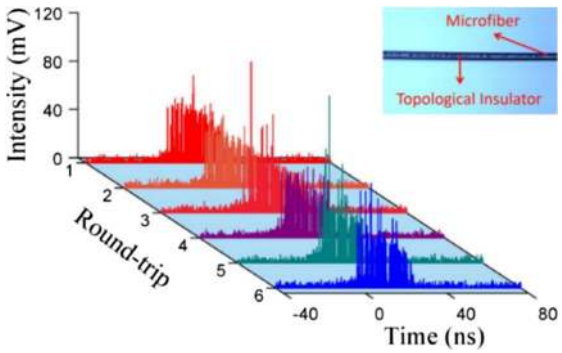

Fig. 20. Evolution of chaotic multi-pulse bunch over several cavity round-trips in a mode-locked EDFL based on the Bi_2Se_3 SA. Inset: Microscopy image of the TI-deposited microfiber. Selected from Ref. [563].

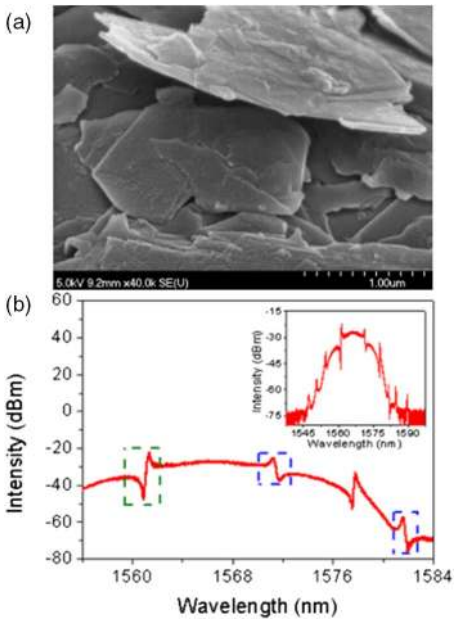

Fig. 21. Material characterization: (a) The photograph of few-layer WS_2; (b) the optical spectrum of the second-order form of the dual-peak–dip sidebands generated from a mode-locked EDFL based on a WS_2 SA. Selected from Ref. [573].

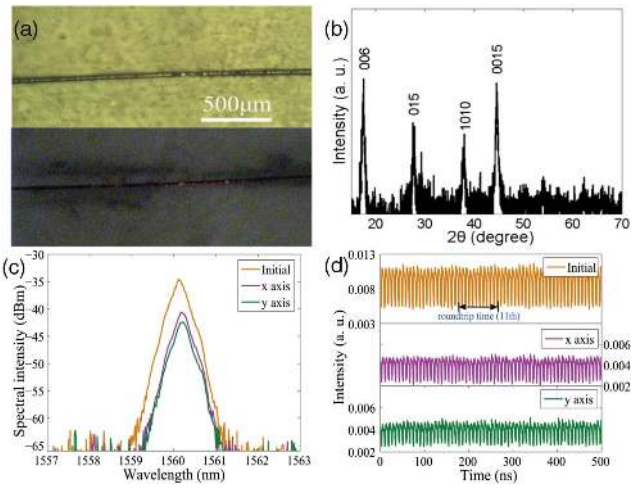

Fig. 22. Material characterization: (a) Microscope image and the evanescent field of microfiber-based Bi_2Te_3 SA observed using visible light and (b) the XRD pattern. Mode-locking characteristics of an EDFL based on a Bi_2Te_3 SA: (c) Pulse traces and (d) corresponding optical spectra of harmonic mode-locked vector dark pulses. Selected from Ref. [566].

corresponding to the 14th harmonics. Single- and multiple-pulse emissions are also observed by changing the pump power. In addition, Chen *et al.* observed the transition dynamics from a bunched state of pulses to harmonic mode-locking, which was up to the 26th order[299].

A dark soliton pulse was also observed in the EDFL mode-locked by 2D materials. For example, Liu *et al.* demonstrated the dark soliton with a repetition rate of 94 MHz in an EDFL based on a Sb_2Te_3 SA, which was fabricated by using the PLD method[570]. They also obtained dark solitons with a repetition rate of 116.5 MHz in a fiber laser with a WS_2 SA[574]. The obtained results provide an enhanced understanding of dynamics of the dark soliton.

Furthermore, Liu *et al.* also observed a rich variety of dynamic states, including polarization-locked dark pulses, polarization-locked noise-like pulses and their harmonic form, and incoherently coupled polarization domain wall pulses, including bright square pulses, bright–dark pulse pairs, dark pulses and bright-square-pulse–dark-pulse pairs in an EDFL by using a microfiber-based Bi_2Te_3 device[566], as shown in Fig. 22. They also demonstrated a passively mode-locked Er:Yb-doped fiber laser operated in the L-band by using a microfiber-based Bi_2Se_3 SA[567]. With the highest pump power of 5 W, the 91st harmonic mode-locking of soliton bunches with an average output power of 308 mW was obtained.

7. CONCLUSIONS AND PERSPECTIVES

The field of graphene, related 2D materials, and hybrids is now rapidly evolving from pure science to technology. Currently, huge research efforts have been focused mainly on graphene, TIs, TMDCs, and BP. However, we believe that pulsed lasers based on novel 2D materials, such as bismuthene and antimonene, will be investigated in the near future for ultrafast photonic applications given the increasing research activity on these materials.

Various mode-locked/Q-switched lasers (e.g., fiber, solid-state, disk, and waveguide lasers) based on 2D materials will be further developed. Future investigations would be targeted to improve output performance (e.g., the output power, pulse duration, and pulse energy) of these pulsed lasers. More improvements can be envisioned by innovative cavity design, 2D material frabrication, and device optimization. This is particularly important in view of new applications. In the past decade, these 2D materials have been utilized for achieving passive mode-locking/Q-switching in the major lasers ranging from fiber, solid-state, disk, and waveguide lasers to vertical-external-cavity surface-emitting lasers. We believe that research on 2D noncarbon materials-based SAs will continue to grow and provide ultrafast fiber lasers for various applications. For example, besides saturable absorption, 2D materials also exhibit a large nonlinear refractive index. Thus, they can be applied to nonlinear optical processing devices, such as phase shifter and wavelength convertors[575–586]. We believe that this area has not been fully explored yet, so there will be more room for new research opportunities.

We expect to see fast development in 2D materials-based nonlinear optical devices in future decades. As one of the most important fields, 2D materials will improve our understanding and impact human society through brand new technologies in the future.

This work was supported by the Program for Equipment Pre-research Field Funds (No. 6140414040116CB01012), the National Natural Science Foundation of China (Nos. 61575051 and 11704086), and the 111 project of the Harbin Engineering University (No. B13015).

REFERENCES

1. U. Keller, Nature **424**, 831 (2003).
2. B. Oktem, C. Scedil, K. Ulgudur, and F. O. Ilday, Nat. Photon. **4**, 307 (2010).
3. M. E. Fermann and I. Hartl, Nat. Photon. **7**, 868 (2013).
4. L. G. Wright, D. N. Christodoulides, and F. W. Wise, Science **358**, 94 (2017).
5. A. K. Geim and K. S. Novoselov, Nat. Mater. **6**, 183 (2007).
6. K. J. Koski and Y. Cui, ACS Nano **7**, 3739 (2013).
7. H. Zhang, ACS Nano **9**, 9451 (2015).
8. H. Zhang, C. Liu, X. Qi, X. Dai, Z. Fang, and S. Zhang, Nat. Phys. **5**, 438 (2009).
9. Y. Xia, D. Qian, D. Hsieh, L. Wray, A. Pal, H. Lin, A. Bansil, D. Grauer, Y. S. Hor, R. J. Cava, and M. Z. Hasan, Nat. Phys. **5**, 398 (2009).
10. Y. Chen, J. G. Analytis, J. Chu, Z. Liu, S. Mo, X. L. Qi, H. J. Zhang, D. H. Lu, X. Dai, Z. Fang, S. C. Zhang, I. R. Fisher, Z. Hussain, and Z. X. Shen, Science **325**, 178 (2009).
11. Y. Zhang, K. He, C. Chang, C. Song, L. Wang, X. Chen, J. F. Jia, Z. Fang, X. Dai, W. Y. Shan, S. Q. Shen, Q. Niu, X. L. Qi, S. C. Zhang, X. C. Ma, and Q. Xue, Nat. Phys. **6**, 584 (2010).
12. J. Moore, Nature **464**, 194 (2010).
13. M. Z. Hasan and C. L. Kane, Rev. Mod. Phys. **82**, 3045 (2010).
14. X. L. Qi and S. C. Zhang, Rev. Mod. Phys. **83**, 1057 (2011).

15. Y. Ando, J. Phys. Soc. Jpn. **82**, 102001 (2013).
16. C. Tan, Z. Lai, and H. Zhang, Adv. Mater. **29**, 1701392 (2017).
17. A. Molle, J. Goldberger, M. Houssa, Y. Xu, S. C. Zhang, and D. Akinwande, Nat. Mater. **16**, 163 (2017).
18. O. V. Yazyev and Y. P. Chen, Nat. Nanotechnol. **9**, 755 (2014).
19. A. Gupta, T. Sakthivel, and S. Seal, Prog. Mater. Sci. **73**, 44 (2015).
20. G. R. Bhimanapati, Z. Lin, V. Meunier, Y. Jung, J. Cha, S. Das, D. Xiao, Y. Son, M. S. Strano, V. R. Cooper, L. Liang, S. G. Louie, E. Ringe, W. Zhou, S. S. Kim, R. R. Naik, B. G. Sumpter, H. Terrones, F. Xia, Y. Wang, J. Zhu, D. Akinwande, N. Alem, J. A. Schuller, R. E. Schaak, M. Terrones, and J. A. Robinson, ACS Nano **9**, 11509 (2015).
21. M. Xu, T. Liang, M. Shi, and H. Chen, Chem. Rev. **113**, 3766 (2013).
22. X. Kong, Q. Liu, C. Zhang, Z. Peng, and Q. Chen, Chem. Soc. Rev. **46**, 2127 (2017).
23. C. Tan, X. Cao, X. J. Wu, Q. He, J. Yang, X. Zhang, J. Chen, W. Zhao, S. Han, G. H. Nam, M. Sindoro, and M. Sindoro, Chem. Rev. **117**, 6225 (2017).
24. F. Bonaccorso, Z. Sun, T. Hasan, and A. C. Ferrari, Nat. Photon. **4**, 611 (2010).
25. H. Chang and H. Wu, Adv. Funct. Mater. **23**, 1984 (2013).
26. F. Xia, H. Wang, D. Xiao, M. Dubey, and A. Ramasubramaniam, Nat. Photon. **8**, 899 (2014).
27. F. Bonaccorso and Z. Sun, Opt. Mater. Express **4**, 63 (2014).
28. A. C. Ferrari, F. Bonaccorso, V. Fal'ko, K. S. Novoselov, S. Roche, P. Bøggild, S. Borini, F. H. L. Koppens, V. Palermo, N. Pugno, J. A. Garrido, R. Sordan, A. Bianco, L. Ballerini, M. Prato, E. Lidorikis, J. Kivioja, C. Marinelli, T. Ryhänen, A. Morpurgo, J. N. Coleman, V. Nicolosi, L. Colombo, A. Fert, M. Garcia-Hernandez, A. Bachtold, G. F. Schneider, F. Guinea, C. Dekker, M. Barbone, Z. Sun, C. Galiotis, A. N. Grigorenko, G. Konstantatos, A. Kis, M. Katsnelson, L. Vandersypen, A. Loiseau, V. Morandi, D. Neumaier, E. Treoss, V. Pellegrini, M. Polini, A. Tredicucci, G. M. Williams, B. H. Hong, J.-H. Ahn, J. M. Kim, H. Zirath, B. J. van Wees, H. van der Zant, L. Occhipinti, A. Di Matteo, I. A. Kinloch, T. Seyller, E. Quesnel, X. Feng, K. Teo, N. Rupesinghe, P. Hakonen, S. R. T. Neil, Q. Tannock, T. Löfwanderaq, and J. Kinaretba, Nanoscale **7**, 4598 (2015).
29. J. Wang, X. Zhang, S. Zhang, P. Zhao, and L. Zhang, Chin. J. Laser. **44**, 0703004 (2017).
30. Z. Ma, R. Wei, Z. Hu, and J. Qiu, Chin. J. Laser. **44**, 0703002 (2017).
31. Q. Guo, X. Liu, and J. Qiu, Chin. J. Laser. **44**, 0703005 (2017).
32. T. Low, A. Chaves, J. D. Caldwell, A. Kumar, N. X. Fang, P. Avouris, T. F. Heinz, F. Guinea, L. M. Moreno, and F. H. Koppens, Nat. Mater. **16**, 182 (2016).
33. Z. Sun, T. Hasan, and A. C. Ferrari, Phys. E **44**, 1082 (2012).
34. A. Martinez and Z. Sun, Nat. Photon. **7**, 842 (2013).
35. S. Yamashita, A. Martinez, and B. Xu, Opt. Fiber Technol. **20**, 702 (2014).
36. R. I. Woodward, R. C. T. Howe, G. Hu, F. Torrisi, M. Zhang, T. Hasan, and E. J. R. Kelleher, Photon. Res. **3**, A30 (2015).
37. R. I. Woodward and E. J. Kelleher, Appl. Sci. **5**, 1440 (2015).
38. G. Sobon, Photon. Res. **3**, A56 (2015).
39. Z. Sun, A. Martinez, and F. Wang, Nat. Photon. **10**, 227 (2016).
40. S. Yu, X. Wu, Y. Wang, X. Guo, and L. Tong, Adv. Mater. **29**, 1606128 (2017).
41. X. Liu, Q. Guo, and J. Qiu, Adv. Mater. **29**, 1605886 (2017).
42. K. Wu, B. Chen, X. Zhang, S. Zhang, C. Guo, C. Li, P. Xiao, J. Wang, L. Zhou, W. Zou, and J. Chen, Opt. Commun. **466**, 214 (2017).
43. C. Wei, H. Shi, H. Luo, J. Xie, B. Zhai, F. Yuan, and Y. Liu, Chin. J. Laser. **44**, 0703009 (2017).
44. W. Tian, W. Yu, J. Shi, and Y. Wang, Material **10**, 814 (2017).
45. S. Dhanabalan, J. Ponraj, Z. Guo, S. Li, Q. Bao, and H. Zhang, Adv. Sci. **4**, 1600305 (2017).
46. V. Nicolosi, M. Chhowalla, M. G. Kanatzidis, M. S. Strano, and J. N. Coleman, Science **340**, 1226419 (2013).
47. F. Bernard, H. Zhang, S. P. Gorza, and P. Emplit, *Nonlinear Photonics*, OSA Technical Digest (Optical Society of America, 2012), paper NTh1A.5.
48. S. Lu, C. Zhao, Y. Zou, S. Chen, Y. Chen, Y. Li, H. Zhang, S. Wen, and D. Tang, Opt. Express **21**, 2072 (2013).
49. S. Chen, C. Zhao, Y. Li, H. Huang, S. Lu, H. Zhang, and S. Wen, Opt. Mater. Express **4**, 587 (2014).
50. B. Shi, L. Miao, Q. Wang, J. Du, P. Tang, J. Liu, C. Zhao, and S. Wen, Appl. Phys. Lett. **107**, 151101 (2015).
51. H. Zhang, X. He, W. Lin, R. Wei, F. Zhang, X. Du, G. Dong, and J. Qiu, Opt. Express **23**, 13376 (2015).
52. Y. Wang, H. Mu, X. Li, J. Yuan, J. Chen, S. Xiao, Q. Bao, Y. Gao, and J. He, Appl. Phys. Lett. **108**, 221901 (2016).
53. L. Miao, J. Yi, Q. Wang, D. Feng, H. He, S. Lu, C. Zhao, H. Zhang, and S. Wen, Opt. Mater. Express **6**, 2244 (2016).
54. X. Li, R. Liu, H. Xie, Y. Zhang, B. Lyu, P. Wang, J. Wang, Q. Fan, Y. Ma, S. Tao, S. Xiao, X. Yu, Y. Gao, and J. He, Opt. Express **25**, 18346 (2017).
55. K. Wang, Y. Feng, C. Chang, J. Zhan, C. Wang, Q. Zhao, J. N. Coleman, L. Zhang, W. J. Blau, and J. Wang, Nanoscale **6**, 10530 (2014).
56. K. G. Zhou, M. Zhao, M. J. Chang, Q. Wang, X. Z. Wu, Y. Song, and H. L. Zhang, Small **11**, 694 (2015).
57. G. Wang, S. Zhang, X. Zhang, L. Zhang, Y. Cheng, D. Fox, H. Zhang, J. N. Coleman, W. J. Blau, and J. Wang, Photon. Res. **3**, A51 (2015).
58. A. G. Čabo, J. A. Miwa, S. S. Grønborg, J. M. Riley, J. C. Johannsen, C. Cacho, O. Alexander, R. T. Chapman, E. Springate, M. Grioni, J. V. Lauritsen, P. D. C. King, P. Hofmann, and S. Ulstrup, Nano Lett. **15**, 5883 (2015).
59. L. Liu, K. Xu, X. Wan, J. Xu, C. Y. Wong, and H. K. Tsang, Photon. Res. **3**, 206 (2015).
60. Y. Jiang, L. Miao, G. Jiang, Y. Chen, X. Qi, X. F. Jiang, H. Zhang, and S. Wen, Sci. Rep. **5**, 16372 (2015).
61. S. Bikorimana, P. Lama, A. Walser, R. Dorsinville, S. Anghel, A. Mitioglu, A. Micu, and L. Kulyuk, Opt. Express **24**, 20685 (2016).
62. R. Wei, X. Tian, Z. Hu, H. Zhang, T. Qiao, X. He, Q. Chen, Z. Chen, and J. Qiu, Opt. Express **24**, 25337 (2016).
63. J. Sun, Y. J. Gu, D. Y. Lei, S. P. Lau, W. T. Wong, K. Y. Wong, and H. L. W. Chan, ACS Photon. **3**, 2434 (2016).
64. X. Fan, Y. Jiang, X. Zhuang, H. Liu, T. Xu, W. Zheng, P. Fan, H. Li, X. Wu, X. Zhu, Q. Zhang, H. Zhou, W. Hu, X. Wang, L. Sun, X. Duan, and A. Pan, ACS Nano **11**, 4892 (2017).
65. P. Steinleitner, P. Merkl, P. Nagler, J. Mornhinweg, C. Schüller, T. Korn, A. Chernikov, and R. Huber, Nano Lett. **17**, 1455 (2017).
66. S. B. Lu, L. L. Miao, Z. N. Guo, X. Qi, C. J. Zhao, H. Zhang, S. C. Wen, D. Y. Tang, and D. Y. Fan, Opt. Express **23**, 11183 (2015).
67. Z. Guo, H. Zhang, S. Lu, Z. Wang, S. Tang, J. Shao, Z. Sun, H. Xie, H. Wang, X. F. Yu, and P. K. Chu, Adv. Funct. Mater. **25**, 6996 (2015).
68. J. Zhang, X. Yu, W. Han, B. Lv, X. Li, S. Xiao, Y. Gao, and J. He, Opt. Lett. **41**, 1704 (2016).
69. K. Wang, B. M. Szydłowska, G. Wang, X. Zhang, J. J. Wang, J. J. Magan, L. Zhang, J. N. Coleman, J. Wang, and W. J. Blau, ACS Nano **10**, 6923 (2016).
70. R. Chen, Y. Tang, X. Zheng, and T. Jiang, Appl. Opt. **55**, 10307 (2016).
71. S. W. Kim, H. Jung, H. J. Kim, J. H. Choi, S. H. Wei, and J. H. Cho, Phys. Rev. B **96**, 075416 (2017).

72. S. Tang, Z. He, G. Liang, S. Chen, Y. Ge, D. K. Sang, J. X. Lu, and H. Zhang, Opt. Commun. **406**, 244 (2018).
73. X. Zheng, Y. Zhang, R. Chen, Z. Xu, and T. Jiang, Opt. Express **23**, 15616 (2015).
74. X. Zheng, R. Chen, G. Shi, J. Zhang, Z. Xu, and T. Jiang, Opt. Lett. **40**, 3480 (2015).
75. D. Liu, B. Gu, B. Ren, C. Lu, J. He, Q. Zhan, and Y. Cui, J. Appl. Phys. **119**, 073103 (2016).
76. K. Wang, J. Wang, J. Fan, M. Lotya, A. O'Neill, D. Fox, Y. Feng, X. Zhang, B. Jiang, Q. Zhao, H. Zhang, J. N. Coleman, L. Zhang, and W. J. Blau, ACS Nano **7**, 9260 (2013).
77. X. Fu, J. Qian, X. Qiao, P. Tan, and Z. Peng, Opt. Lett. **39**, 6450 (2014).
78. S. Wang, H. Yu, H. Zhang, A. Wang, M. Zhao, Y. Chen, L. Mei, and J. Wang, Adv. Mater. **26**, 3538 (2014).
79. Q. Ouyang, H. Yu, K. Zhang, and Y. Chen, J. Mater. Chem. C **2**, 6319 (2014).
80. Y. Wang, G. Huang, H. Mu, S. Lin, J. Chen, S. Xiao, Q. Bao, and J. He, Appl. Phys. Lett. **107**, 091905 (2015).
81. S. Zhang, N. Dong, N. McEvoy, M. O'Brien, S. Winters, N. C. Berner, C. Yim, Y. Li, X. Zhang, Z. Chen, L. Zhang, G. S. Duesberg, and J. Wang, ACS Nano **9**, 7142 (2015).
82. N. Dong, Y. Li, S. Zhang, N. McEvoy, X. Zhang, Y. Cui, L. Zhang, G. S. Duesberg, and J. Wang, Opt. Lett. **41**, 3936 (2016).
83. F. Zhou and W. Ji, Opt. Lett. **42**, 3113 (2017).
84. R. I. Woodward, R. T. Murray, C. F. Phelan, R. E. P. de Oliveira, T. H. Runcorn, E. J. R. Kelleher, S. Li, E. C. de Oliveira, G. J. M. Fechine, G. Eda, and C. J. S. De Matos, 2D Mater. **4**, 011006 (2016).
85. X. Yin, Z. Ye, D. A. Chenet, Y. Ye, K. O'Brien, J. C. Hone, and X. Zhang, Science **344**, 488 (2014).
86. M. Trushin, E. J. Kelleher, and T. Hasan, Phys. Rev. B **94**, 155301 (2016).
87. R. Wang, H. C. Chien, J. Kumar, N. Kumar, H. Y. Chiu, and H. Zhao, ACS Appl. Mater. Interf. **6**, 314 (2013).
88. M. Weismann and N. C. Panoiu, Phys. Rev. B **94**, 035435 (2016).
89. H. Y. Wu, Y. Yen, and C. H. Liu, Appl. Phys. Lett. **109**, 261902 (2016).
90. N. Youngblood, R. Peng, A. Nemilentsau, T. Low, and M. Li, ACS Photon. **4**, 8 (2016).
91. T. Jakubczyk, V. Delmonte, M. Koperski, K. Nogajewski, C. Faugeras, W. Langbein, M. Potemski, and J. Kasprzak, Nano Lett. **16**, 5333 (2016).
92. Q. Bao, H. Zhang, Y. Wang, Z. Ni, Y. Yan, Z. Shen, K. P. Loh, and D. Tang, Adv. Funct. Mater. **19**, 3077 (2009).
93. H. Zhang, Q. Bao, D. Tang, L. Zhao, and K. Loh, Appl. Phys. Lett. **95**, 141103 (2009).
94. H. Zhang, D. Tang, L. M. Zhao, Q. Bao, and K. P. Loh, Opt. Express **17**, 17630 (2009).
95. Z. Sun, T. Hasan, F. Torrisi, D. Popa, G. Privitera, F. Wang, F. Bonaccorso, D. M. Basko, and A. C. Ferrari, ACS Nano **4**, 803 (2010).
96. Q. Bao, H. Zhang, J. Yang, S. Wang, D. Tang, R. Jose, S. Ramakrishna, C. T. Lim, and K. P. Loh, Adv. Funct. Mater. **20**, 782 (2010).
97. Y. W. Song, S. Y. Jang, W. S. Han, and M. K. Bae, Appl. Phys. Lett. **96**, 051122 (2010).
98. D. Popa, Z. Sun, F. Torrisi, T. Hasan, F. Wang, and A. C. Ferrari, Appl. Phys. Lett. **97**, 203106 (2010).
99. Y. M. Chang, H. Kim, J. H. Lee, and Y. W. Song, Appl. Phys. Lett. **97**, 211102 (2010).
100. Z. Sun, D. Popa, T. Hasan, F. Torrisi, F. Wang, E. J. Kelleher, J. C. Travers, V. Nicolosi, and A. C. Ferrari, Nano Res. **3**, 653 (2010).
101. A. Martinez, K. Fuse, B. Xu, and S. Yamashita, Opt. Express **18**, 23054 (2010).
102. H. Kim, J. Cho, S. Y. Jang, and Y. W. Song, Appl. Phys. Lett. **98**, 021104 (2011).
103. A. Martinez, K. Fuse, and S. Yamashita, Appl. Phys. Lett. **99**, 121107 (2011).
104. B. V. Cunning, C. L. Brown, and D. Kielpinski, Appl. Phys. Lett. **99**, 261109 (2011).
105. Z. Liu, X. He, and D. N. Wang, Opt. Lett. **36**, 3024 (2011).
106. Q. Bao, H. Zhang, Z. Ni, Y. Wang, L. Polavarapu, Z. Shen, Q. H. Xu, D. Tang, and K. P. Loh, Nano Res. **4**, 297 (2011).
107. G. Sobon, J. Sotor, and K. M. Abramski, Appl. Phys. Lett. **100**, 161109 (2012).
108. A. Martinez and S. Yamashita, Appl. Phys. Lett. **101**, 041118 (2012).
109. J. Sotor, G. Sobon, and K. M. Abramski, Opt. Lett. **37**, 2166 (2012).
110. X. He, Z. Liu, and D. N. Wang, Opt. Lett. **37**, 2394 (2012).
111. P. L. Huang, S. Lin, C. Yeh, H. Kuo, S. Huang, G. Lin, L. Li, C. Su, and W. Cheng, Opt. Express **20**, 2460 (2012).
112. S. Y. Choi, D. K. Cho, Y. Song, K. Oh, K. Kim, F. Rotermund, and D. Yeom, Opt. Express **20**, 5652 (2012).
113. G. Sobon, J. Sotor, J. Jagiello, R. Kozinski, M. Zdrojek, M. Holdynski, P. Paletko, J. Boguslawski, L. Lipinska, and K. M. Abramski, Opt. Express **20**, 19463 (2012).
114. J. Xu, J. Liu, S. Wu, Q. Yang, and P. Wang, Opt. Express **20**, 15474 (2012).
115. G. Sobon, J. Sotor, I. Pasternak, K. Grodecki, P. Paletko, W. Strupinski, Z. Jankiewicz, and K. M. Abramski, J. Lightwave Technol. **30**, 2770 (2012).
116. X. He, Z. Liu, D. N. Wang, M. Yang, C. Liao, and X. Zhao, J. Lightwave Technol. **30**, 984 (2012).
117. C. E. Castellani, E. J. Kelleher, Z. Luo, K. Wu, C. Ouyang, P. P. Shum, Z. Shen, S. V. Popov, and J. R. Taylor, Laser Phys. Lett. **9**, 223 (2012).
118. Y. Meng, S. Zhang, X. Li, H. F. Li, J. Du, and Y. Hao, Laser Phys. Lett. **9**, 537 (2012).
119. G. Sobon, J. Sotor, and K. M. Abramski, Laser Phys. Lett. **9**, 581 (2012).
120. J. Wang, Z. Luo, M. Zhou, C. Ye, H. Fu, Z. Cai, H. Cheng, H. Xu, and W. Qi, IEEE Photon. J. **4**, 1295 (2012).
121. L. Zhang, G. Wang, J. Hu, J. Wang, J. Fan, J. Wang, and Y. Feng, IEEE Photon. J. **4**, 1809 (2012).
122. J. Sotor, G. Sobon, and K. M. Abramski, Opto-Electron. Rev. **20**, 362 (2012).
123. Y. Lin, C. C. Yang, J. Liou, C. Yu, and G. Lin, Opt. Express **21**, 16763 (2013).
124. J. H. Lee, J. Koo, P. Debnat, Y. Song, and J. H. Lee, Laser Phys. Lett. **10**, 035103 (2013).
125. Y. F. Song, L. Li, D. Y. Tang, and D. Y. Shen, Laser Phys. Lett. **10**, 125103 (2013).
126. G. Sobon, J. Sotor, I. Pasternak, W. Strupinski, K. Krzempek, P. Kaczmarek, and K. M. Abramski, Laser Phys. Lett. **10**, 035104 (2013).
127. P. Zhu, Z. Lin, Q. Ning, Z. Cai, X. Xing, J. Liu, W. C. Chen, Z. C. Luo, A. P. Luo, and W. Xu, Laser Phys. Lett. **10**, 105107 (2013).
128. H. Ahmad, F. D. Muhammad, M. Z. Zulkifli, and S. W. Harun, IEEE Photon. J. **5**, 1501709 (2013).
129. Z. Wang, S. E. Zhu, Y. Chen, M. Wu, C. Zhao, H. Zhang, G. Janssen, and S. Wen, Opt. Commun. **300**, 17 (2013).
130. J. Zhao, S. Ruan, P. Yan, H. Zhang, Y. Yu, H. Wei, and J. Luo, Opt. Eng. **52**, 106105 (2013).
131. M. C. Paul, G. Sobon, J. Sotor, K. M. Abramski, J. Jagiello, R. Kozinski, L. Lipinska, and M. Pal, Laser Phys. **23**, 035110 (2013).
132. G. Sobon, J. Sotor, I. Pasternak, K. Krzempek, W. Strupinski, and K. M. Abramski, Laser Phys. **23**, 125101 (2013).

133. Q. W. Sheng, M. Feng, W. Xin, H. Guo, T. Y. Han, Y. G. Li, Y. G. Liu, F. Gao, F. Song, Z. B. Liu, and J. G. Tian, Appl. Phys. Lett. **105**, 041901 (2014).
134. I. Baylam, S. Özharar, N. Kakenov, C. Kocabaş, and A. Sennaroğlu, Opt. Lett. **39**, 5180 (2014).
135. Y. Yang, M. Loeblein, S. H. Tsang, K. K. Chow, and E. H. T. Teo, Opt. Express **22**, 31458 (2014).
136. B. Fu, Y. Hua, X. Xiao, H. Zhu, Z. Sun, and C. Yang, IEEE J. Sel. Top. Quantum Electron. **20**, 411 (2014).
137. H. Ahmad, K. Thambiratnam, F. Muhammad, M. Zulkifli, A. Zulkifli, M. Paul, and S. W. Harun, IEEE J. Sel. Top. Quantum Electron. **20**, 1100108 (2014).
138. X. Li, Y. Tang, Z. Yan, Y. Wang, B. Meng, G. Liang, H. Sun, X. Yu, Y. Zhang, X. Cheng, and Q. J. Wang, IEEE J. Sel. Top. Quantum Electron. **20**, 441 (2014).
139. W. Xin, Z. Liu, Q. Sheng, M. Feng, L. Huang, P. Wang, W. Jiang, F. Xing, Y. Liu, and J. Tian, Opt. Express **22**, 10239 (2014).
140. Y. Meng, A. Niang, K. Guesmi, M. Salhi, and F. Sanchez, Opt. Express **22**, 29921 (2014).
141. X. He, D. N. Wang, and Z. Liu, IEEE Photon. Technol. Lett. **26**, 360 (2014).
142. J. Xu, S. Wu, J. Liu, Y. Li, J. Ren, Q. Yang, and P. Wang, IEEE Photon. Technol. Lett. **26**, 346 (2014).
143. T. Chen, C. Liao, D. N. Wang, and Y. Wang, Appl. Opt. **53**, 2828 (2014).
144. H. Xia, H. Li, Z. Wang, Y. Chen, X. Zhang, X. Tang, and Y. Liu, Opt. Commun. **330**, 147 (2014).
145. E. J. Lee, S. Y. Choi, H. Jeong, N. H. Park, W. Yim, M. H. Kim, J. K. Park, S. Son, S. Bae, S. J. Kim, K. Lee, Y. H. Ahn, K. J. Ahn, B. H. Hong, J. Y. Park, F. Rotermund, and D. Yeom, Nat. Commun. **6**, 6851 (2015).
146. D. G. Purdie, D. Popa, V. J. Wittwer, Z. Jiang, G. Bonacchini, F. Torrisi, S. Milana, E. Lidorikis, and A. C. Ferrari, Appl. Phys. Lett. **106**, 253101 (2015).
147. C. Mou, R. Arif, A. S. Lobach, D. V. Khudyakov, N. G. Spitsina, V. A. Kazakov, S. Turitsyn, and A. Rozhin, Appl. Phys. Lett. **106**, 061106 (2015).
148. J. Boguslawski, J. Sotor, G. Sobon, R. Kozinski, K. Librant, M. Aksienionek, L. Lipinska, and K. M. Abramski, Photon. Res. **3**, 119 (2015).
149. J. Park, K. Park, D. Spoor, B. Hall, and Y. Song, Opt. Express **23**, 7940 (2015).
150. K. Wu, X. Li, Y. Wang, Q. J. Wang, P. P. Shum, and J. Chen, Opt. Express **23**, 501 (2015).
151. Y. Qi, H. Liu, H. Cui, Y. Huang, Q. Ning, M. Liu, Z. C. Luo, A. P. Luo, and W. Xu, Opt. Express **23**, 17720 (2015).
152. S. Yu, C. Meng, B. Chen, H. Wang, X. Wu, W. Liu, S. Zhang, Y. Liu, Y. Su, and L. Tong, Opt. Express **23**, 10764 (2015).
153. H. Lee, W. S. Kwon, J. H. Kim, D. Kang, and S. Kim, Opt. Express **23**, 22116 (2015).
154. J. Sotor, I. Pasternak, A. Krajewska, W. Strupinski, and G. Sobon, Opt. Express **23**, 27503 (2015).
155. N. H. Park, H. Jeong, S. Y. Choi, M. H. Kim, F. Rotermund, and D. Yeom, Opt. Express **23**, 19806 (2015).
156. T. Chen, H. Chen, and D. N. Wang, J. Lightwave Technol. **33**, 2332 (2015).
157. J. Deng, H. Chen, B. Lu, M. Yin, D. Li, M. Jiang, and J. Bai, J. Opt. **17**, 025802 (2015).
158. G. X. Liu, D. J. Feng, M. S. Zhang, S. Z. Jiang, and C. Zhang, Opt. Laser Technol. **72**, 70 (2015).
159. X. Li, K. Wu, Z. Sun, B. Meng, Y. G. Wang, Y. Wang, X. Yu, Y. Zhang, P. P. Shum, and Q. J. Wang, Sci. Rep. **6**, 1 (2016).
160. J. D. Zapata, D. Steinberg, L. A. Saito, R. E. De Oliveira, A. M. Cardenas, and E. A. De Souza, Sci. Rep. **6**, 20644 (2016).
161. X. M. Liu, H. R. Yang, Y. Cui, G. W. Chen, Y. Yang, X. Q. Wu, X. K. Yao, D. D. Han, X. X. Han, C. Zeng, J. Guo, W. L. Li, G. Cheng, and L. M. Tong, Sci. Rep. **6**, 26024 (2016).
162. L. Gao, T. Zhu, Y. J. Li, W. Huang, and M. Liu, IEEE Photon. Technol. Lett. **28**, 1245 (2016).
163. P. Mouchel, G. Semaan, A. Niang, M. Salhi, M. Le Flohic, and F. Sanchez, Appl. Phys. Lett. **111**, 031106 (2017).
164. D. Popa, Z. Jiang, G. E. Bonacchini, Z. Zhao, L. Lombardi, F. Torrisi, A. K. Ott, E. Lidorikis, and A. C. Ferrari, Appl. Phys. Lett. **110**, 243102 (2017).
165. T. Chen, Y. Lin, C. Cheng, C. Tsai, Y. Chi, and G. Lin, IEEE J. Sel. Top. Quantum Electron. **23**, 1 (2017).
166. J. Q. Zhao, F. Zhao, Y. Wang, Y. Wang, H. Wang, and Y. Cai, Chin. Opt. Lett. **15**, 101402 (2017).
167. H. G. Rosa, J. A. Castañeda, C. H. B. Cruz, L. A. Padilha, J. C. Gomes, E. A. T. de Souza, and H. L. Fragnito, Opt. Mater. Express **7**, 2528 (2017).
168. H. Xu, X. Wan, Q. Ruan, R. Yang, T. Du, N. Chen, Z. Cai, and Z. Luo, IEEE J. Sel. Top. Quantum Electron. **23**, 1100209 (2018).
169. Z. Luo, M. Zhou, J. Weng, G. Huang, H. Xu, C. Ye, and Z. Cai, Opt. Lett. **35**, 3709 (2010).
170. D. Popa, Z. Sun, T. Hasan, F. Torrisi, F. Wang, and A. C. Ferrari, Appl. Phys. Lett. **98**, 073106 (2011).
171. J. Liu, S. Wu, Q. H. Yang, and P. Wang, Opt. Lett. **36**, 4008 (2011).
172. Z. Luo, M. Zhou, D. Wu, C. Ye, J. Weng, J. Dong, H. Xu, Z. Cai, and L. Chen, J. Lightwave Technol. **29**, 2732 (2011).
173. W. J. Cao, H. Y. Wang, A. P. Luo, Z. C. Luo, and W. C. Xu, Laser Phys. Lett. **9**, 54 (2011).
174. G. Sobon, J. Sotor, J. Jagiello, R. Kozinski, K. Librant, M. Zdrojek, L. Lipinska, and K. M. Abramski, Appl. Phys. Lett. **101**, 241106 (2012).
175. J. Liu, J. Xu, and P. Wang, Opt. Commun. **285**, 5319 (2012).
176. Z. T. Wang, Y. Chen, C. J. Zhao, H. Zhang, and S. C. Wen, IEEE Photon. J. **4**, 869 (2012).
177. H. Ahmad, F. D. Muhammad, M. Z. Zulkifli, and S. W. Harun, IEEE Photon. J. **4**, 2205 (2012).
178. Y. K. Yap, M. Richard, C. H. Pua, S. W. Harun, and H. Ahmad, Chin. Opt. Lett. **10**, 041405 (2012).
179. L. Zhang, J. T. Fan, J. H. Wang, J. M. Hu, M. Lotya, G. Z. Wang, R. H. Li, L. Zhang, W. J. Blau, J. N. Coleman, J. Wang, and Y. Feng, Laser Phys. Lett. **9**, 888 (2012).
180. J. Q. Zhao, Y. G. Wang, P. G. Yan, S. C. Ruan, J. Q. Chen, G. G. Du, Y. Q. Yu, G. L. Zhang, H. F. Wei, J. Luo, and Y. H. Tsang, Chin. Phys. Lett. **29**, 114206 (2012).
181. C. Wei, X. Zhu, F. Wang, Y. Xu, K. Balakrishnan, F. Song, R. A. Norwood, and N. Peyghambarian, Opt. Lett. **38**, 3233 (2013).
182. C. Liu, C. Ye, Z. Luo, H. Cheng, D. Wu, Y. Zheng, Z. Liu, and B. Qu, Opt. Express **21**, 204 (2013).
183. M. Jiang, H. F. Ma, Z. Y. Ren, X. M. Chen, J. Y. Long, M. Qi, D. Y. Shen, Y. S. Wang, and J. T. Bai, Laser Phys. Lett. **10**, 055103 (2013).
184. H. P. Li, H. D. Xia, Z. G. Wang, X. X. Zhang, Y. F. Chen, S. J. Zhang, X. G. Tang, and Y. Liu, Chin. Phys. B **23**, 024209 (2013).
185. B. Lu, H. Chen, M. Jiang, X. Chen, Z. Ren, and J. Bai, Laser Phys. **23**, 045111 (2013).
186. H. Ahmad, M. Z. Zulkifli, F. D. Muhammad, A. Z. Zulkifli, and S. W. Harun, J. Mod. Opt. **60**, 202 (2013).
187. H. Ahmad, F. D. Muhammad, M. Z. Zulkifli, and S. W. Harun, J. Mod. Opt. **60**, 1563 (2013).
188. Y. Tang, X. Yu, X. Li, Z. Yan, and Q. J. Wang, Opt. Lett. **39**, 614 (2014).

189. D. Wu, Z. Luo, F. Xiong, C. Zhang, Y. Huang, S. Chen, W. Cai, Z. Cai, and H. Xu, IEEE Photon. Technol. Lett. **26**, 1474 (2014).
190. H. Ahmad, M. R. K. Soltanian, C. H. Pua, M. Alimadad, and S. W. Harun, Appl. Opt. **53**, 3581 (2014).
191. D. Wu, F. Xiong, C. Zhang, S. Chen, H. Xu, Z. Cai, W. Cai, K. Che, and Z. Luo, Appl. Opt. **53**, 4089 (2014).
192. R. Z. R. R. Rosdin, F. Ahmad, N. M. Ali, S. W. Harun, and H. Arof, Chin. Opt. Lett. **12**, 091404 (2014).
193. A. Ren, M. Feng, F. Song, Y. Ren, S. Yang, Z. Yang, Y. Li, Z. Liu, and J. Tian, Opt. Express **23**, 21490 (2015).
194. J. Gene, N. H. Park, H. Jeong, S. Y. Choi, F. Rotermund, D. I. Yeom, and B. Y. Kim, Opt. Express **24**, 21301 (2016).
195. J. Zhao, Z. Zheng, D. Ouyang, M. Liu, X. Ren, S. Ruan, and W. Xie, IEEE J. Sel. Top. Quantum Electron. **23**, 13 (2017).
196. B. C. Yao, Y. J. Rao, S. W. Huang, Y. Wu, Z. Y. Feng, C. Choi, H. Liu, H. F. Qi, X. F. Duan, G. D. Peng, and C. W. Wong, Opt. Express **25**, 8202 (2017).
197. Z. Luo, Y. Huang, J. Weng, H. Cheng, Z. Lin, B. Xu, Z. Cai, and H. Xu, Opt. Express **21**, 29516 (2013).
198. Y. Chen, C. Zhao, H. Huang, S. Chen, P. Tang, Z. Wang, S. Lu, H. Zhang, S. Wen, and D. Tang, J. Lightwave Technol. **31**, 2857 (2013).
199. Z. Luo, C. Liu, Y. Huang, D. Wu, J. Wu, H. Xu, Z. Cai, Z. Lin, L. Sun, and J. Weng, IEEE J. Sel. Top. Quantum Electron. **20**, 1 (2014).
200. L. Sun, Z. Lin, J. Peng, J. Weng, Y. Huang, and Z. Luo, Sci. Rep. **4**, 4794 (2014).
201. Z. Yu, Y. Song, J. Tian, Z. Dou, H. Guoyu, K. Li, H. Li, and X. Zhang, Opt. Express **22**, 11508 (2014).
202. H. Y. Lin, W. S. Li, J. L. Lan, X. F. Guan, H. Y. Xu, and Z. P. Cai, Appl. Opt. **56**, 802 (2017).
203. L. Gao, W. Huang, J. D. Zhang, T. Zhu, H. Zhang, C. J. Zhao, W. Zhang, and H. Zhang, Appl. Opt. **53**, 5117 (2014).
204. Y. Chen, C. Zhao, S. Chen, J. Du, P. Tang, G. Jiang, H. Zhang, S. Wen, and D. Tang, IEEE J. Sel. Top. Quantum Electron. **20**, 315 (2014).
205. J. Yu, D. Lin, G. Jiang, and C. Zhao, Chin. J. Laser. **44**, 0703014 (2017).
206. J. Koo, J. Lee, C. Chi, and J. H. Lee, J. Opt. Soc. Am. B **31**, 2157 (2014).
207. J. Koo, J. Lee, and J. H. Lee, J. Lightwave Technol. **35**, 2175 (2017).
208. K. Yan, J. Lin, Y. Zhou, C. Gu, L. Xu, A. Wang, P. Yao, and Q. Zhan, Appl. Opt. **55**, 3026 (2016).
209. J. Li, H. Luo, L. Wang, C. Zhao, H. Zhang, H. Li, and Y. Liu, Opt. Lett. **40**, 3659 (2015).
210. P. Yan, H. Chen, K. Li, C. Guo, S. Ruan, J. Wang, J. Ding, X. Zhang, and T. Guo, IEEE Photon. J. **8**, 1 (2016).
211. J. Bogusławski, G. Soboń, K. Tarnowski, R. Zybała, K. Mars, A. Mikuła, K. M. Abramski, and J. Sotor, Opt. Eng. **55**, 081316 (2016).
212. Y. Huang, Z. Luo, Y. Li, M. Zhong, B. Xu, K. Che, H. Xu, Z. Cai, J. Peng, and J. Weng, Opt. Express **22**, 25258 (2014).
213. Z. Luo, Y. Huang, M. Zhong, Y. Li, J. Wu, B. Xu, H. Xu, Z. Cai, J. Peng, and J. Weng, J. Lightwave Technol. **32**, 4679 (2014).
214. R. I. Woodward, E. J. R. Kelleher, R. C. T. Howe, G. Hu, F. Torrisi, T. Hasan, S. V. Popov, and J. R. Taylor, Opt. Express **22**, 31113 (2014).
215. R. Khazaeinezhad, S. H. Kassani, T. Nazari, H. Jeong, J. Kim, K. Choi, J. U. Lee, J. H. Kim, H. Cheong, D. Yeom, and K. Oh, Opt. Commun. **335**, 224 (2015).
216. J. Ren, S. Wang, Z. Cheng, H. Yu, H. Zhang, Y. Chen, L. Mei, and P. Wang, Opt. Express **23**, 5607 (2015).
217. J. H. Chen, G. Q. Deng, S. C. Yan, C. Li, K. Xi, F. Xu, and Y. Q. Lu, Opt. Lett. **40**, 3576 (2015).
218. H. Li, H. Xia, C. Lan, C. Li, X. Zhang, J. Li, and Y. Liu, IEEE Photon. Technol. Lett. **27**, 69 (2015).
219. H. Xia, H. Li, C. Lan, C. Li, J. Du, S. Zhang, and Y. Liu, Photon. Res. **3**, A92 (2015).
220. R. Wei, H. Zhang, Z. Hu, T. Qiao, X. He, Q. Guo, X. Tian, Z. Chen, and J. Qiu, Nanotechnology **27**, 305203 (2016).
221. J. Lin, Y. Hu, C. Chen, C. Gu, and L. Xu, Opt. Express **23**, 29059 (2015).
222. M. Zhang, G. Hu, G. Hu, R. C. T. Howe, L. Chen, Z. Zheng, and T. Hasan, Sci. Rep. **5**, 17482 (2015).
223. J. Lin, K. Yan, Y. Zhou, L. X. Xu, C. Gu, and Q. W. Zhan, Appl. Phys. Lett. **107**, 191108 (2015).
224. B. Chen, X. Zhang, C. Guo, K. Wu, J. Chen, and J. Wang, Opt. Eng. **55**, 081306 (2016).
225. Z. Luo, D. Wu, B. Xu, H. Xu, Z. Cai, J. Peng, J. Weng, S. Xu, C. Zhu, F. Wang, Z. Sun, and H. Zhang, Nanoscale **8**, 1066 (2016).
226. W. Li, J. Peng, Y. Zhong, D. Wu, H. Lin, Y. Cheng, Z. Luo, J. Weng, H. Xu, and Z. Cai, Opt. Mater. Express **6**, 2031 (2016).
227. S. H. Kassani, R. Khazaeinezhad, H. Jeong, T. Nazari, D. I. Yeom, and K. Oh, Opt. Mater. Express **5**, 373 (2015).
228. C. Yang, M. Liu, W. Yu, Y. Zhang, and W. Liu, Chin. J. Laser. **44**, 0703015 (2017).
229. H. Chen, Y. Chen, J. Yin, X. Zhang, T. Guo, and P. Yan, Opt. Express **24**, 16287 (2016).
230. L. Li, Y. Wang, Z. F. Wang, X. Wang, and G. Yang, Opt. Commun. **406**, 80 (2018).
231. R. I. Woodward, R. C. T. Howe, T. H. Runcorn, G. Hu, F. Torrisi, E. J. R. Kelleher, and T. Hasan, Opt. Express **23**, 20051 (2015).
232. B. Chen, X. Zhang, K. Wu, H. Wang, J. Wang, and J. Chen, Opt. Express **23**, 26723 (2015).
233. C. Guo, B. Chen, H. Wang, K. Wu, and J. Chen, Chin. J. Laser. **44**, 0703018 (2017).
234. K. Niu, Q. Chen, R. Sun, B. Man, and H. Zhang, Opt. Mater. Express **7**, 3934 (2017).
235. W. Liu, M. Liu, M. Lei, S. Fang, and Z. Wei, IEEE J. Sel. Top. Quantum Electron. **24**, 1 (2018).
236. Y. Chen, G. Jiang, S. Chen, Z. Guo, X. Yu, C. Zhao, H. Zhang, Q. Bao, S. Wen, D. Tang, and D. Fan, Opt. Express **23**, 12823 (2015).
237. H. Mu, S. Lin, Z. Wang, S. Xiao, P. Li, Y. Chen, H. Zhang, H. Bao, S. P. Lau, C. Pan, D. Fan, and Q. Bao, Adv. Opt. Mater. **3**, 1447 (2015).
238. H. Yu, X. Zheng, K. Yin, and T. Jiang, Opt. Mater. Express **6**, 603 (2016).
239. D. Wu, Z. Cai, Y. Zhong, J. Peng, Y. Cheng, J. Weng, Z. Luo, and H. Xu, IEEE J. Sel. Top. Quantum Electron. **23**, 1 (2017).
240. R. Zhao, J. He, X. Su, Y. Wang, X. Sun, H. Nie, B. Zhang, and K. Yang, IEEE J. Sel. Top. Quantum Electron. **24**, 1 (2018).
241. T. Jiang, K. Yin, X. Zheng, H. Yu, and X. A. Cheng, "Black phosphorous as a new broadband saturable absorber for infrared passively *Q*-switched fiber lasers," arXiv:1504.07341 (2015).
242. K. X. Huang, B. L. Lu, D. Li, X. Y. Qi, H. W. Chen, N. Wang, Z. Wen, and J. T. Bai, Appl. Opt. **56**, 6427 (2017).
243. Z. Wang, R. Zhao, J. He, B. Zhang, J. Ning, Y. Wang, X. Su, J. Hou, F. Lou, K. Yang, Y. Fan, J. Bian, and Y. Fan, Opt. Express **24**, 1598 (2016).
244. Z. Qin, G. Xie, H. Zhang, C. Zhao, P. Yuan, S. Wen, and L. Qian, Opt. Express **23**, 24713 (2015).
245. C. Zhao, Y. Zou, Y. Chen, Z. Wang, S. Lu, H. Zhang, S. Wen, and D. Tang, Opt. Express **20**, 27888 (2012).
246. H. Liu, X. W. Zheng, M. Liu, N. Zhao, A. P. Luo, Z. C. Luo, W. Xu, H. Zhang, C. J. Zhao, and S. C. Wen, Opt. Express **22**, 6868 (2014).
247. H. Xu, X. Wan, Q. Ruan, R. Yang, T. Du, N. Chen, Z. Cai, and Z. Luo, IEEE J. Sel. Top. Quantum Electron. **24**, 1 (2018).

248. L. Gao, T. Zhu, W. Huang, and Z. Luo, IEEE Photon. J. **7**, 1 (2015).
249. Y. Xu, H. Xie, G. Jiang, L. Miao, K. Wang, S. Tang, S. Yu, H. Zhang, and Q. Bao, Opt. Commun. **395**, 55 (2017).
250. C. Zhao, H. Zhang, X. Qi, Y. Chen, Z. Wang, S. Wen, and D. Tang, Appl. Phys. Lett. **101**, 211106 (2012).
251. Z. C. Luo, M. Liu, H. Liu, X. W. Zheng, A. P. Luo, C. J. Zhao, H. Zhang, S. C. Wen, and W. C. Xu, Opt. Lett. **38**, 5212 (2013).
252. S. Chen, Q. Wang, C. Zhao, Y. Li, H. Zhang, and S. Wen, J. Lightwave Technol. **32**, 3836 (2014).
253. P. Yan, R. Lin, S. Ruan, A. Liu, and H. Chen, Opt. Express **23**, 154 (2015).
254. L. N. Duan, Y. G. Wang, C. W. Xu, L. Li, and Y. S. Wang, IEEE Photon. J. **7**, 1 (2015).
255. J. Lee, J. Koo, Y. M. Jhon, and J. H. Lee, Opt. Express **22**, 6165 (2014).
256. J. Lee, J. Koo, Y. M. Jhon, and J. H. Lee, Opt. Express **23**, 6359 (2015).
257. Y. S. Chen, P. G. Yan, H. Chen, A. J. Liu, and S. C. Ruan, Photonics **2**, 342 (2015).
258. P. Yan, R. Lin, H. Chen, H. Zhang, A. Liu, H. Yang, and S. Ruan, IEEE Photon. Technol. Lett. **27**, 951 (2015).
259. Q. Wang, Y. Chen, G. Jiang, L. Miao, C. Zhao, X. Fu, S. Wen, and H. Zhang, IEEE Photon. J. **7**, 1 (2015).
260. D. Mao, B. Jiang, X. Gan, C. Ma, Y. Chen, C. Zhao, H. Zhang, J. Zheng, and J. Zhao, Photon. Res. **3**, A43 (2015).
261. Y. H. Lin, S. F. Lin, Y. C. Chi, C. L. Wu, C. H. Cheng, W. H. Tseng, J. H. He, C. Wu, C. K. Lee, and G. R. Lin, ACS Photon. **2**, 481 (2015).
262. J. Sotor, G. Sobon, W. Macherzynski, P. Paletko, K. Grodecki, and K. M. Abramski, Opt. Mater. Express **4**, 1 (2014).
263. J. Sotor, G. Sobon, W. Macherzynski, and K. M. Abramski, Laser Phys. Lett. **11**, 055102 (2014).
264. J. Sotor, G. Sobon, K. Grodecki, and K. M. Abramski, Appl. Phys. Lett. **104**, 251112 (2014).
265. J. Bogusławski, G. Soboń, R. Zybała, K. Mars, A. Mikuła, K. M. Abramski, and J. Sotor, Opt. Express **23**, 29014 (2015).
266. M. Kowalczyk, J. Bogusławski, R. Zybała, K. Mars, A. Mikuła, G. Soboń, and J. Sotor, Opt. Mater. Express **6**, 2273 (2016).
267. W. Liu, L. Pang, H. Han, W. Tian, H. Chen, M. Lei, P. Yan, and Z. Wei, Sci. Rep. **6**, 19997 (2016).
268. K. F. Mak, C. Lee, J. Hone, J. Shan, and T. F. Heinz, Phys. Rev. Lett. **105**, 136805 (2010).
269. J. N. Coleman, M. Lotya, A. O. Neill, S. D. Bergin, P. J. King, U. Khan, K. Young, A. Gaucher, S. De, R. J. Smith, I. V. Shvets, S. K. Arora, G. Stanton, H. Y. Kim, K. Lee, G. T. Kim, G. S. Duesberg, T. Hallam, J. J. Boland, J. J. Wang, J. F. Donegan, J. C. Grunlan, G. Moriarty, A. Shmeliov, R. J. Nicholls, J. M. Perkins, E. M. Grieveson, K. Theuwissen, D. W. McComb, P. D. Nellist, and V. Nicolosi, Science **331**, 568 (2011).
270. Q. H. Wang, K. Kalantarzadeh, A. Kis, J. N. Coleman, and M. S. Strano, Nat. Nanotechnol. **7**, 699 (2012).
271. M. Chhowalla, H. S. Shin, G. Eda, L. J. Li, K. P. Loh, and H. Zhang, Nat. Chem. **5**, 263 (2013).
272. S. Butler, S. M. Hollen, L. Cao, Y. Cui, J. A. Gupta, H. R. Gutierrez, T. F. Heinz, S. S. Hong, J. Huang, A. F. Ismach, E. J. Halperin, M. Kuno, V. V. Plashnitsa, R. D. Robinson, R. S. Ruoff, S. Salahuddin, J. Shan, L. Shi, M. G. Spencer, M. Terrones, W. Windl, and J. E. Goldberger, ACS Nano **7**, 2898 (2013).
273. G. Eda and S. A. Maier, ACS Nano **7**, 5660 (2013).
274. Q. Tang and Z. Zhou, Prog. Mater. Sci. **58**, 1244 (2013).
275. K. Zhou and H. Zhang, Small **11**, 3206 (2015).
276. C. Qin, Y. Gao, Z. Qiao, L. Xiao, and S. Jia, Adv. Opt. Mater. **4**, 1429 (2016).
277. J. R. Brent, N. Savjani, and P. O'Brien, Prog. Mater. Sci. **89**, 411 (2017).
278. S. Manzeli, D. Ovchinnikov, D. Pasquier, O. V. Yazyev, and A. Kis, Nat. Rev. Mater. **2**, 17033 (2017).
279. H. Zhang, S. B. Lu, J. Zheng, J. Du, S. C. Wen, D. Y. Tang, and K. P. Loh, Opt. Express **22**, 7249 (2014).
280. H. Xia, H. Li, C. Lan, C. Li, X. Zhang, S. Zhang, and Y. Liu, Opt. Express **22**, 17341 (2014).
281. J. Du, Q. Wang, G. Jiang, C. Xu, C. Zhao, Y. Xiang, Y. Chen, S. Wen, and H. Zhang, Sci. Rep. **4**, 6346 (2014).
282. M. Liu, X. W. Zheng, Y. L. Qi, H. Liu, A. P. Luo, Z. C. Luo, W. C. Xu, C. J. Zhao, and H. Zhang, Opt. Express **22**, 22841 (2014).
283. E. J. Aiub, D. Steinberg, E. Souza, and L. A. Saito, Opt. Express **25**, 10546 (2017).
284. H. Liu, A. P. Luo, F. Z. Wang, R. Tang, M. Liu, Z. C. Luo, W. C. Xu, C. J. Zhao, and H. Zhang, Opt. Lett. **39**, 4591 (2014).
285. K. Wu, X. Zhang, J. Wang, and J. Chen, Opt. Lett. **40**, 1374 (2015).
286. M. Zhang, C. Richard, T. Howe, R. I. Woodward, J. Edmund, R. Kelleher, F. Torrisi, G. Hu, S. V. Popov, J. Taylor, and T. Hasan, Nano Res. **8**, 1522 (2015).
287. Z. C. Luo, F. Z. Wang, H. Liu, M. Liu, R. Tang, A. P. Luo, and W. C. Xu, Opt. Eng. **55**, 081308 (2016).
288. M. Ahmed, A. Latiff, H. Arof, H. Ahmad, and S. W. Harun, IET Optoelectron. **10**, 169 (2016).
289. Z. Jiang, J. Li, H. Chen, J. Wang, W. Zhang, and P. Yan, Opt. Commun. **406**, 44 (2018).
290. K. Wu, X. Zhang, J. Wang, X. Li, and J. Chen, Opt. Express **23**, 11453 (2015).
291. P. Yan, A. Liu, Y. Chen, H. Chen, S. Ruan, C. Guo, S. Chen, I. Li, H. Yang, J. Hu, and G. Cao, Opt. Mater. Express **5**, 479 (2015).
292. R. Khazaeinezhad, S. H. Kassani, H. Jeong, K. J. Park, B. Y. Kim, D. I. Yeom, and K. Oh, IEEE Photon. Technol. Lett. **27**, 1581 (2015).
293. R. Khazaeinezhad, S. H. Kassani, H. Jeong, D. I. Yeom, and K. Oh, J. Lightwave Technol. **33**, 3550 (2015).
294. W. Liu, L. Pang, H. Han, K. Bi, M. Lei, and Z. Wei, Nanoscale **9**, 5806 (2017).
295. W. Liu, L. Pang, H. Han, M. Liu, M. Lei, S. Fang, H. Teng, and Z. Wei, Opt. Express **25**, 2950 (2017).
296. D. Mao, Y. Wang, C. Ma, L. Han, B. Jiang, X. Gan, S. Hua, W. Zhang, T. Mei, and J. Zhao, Sci. Rep. **5**, 12587 (2015).
297. L. Li, Y. Su, Y. Wang, X. Wang, Y. Wang, X. Li, D. Mao, and J. Si, IEEE J. Sel. Top. Quantum Electron. **23**, 44 (2017).
298. P. Yan, A. Liu, Y. Chen, J. Wang, S. Ruan, H. Chen, and J. Ding, Sci. Rep. **5**, 12587 (2015).
299. H. Chen, I. L. Li, S. Ruan, T. Guo, and P. Yan, Opt. Eng. **55**, 081318 (2016).
300. P. Yan, H. Chen, A. Liu, K. Li, S. Ruan, J. Ding, X. Qiu, and T. Guo, IEEE J. Sel. Top. Quantum Electron. **23**, 1 (2017).
301. P. Yan, H. Chen, J. Yin, Z. Xu, J. Li, Z. Jiang, W. Zhang, J. Wang, I. L. Li, Z. Sun, and S. Ruan, Nanoscale **9**, 1871 (2017).
302. M. Liu, W. Liu, L. Pang, H. Teng, S. Fang, and Z. Wei, Opt. Commun. **406**, 72 (2018).
303. J. Yin, J. Li, H. Chen, J. Wang, P. Yan, M. Liu, W. Liu, W. Lu, Z. Xu, W. Zhang, J. Wang, Z. Sun, and S. Ruan, Opt. Express **25**, 30020 (2017).
304. D. Mao, X. Cui, X. Gan, M. Li, W. Zhang, H. Lu, and J. Zhao, IEEE J. Sel. Top. Quantum Electron. **23**, 1 (2018).
305. Z. Luo, Y. Li, M. Zhong, Y. Huang, X. Wan, J. Peng, and J. Weng, Photon. Res. **3**, A79 (2015).
306. J. Koo, J. Park, J. Lee, Y. M. Jhon, and J. H. Lee, Opt. Express **24**, 10575 (2016).
307. H. R. Yang and X. M. Liu, Appl. Phys. Lett. **110**, 171106 (2017).

308. J. Li, Y. Zhao, Q. Chen, K. Niu, R. Sun, and H. Zhang, IEEE Photon. J. **9**, 1 (2017).
309. X. Ling, H. Wang, S. Huang, F. Xia, and M. S. Dresselhaus, PNAS **112**, 4523 (2015).
310. X. Wang and S. Lan, Adv. Opt. Photon. **8**, 618 (2016).
311. M. Batmunkh, M. Baterdene, and J. G. Shapter, Adv. Mater. **28**, 8586 (2016).
312. A. J. Mannix, B. Kiraly, M. C. Hersam, and N. P. Guisinger, Nat. Rev. Chem. **1**, 0014 (2017).
313. Z. C. Luo, M. Liu, Z. N. Guo, X. F. Jiang, A. P. Luo, C. J. Zhao, X. F. Yu, W. C. Xu, and H. Zhang, Opt. Express **23**, 20030 (2015).
314. Y. Chen, S. Chen, J. Liu, Y. Gao, and W. Zhang, Opt. Express **24**, 13316 (2016).
315. D. Li, H. Jussila, L. Karvonen, G. Ye, H. Lipsanen, X. Chen, and Z. Sun, Sci. Rep. **5**, 15899 (2015).
316. J. Sotor, G. Sobon, W. Macherzynski, P. Paletko, and K. M. Abramski, Appl. Phys. Lett. **107**, 051108 (2015).
317. Y. Chen, H. Mu, P. Li, S. Lin, B. N. Shivananju, and Q. Bao, Opt. Eng. **55**, 081317 (2016).
318. Y. Xu, X. F. Jiang, Y. Ge, Z. Guo, Z. Zeng, Q. Xu, H. Zhang, X. Yu, and D. Fan, J. Mater. Chem. C **5**, 3007 (2017).
319. M. Hisyam, M. Rusdi, A. Latiff, and S. Harun, IEEE J. Sel. Top. Quantum Electron. **23**, 39 (2017).
320. D. Mao, M. Li, X. Cui, W. Zhang, H. Lu, K. Song, and J. Zhao, Opt. Commun. **406**, 254 (2018).
321. B. Gao, W. Guo, J. Huo, G. Wu, C. Ma, J. Li, and J. Wang, Opt. Commun. **406**, 192 (2018).
322. H. Zhang, D. Tang, R. J. Knize, L. M. Zhao, Q. Bao, and K. P. Loh, Appl. Phys. Lett. **96**, 111112 (2010).
323. H. Zhang, D. Tang, L. M. Zhao, Q. Bao, K. P. Loh, B. Lin, and S. C. Tjin, Laser Phys. Lett. **7**, 591 (2010).
324. H. Zhang, D. Tang, L. M. Zhao, Q. Bao, and K. P. Loh, Opt. Commun. **283**, 3334 (2010).
325. J. Xu, S. Wu, H. Li, J. Liu, R. Sun, F. Tan, Q. H. Yang, and P. Wang, Opt. Express **20**, 23653 (2012).
326. Y. Cui and X. Liu, Opt. Express **21**, 18969 (2013).
327. X. Li, Y. G. Wang, Y. Wang, Y. Z. Zhang, K. Wu, P. P. Shum, X. Yu, Y. Zhang, and Q. J. Wang, Laser Phys. Lett. **10**, 075108 (2013).
328. S. Y. Choi, H. Jeong, B. H. Hong, F. Rotermund, and D. Yeom, Laser Phys. Lett. **11**, 015101 (2014).
329. L. M. Zhao, D. Y. Tang, H. Zhang, X. Wu, Q. Bao, and K. P. Loh, Opt. Lett. **35**, 3622 (2010).
330. L. Gao, T. Zhu, W. Huang, and J. Zeng, Appl. Opt. **53**, 6452 (2014).
331. Z. Cheng, H. Li, H. Shi, J. Ren, Q. Yang, and P. Wang, Opt. Express **23**, 7000 (2015).
332. Z. Dou, Y. Song, J. Tian, J. Liu, Z. Yu, and X. Fang, Opt. Express **22**, 24055 (2014).
333. Q. Wang, Y. Chen, L. Miao, G. Jiang, S. Chen, J. Liu, X. Fu, C. Zhao, and H. Zhang, Opt. Express **23**, 7681 (2015).
334. J. Lee, J. Koo, and J. H. Lee, Opt. Eng. **55**, 081309 (2016).
335. J. Sotor, G. Sobon, and K. M. Abramski, Opt. Express **22**, 13244 (2014).
336. J. Boguslawski, G. Sobon, R. Zybala, and J. Sotor, Opt. Lett. **40**, 2786 (2015).
337. M. Kowalczyk, J. Bogusławski, R. Zybała, K. Mars, A. Mikuła, G. Soboń, and J. Sotor, Opt. Mater. Express **6**, 2273 (2016).
338. R. Khazaeizhad, S. H. Kassani, H. Jeong, D. I. Yeom, and K. Oh, Opt. Express **22**, 23732 (2014).
339. S. Samikannu and S. Sivaraj, Opt. Eng. **55**, 081311 (2016).
340. L. Li, S. Jiang, Y. Wang, X. Wang, L. Duan, D. Mao, Z. Li, B. Man, and J. Si, Opt. Express **23**, 28698 (2015).
341. D. Mao, S. Zhang, Y. Wang, X. Gan, W. Zhang, T. Mei, Y. G. Wang, Y. Wang, H. Zeng, and J. Zhao, Opt. Express **23**, 27509 (2015).
342. C. Ma, X. Tian, B. Gao, and G. Wu, Opt. Commun. **406**, 177 (2018).
343. B. Guo, Y. Yao, and Y. F. Yang, *In Optoelectronic Devices and Integration* (Optical Society of America, 2015), p. OW2C-4.
344. M. Zhang, E. J. Kelleher, F. Torrisi, Z. Sun, T. Hasan, D. Popa, F. Wang, A. C. Ferrari, S. V. Popov, and J. R. Taylor, Opt. Express **20**, 25077 (2012).
345. M. Jung, J. Koo, P. C. Debnath, Y. Song, and J. H. Lee, Appl. Phys. Express **5**, 112702 (2012).
346. Q. Wang, T. Chen, B. Zhang, M. Li, Y. Lu, and K. P. Chen, Appl. Phys. Lett. **102**, 131117 (2013).
347. G. Sobon, J. Sotor, I. Pasternak, A. Krajewska, W. Strupinski, and K. M. Abramski, Opt. Express **21**, 12797 (2013).
348. B. Fu, L. Gui, X. Li, X. Xiao, H. Zhu, and C. Yang, IEEE Photon. Technol. Lett. **25**, 1447 (2013).
349. D. I. Zen, N. Saidin, S. S. Damanhuri, S. W. Harun, H. Ahmad, M. A. Ismail, K. Dimyati, A. Halder, M. C. Paul, S. Das, M. Pal, and S. K. Bhadra, Appl. Opt. **52**, 1226 (2013).
350. M. Currie, T. J. Anderson, V. D. Wheeler, L. O. Nyakiti, N. Y. Garces, R. L. Myersward, C. R. Eddy, F. J. Kub, D. K. Gaskill, and D. K. Gaskill, Opt. Eng. **52**, 076101 (2013).
351. G. Sobon, J. Sotor, I. Pasternak, A. Krajewska, W. Strupinski, and K. M. Abramski, Opt. Express **23**, 9339 (2015).
352. S. M. Azooz, S. W. Harun, H. Ahmad, A. Halder, M. C. Paul, M. Pal, and S. K. Bhadra, Chin. Phys. Lett. **32**, 014204 (2015).
353. J. Sotor, M. Pawliszewska, G. Sobon, P. Kaczmarek, A. Przewolka, I. Pasternak, J. Cajzl, P. Peterka, P. Honzatko, I. Kasik, W. Strupinski, and K. M. Abramski, Opt. Lett. **41**, 2592 (2016).
354. G. Sobon, J. Sotor, A. Przewolka, I. Pasternak, W. Strupinski, and K. M. Abramski, Opt. Express **24**, 20359 (2016).
355. H. Jeong, S. Y. Choi, M. H. Kim, F. Rotermund, Y. Cha, D. Jeong, S. B. Lee, K. Lee, and D. Yeom, Opt. Express **24**, 14152 (2016).
356. G. Yang, Y. G. Liu, Z. Wang, J. Lou, Z. Wang, and Z. Liu, Laser Phys. Lett. **13**, 065105 (2016).
357. J. Sotor, J. Bogusławski, T. Martynkien, P. Mergo, A. Krajewska, A. Przewłoka, W. Strupinski, and G. Sobon, Opt. Lett. **42**, 1592 (2017).
358. M. Jung, J. Lee, J. Koo, J. Park, Y. W. Song, K. Lee, S. Lee, and J. H. Lee, Opt. Express **22**, 7865 (2014).
359. K. Yin, B. Zhang, L. Li, T. Jiang, X. Zhou, and J. Hou, Photon. Res. **3**, 72 (2015).
360. Z. Tian, K. Wu, L. Kong, N. Yang, Y. Wang, R. Chen, W. Hu, J. Xu, and Y. Tang, Laser Phys. Lett. **12**, 065104 (2015).
361. M. Jung, J. Lee, J. Park, J. Koo, Y. M. Jhon, and J. H. Lee, Opt. Express **23**, 19996 (2015).
362. J. Wang, Z. Jiang, H. Chen, J. Li, J. Yin, J. Wang, T. He, P. Yan, and S. Ruan, Opt. Lett. **42**, 5010 (2017).
363. J. Sotor, G. Sobon, M. Kowalczyk, W. Macherzynski, P. Paletko, and K. M. Abramski, Opt. Lett. **40**, 3885 (2015).
364. M. Pawliszewska, Y. Ge, Z. Li, H. Zhang, and J. Sotor, Opt. Express **25**, 16916 (2017).
365. K. Yin, T. Jiang, X. Zheng, H. Yu, X. Cheng, and J. Hou, "Mid-infrared ultra-short mode-locked fiber laser utilizing topological insulator Bi_2Te_3 nano-sheets as the saturable absorber," arXiv:1505.06322 (2015).
366. Z. Qin, G. Xie, C. Zhao, S. Wen, P. Yuan, and L. Qian, Opt. Lett. **41**, 56 (2016).
367. J. Li, H. Luo, B. Zhai, R. Lu, Z. Guo, H. Zhang, and Y. Liu, Sci. Rep. **6**, 30361 (2016).
368. Q. Guo, Y. Yao, Z. C. Luo, Z. Qin, G. Xie, M. Liu, J. Kang, S. Zhang, G. Bi, X. Liu, and J. Qiu, ACS Nano **10**, 9463 (2016).
369. G. Zhu, X. Zhu, F. Wang, S. Xu, Y. Li, X. Guo, K. Balakrishnan, R. A. Norwood, and N. Peyghambarian, IEEE Photon. Technol. Lett. **28**, 7 (2016).

370. C. Wei, H. Shi, H. Luo, H. Zhang, Y. Lyu, and Y. Liu, Opt. Express **25**, 19170 (2017).
371. Z. Q. Luo, J. Z. Wang, M. Zhou, H. Y. Xu, Z. P. Cai, and C. C. Ye, Laser Phys. Lett. **9**, 229 (2012).
372. Z. Q. Luo, Y. Huang, J. Wang, H. Cheng, Z. Cai, and C. Ye, IEEE Photon. Technol. Lett. **24**, 1539 (2012).
373. N. Zhao, M. Liu, H. Liu, X. W. Zheng, Q. Y. Ning, A. P. Luo, Z. C. Luo, and W. C. Xu, Opt. Express **22**, 10906 (2014).
374. S. Huang, Y. Wang, P. Yan, J. Zhao, H. Li, and R. Lin, Opt. Express **22**, 11417 (2014).
375. J. Zhou, A. Luo, Z. Luo, X. Wang, X. Feng, and B. O. Guan, Photon. Res. **3**, A21 (2015).
376. B. Guo, Y. Yao, Y. F. Yang, Y. J. Yuan, R. L. Wang, S. G. Wang, Z. H. Ren, and B. Yan, J. Appl. Phys. **117**, 063108 (2015).
377. B. Guo, Y. Yao, Y. F. Yang, Y. J. Yuan, L. Jin, B. Yan, and J. Y. Zhang, Photon. Res. **3**, 94 (2015).
378. B. Guo and Y. Yao, Opt. Eng. **55**, 081315 (2016).
379. M. Liu, N. Zhao, H. Liu, X. W. Zheng, A. P. Luo, Z. C. Luo, W. C. Xu, C. J. Zhao, H. Zhang, and S. C. Wen, IEEE Photon. Technol. Lett. **26**, 983 (2014).
380. B. Guo, Y. Yao, P. G. Yan, K. Xu, J. J. Liu, S. G. Wang, and Y. Li, IEEE Photon. Technol. Lett. **28**, 323 (2016).
381. B. Guo, S. Li, Y. X. Fan, and P. Wang, Opt. Commun. **406**, 66 (2018).
382. Z. C. Tiu, H. Ahmad, A. Zarei, and S. W. Harun, Chin. Opt. Lett. **14**, 041901 (2016).
383. R. Zhao, J. Li, B. Zhang, X. Li, X. Su, Y. Wang, F. Lou, H. Zhang, and J. He, Appl. Phys. Express **9**, 092701 (2016).
384. L. Yun, Opt. Express **25**, 32380 (2017).
385. M. Liu, Y. Yan, X. Wang, A. Luo, W. Xu, and Z. Luo, Chin. J. Laser. **44**, 0703013 (2017).
386. B. Guo, Q. Ouyang, S. Li, Z. Fang, and P. Wang, Chin. J. Laser. **44**, 0703012 (2017).
387. H. Yu, X. Chen, H. Zhang, X. Xu, X. Hu, Z. Wang, J. Wang, S. Zhuang, and M. Jiang, ACS Nano **4**, 7582 (2010).
388. X. L. Li, J. L. Xu, Y. Z. Wu, J. L. He, and X. P. Hao, Opt. Express **19**, 9950 (2011).
389. Q. Wang, H. Teng, Y. Zou, Z. Zhang, D. Li, R. Wang, C. Gao, J. Lin, L. Guo, and Z. Wei, Opt. Lett. **37**, 395 (2012).
390. C. Gao, R. Wang, L. Zhu, M. Gao, Q. Wang, Z. Zhang, Z. Wei, J. Lin, and L. Guo, Opt. Lett. **37**, 632 (2012).
391. J. L. Xu, X. L. Li, J. L. He, X. P. Hao, Y. Yang, Y. Z. Wu, S. D. Liu, and B. T. Zhang, Opt. Lett. **37**, 2652 (2012).
392. S. Men, Z. Liu, X. Zhang, Q. Wang, H. Shen, F. Bai, L. Gao, X. Xu, R. Wei, and X. Chen, Laser Phys. Lett. **10**, 035803 (2013).
393. L. Zhang, H. Yu, S. Yan, W. Zhao, W. Sun, Y. Yang, L. Wang, W. Hou, X. Lin, Y. G. Wang, and Y. Wang, J. Mod. Opt. **60**, 1287 (2013).
394. P. Matía-Hernando, J. M. Guerra, and R. Weigand, Laser Phys. **23**, 025003 (2013).
395. L. Li, X. Zheng, C. Jin, M. Qi, X. Chen, Z. Ren, J. Bai, and Z. Sun, Appl. Phys. Lett. **105**, 221103 (2014).
396. Q. Wen, X. Zhang, Y. G. Wang, Y. Wang, and H. Niu, IEEE Photon. J. **6**, 1 (2014).
397. T. Zhao, Y. Wang, H. Chen, and D. Shen, Appl. Phys. B **116**, 947 (2014).
398. J. Hou, B. Zhang, J. He, Z. Wang, F. Lou, J. Ning, R. Zhao, and X. Su, Appl. Opt. **53**, 4968 (2014).
399. H. N. Zhang, M. Li, X. H. Chen, Q. P. Wang, and P. Li, Chin. Phys. Lett. **31**, 074201 (2014).
400. S. Han, X. Li, H. Xu, Y. Zhao, H. Yu, H. Zhang, Y. Wu, Z. Wang, X. Hao, and X. Xu, Chin. Opt. Lett. **12**, 011401 (2014).
401. S. Liu, X. Zhu, G. Zhu, K. Balakrishnan, J. Zong, K. Wiersma, A. C. Pirson, R. A. Norwood, and N. Peyghambarian, Opt. Lett. **40**, 147 (2015).
402. J. M. Serres, P. Loiko, X. Mateos, K. Yumashev, U. Griebner, V. Petrov, M. Aguilo, and F. Díaz, Opt. Express **23**, 14108 (2015).
403. H. Chu, S. Zhao, T. Li, K. Yang, G. Li, D. Li, J. Zhao, W. Qiao, J. Xu, and Y. Hang, IEEE J. Sel. Top. Quantum Electron. **21**, 343 (2015).
404. J. M. Serres, V. Jambunathan, X. Mateos, P. Loiko, A. Lucianetti, T. Mocek, K. Yumashev, V. Petrov, U. Griebner, M. Aguiló, and F. Díaz, IEEE Photon. J. **7**, 1 (2015).
405. Z. W. Wang, X. F. Chen, J. L. He, X. G. Xu, B. T. Zhang, K. J. Yang, R. H. Wang, and X. M. Liu, IEEE J. Quantum Electron. **51**, 1 (2015).
406. Q. Song, G. Wang, B. Zhang, W. Wang, M. Wang, Q. Zhang, G. Sun, Y. Bo, and Q. Peng, Appl. Opt. **54**, 2688 (2015).
407. J. Guo, H. Zhang, and P. Li, Appl. Opt. **54**, 6694 (2015).
408. C. Luan, K. J. Yang, J. Zhao, S. Z. Zhao, W. C. Qiao, T. Li, T. Feng, C. Liu, J. P. Qiao, L. H. Zheng, J. Xu, Q. G. Wang, and L. B. Su, Appl. Opt. **54**, 8024 (2015).
409. Q. Song, G. Wang, B. Zhang, Q. Zhang, W. Wang, M. Wang, G. Sun, Y. Bo, and Q. Peng, Opt. Commun. **347**, 64 (2015).
410. B. Zhang, Q. Song, G. Wang, Y. Gao, Q. Zhang, M. Wang, and W. Wang, Opt. Eng. **55**, 081305 (2016).
411. K. Gorbachenya, V. Kisel, A. Yasukevich, P. Loiko, X. Mateos, V. Maltsev, N. Leonyuk, M. Aguilo, F. Diaz, U. Griebner, and V. Petrov, Appl. Opt. **56**, 4745 (2017).
412. H. Lin, W. Zhu, F. Xiong, and J. Ruan, Appl. Opt. **56**, 948 (2017).
413. H. Yu, H. Zhang, Y. Wang, C. Zhao, B. Wang, S. Wen, H. J. Zhang, and J. Wang, Laser Photon. Rev. **7**, L77 (2013).
414. B. Wang, H. Yu, H. Zhang, C. Zhao, S. Wen, H. Zhang, and J. Wang, IEEE Photon. J. **6**, 1 (2014).
415. F. Jia, H. Chen, P. Liu, Y. Huang, and Z. Luo, IEEE J. Sel. Top. Quantum Electron. **21**, 369 (2015).
416. B. Xu, Y. Wang, J. Peng, Z. Luo, H. Xu, Z. Cai, and J. Weng, Opt. Express **23**, 7674 (2015).
417. S. Luo, X. Yan, B. Xu, L. Xiao, H. Xu, Z. Cai, and J. Weng, Opt. Commun. **406**, 61 (2018).
418. Y. J. Sun, C. K. Lee, J. L. Xu, Z. J. Zhu, Y. Q. Wang, S. F. Gao, H. P. Xia, Z. Y. You, and C. Y. Tu, Photon. Res. **3**, A97 (2015).
419. X. Liu, K. Yang, S. Zhao, T. Li, W. Qiao, H. Zhang, B. Zhang, J. He, J. Bian, L. Zheng, L. Su, and J. Xu, Photon. Res. **5**, 461 (2017).
420. Z. You, Y. Sun, D. Sun, Z. Zhu, Y. Wang, J. Li, C. Tu, and J. Xu, Opt. Lett. **42**, 871 (2017).
421. B. Xu, Y. Cheng, Y. Wang, Y. Huang, J. Peng, Z. Luo, H. Xu, Z. Cai, J. Weng, and R. Moncorgé, Opt. Express **22**, 28934 (2014).
422. F. Lou, R. Zhao, J. He, Z. Jia, X. Su, Z. Wang, J. Hou, and B. Zhang, Photon. Res. **3**, A25 (2015).
423. L. C. Kong, G. Q. Xie, P. Yuan, L. J. Qian, S. X. Wang, H. H. Yu, and H. J. Zhang, Photon. Res. **3**, A47 (2015).
424. P. Ge, J. Liu, S. Jiang, Y. Xu, and B. Man, Photon. Res. **3**, 256 (2015).
425. M. Fan, T. Li, S. Zhao, G. Li, H. Ma, X. Gao, C. Krankel, and G. Huber, Opt. Lett. **41**, 540 (2016).
426. C. Luan, X. Zhang, K. Yang, J. Zhao, S. Zhao, T. Li, W. Qiao, H. Chu, J. Qiao, J. Wang, L. Zheng, X. Xu, and L. Zheng, IEEE J. Sel. Top. Quantum Electron. **23**, 66 (2017).
427. J. Qiao, S. Zhao, K. Yang, J. Zhao, G. Li, D. Li, T. Li, and W. Qiao, Opt. Express **25**, 4227 (2017).
428. H. Xia, M. Li, T. Li, S. Zhao, G. Li, and K. Yang, Appl. Opt. **56**, 2766 (2017).
429. C. Wang, S. Zhao, T. Li, K. Yang, C. Luan, X. Xu, and J. L. Xu, Opt. Commun. **406**, 249 (2018).

430. L. Guo, M. Li, T. Li, S. Zhang, K. Yang, M. Fan, and S. Zhao, Opt. Commun. **406**, 230 (2017).
431. Y. J. Gao, B. Y. Zhang, Q. Song, G. J. Wang, W. J. Wang, M. H. Hong, R. Q. Dou, D. L. Sun, and Q. L. Zhang, Appl. Opt. **55**, 4929 (2016).
432. C. Luan, K. Yang, J. Zhao, S. Zhao, L. Song, T. Li, H. Chu, J. Qiao, C. Wang, Z. Li, S. Jiang, B. Man, and S. Jiang, Opt. Lett. **41**, 3783 (2016).
433. W. Tang, Y. Wang, K. Yang, J. Zhao, S. Zhao, G. Li, D. Li, T. Li, and W. Qiao, IEEE Photon. Technol. Lett. **29**, 470 (2017).
434. W. Ling, T. Xia, Z. Dong, F. Lu, Q. Liu, X. Zhao, K. Li, and Y. Wang, Chin. J. Laser. **44**, 0703020 (2017).
435. C. Y. Tang, P. K. Cheng, L. Tao, H. Long, L. H. Zeng, Q. Wen, and Y. H. Tsang, J. Lightwave Technol. **35**, 4120 (2017).
436. Q. Song, B. Zhang, G. Wang, and Q. Zhang, Opt. Commun. **406**, 76 (2018).
437. W. Tang, J. Zhao, K. Yang, S. Zhao, G. Li, D. Li, W. Qiao, and Y. Wang, Opt. Mater. Express **7**, 1180 (2017).
438. J. Qiao, S. Zhao, K. Yang, J. Zhao, G. Li, D. Li, T. Li, W. Qiao, and Y. Wang, Opt. Mater. Express **7**, 3998 (2017).
439. Y. Sun, Y. Bai, D. Li, L. Hou, B. Bai, Y. Gong, L. Yu, and J. Bai, Opt. Express **25**, 21037 (2017).
440. X. Su, H. Nie, Y. Wang, G. Li, B. Yan, B. Zhang, K. Yang, and J. He, Opt. Lett. **42**, 3502 (2015).
441. J. J. Liu, J. Liu, Z. Guo, H. Zhang, W. Ma, J. Wang, and L. Su, Opt. Express **24**, 30289 (2016).
442. H. Zhang, J. He, Z. Wang, J. Hou, B. Zhang, R. Zhao, K. Han, K. Yang, H. Nie, and X. Sun, Opt. Mater. Express **6**, 2328 (2016).
443. Z. Chu, J. Liu, Z. Guo, and H. Zhang, Opt. Mater. Express **6**, 2374 (2016).
444. L. Kong, Z. Qin, G. Xie, Z. Guo, H. Zhang, P. Yuan, and L. Qian, Laser Phys. Lett. **13**, 045801 (2016).
445. Y. Xie, L. Kong, Z. Qin, G. Xie, and J. Zhang, Opt. Eng. **55**, 081307 (2016).
446. D. Lu, Z. Pan, R. Zhang, T. Xu, R. Yang, B. Yang, Z. Liu, H. Yu, H. Zhang, and J. Wang, Opt. Eng. **55**, 081312 (2016).
447. H. Nie, P. Zhang, B. Zhang, M. Xu, K. Yang, X. Sun, L. Zhang, Y. Hang, and J. He, IEEE J. Sel. Top. Quantum Electron. **24**, 1 (2018).
448. J. Ma, S. Lu, Z. Guo, X. Xu, H. Zhang, D. Tang, and D. Fan, Opt. Express **23**, 22643 (2015).
449. Q. Liu, B. Zhang, S. Qi, Y. Li, X. Fan, Y. Zhao, W. Zhou, and D. Shen, Opt. Express **24**, 30031 (2016).
450. H. Liu, Z. Sun, X. Wang, Y. Wang, and G. Cheng, Opt. Express **25**, 6244 (2017).
451. C. Li, J. Liu, Z. Guo, H. Zhang, W. Ma, J. Wang, X. Xu, and L. Su, Opt. Commun. **406**, 158 (2018).
452. M. Fan, T. Li, G. Li, H. Ma, S. Zhao, K. Yang, and C. Kränkel, Opt. Lett. **42**, 286 (2017).
453. X. Gao, S. Li, T. Li, G. Li, and H. Ma, Photon. Res. **5**, 33 (2017).
454. Y. H. Kim, S. H. Kwon, J. M. Lee, M. S. Hwang, J. H. Kang, W. I. Park, and H. G. Park, Nat. Commun. **3**, 1123 (2012).
455. X. Su, Y. Wang, B. Zhang, R. Zhao, K. Yang, J. He, Q. Hu, Z. Jia, and X. Tao, Opt. Lett. **41**, 1945 (2016).
456. J. Hou, G. Zhao, Y. Wu, J. He, and X. Hao, Opt. Express **23**, 27292 (2015).
457. B. Zhang, F. Lou, R. Zhao, J. He, J. Li, X. Su, J. Ning, and K. Yang, Opt. Lett. **40**, 3691 (2015).
458. Y. Zhang, H. Yu, R. Zhang, G. Zhao, H. Zhang, Y. Chen, L. Mei, M. Tonelli, and J. Wang, Opt. Lett. **42**, 547 (2017).
459. G. Wang, Q. Song, Y. Gao, B. Zhang, W. Wang, M. Wang, Q. Zhang, W. Liu, D. Sun, F. Peng, and G. Sun, Appl. Opt. **54**, 5829 (2015).
460. W. Tang, J. Zhao, T. Li, K. Yang, S. Zhao, G. Li, D. C. Li, and W. Qiao, Opt. Lett. **42**, 4820 (2017).
461. W. D. Tan, C. Y. Su, R. J. Knize, G. Q. Xie, L. J. Li, and D. Y. Tang, Appl. Phys. Lett. **96**, 031106 (2010).
462. J. L. Xu, X. L. Li, J. L. He, X. P. Hao, Y. Z. Wu, Y. Yang, and K. J. Yang, Appl. Phys. Lett. **99**, 261107 (2011).
463. J. L. Xu, X. L. Li, Y. Z. Wu, X. P. Hao, J. L. He, and K. J. Yang, Opt. Lett. **36**, 1948 (2011).
464. W. B. Cho, J. W. Kim, H. W. Lee, S. Bae, B. H. Hong, S. Y. Choi, I. H. Baek, K. Kim, D. Yeom, and F. Rotermund, Opt. Lett. **36**, 4089 (2011).
465. J. Liu, Y. G. Wang, Z. S. Qu, L. H. Zheng, L. B. Su, and J. Xu, Laser Phys. Lett. **9**, 15 (2011).
466. Y. G. Wang, H. R. Chen, X. M. Wen, W. F. Hsieh, and J. Tang, Nanotechnol. **22**, 455203 (2011).
467. J. Ma, G. Q. Xie, P. Lv, W. L. Gao, P. Yuan, L. J. Qian, H. H. Yu, H. J. Zhang, J. Y. Wang, and D. Y. Tang, Opt. Lett. **37**, 2085 (2012).
468. I. H. Baek, H. W. Lee, S. Bae, B. H. Hong, Y. H. Ahn, D. I. Yeom, and F. Rotermund, Appl. Phys. Express **5**, 032701 (2012).
469. A. A. Lagatsky, Z. Sun, T. S. Kulmala, R. S. Sundaram, S. Milana, F. Torrisi, O. L. Antipov, Y. Lee, J. H. Ahn, C. T. A. Brown, and W. Sibbett, Appl. Phys. Lett. **102**, 013113 (2013).
470. M. N. Cizmeciyan, J. W. Kim, S. Bae, B. H. Hong, F. Rotermund, and A. Sennaroglu, Opt. Lett. **38**, 341 (2013).
471. F. Lou, L. Cui, Y. B. Li, J. Hou, J. L. He, Z. T. Jia, J. Q. Liu, B. T. Zhang, K. J. Yang, Z. W. Wang, and X. T. Tao, Opt. Lett. **38**, 4189 (2013).
472. S. D. Cafiso, E. Ugolotti, A. Schmidt, V. Petrov, U. Griebner, A. Agnesi, W. B. Cho, B. H. Jung, F. Rotermund, S. Bae, B. H. Hong, G. Reali, and F. Pirzio, Opt. Lett. **38**, 1745 (2013).
473. C. A. Zaugg, Z. Sun, V. J. Wittwer, D. Popa, S. Milana, T. S. Kulmala, R. S. Sundaram, M. Mangold, O. D. Sieber, M. Golling, Y. Lee, J. H. Ahn, A. C. Ferrari, and U. Keller, Opt. Express **21**, 31548 (2013).
474. L. Li, Z. Ren, X. Chen, M. Qi, X. Zheng, J. Bai, and Z. Sun, Appl. Phys. Express **6**, 082701 (2013).
475. R. P. Shi, Y. Bai, M. Qi, X. M. Chen, H. D. Wei, Z. Y. Ren, and J. T. Bai, Laser Phys. Lett. **11**, 025001 (2013).
476. Q. J. Huang, S. Z. Jiang, J. Chang, W. Ji, and Q. P. Wang, Laser Phys. **23**, 045807 (2013).
477. C. Feng, J. Liu, Y. Wang, L. Zheng, L. Su, and J. Xu, Laser Phys. **23**, 065802 (2013).
478. J. M. Yang, Q. Yang, J. Liu, Y. G. Wang, and Y. H. Tsang, Chin. Phys. B **22**, 094210 (2013).
479. S. Husaini and R. G. Bedford, Appl. Phys. Lett. **104**, 161107 (2014).
480. N. Tolstik, A. Pospischil, E. Sorokin, and I. T. Sorokina, Opt. Express **22**, 7284 (2014).
481. N. Tolstik, E. Sorokin, and I. T. Sorokina, Opt. Express **22**, 5564 (2014).
482. S. C. Xu, B. Y. Man, S. Z. Jiang, C. S. Chen, M. Liu, C. Yang, S. B. Gao, D. J. Feng, G. D. Hu, Q. J. Huang, X. F. Chen, and C. Zhang, Laser Phys. Lett. **11**, 085801 (2014).
483. S. C. Xu, B. Y. Man, S. Z. Jiang, C. S. Chen, C. Yang, M. Liu, Q. J. Huang, C. Zhang, D. Bi, X. Meng, and F. Y. Liu, Opt. Laser Technol. **56**, 393 (2014).
484. F. Canbaz, N. Kakenov, C. Kocabas, U. Demirbas, and A. Sennaroglu, Opt. Lett. **40**, 4110 (2015).
485. A. Choudhary, S. Dhingra, B. D'Urso, P. Kannan, and D. P. Shepherd, IEEE Photon. Technol. Lett. **27**, 646 (2015).
486. W. Cai, S. Jiang, S. Xu, Y. Li, J. Liu, C. Li, L. Zheng, L. Su, and J. Xu, Opt. Laser Technol. **65**, 1 (2015).

487. I. Baylam, O. Balci, N. Kakenov, C. Kocabas, and A. Sennaroglu, Opt. Lett. **41**, 910 (2016).
488. J. Ma, H. Huang, K. Ning, X. Xu, G. Xie, L. Qian, K. P. Loh, and D. Tang, Opt. Lett. **41**, 890 (2016).
489. W. B. Cho, S. Y. Choi, C. Zhu, M. H. Kim, J. W. Kim, J. S. Kim, H. J. Park, D. H. Shin, M. Y. Jung, F. Wang, and F. Rotermund, Opt. Express **24**, 20774 (2016).
490. H. Zhu, L. Zhao, J. Liu, S. Xu, W. Cai, S. Jiang, L. Zheng, L. Su, and J. Xu, Opt. Eng. **55**, 081304 (2016).
491. I. Baylam, S. Ozharar, N. Kakenov, C. Kocabas, and A. Sennaroglu, Opt. Lett. **42**, 1404 (2017).
492. Y. Wang, W. Chen, M. Mero, L. Zhang, H. Lin, Z. Lin, G. Zhang, F. Rotermund, Y. J. Cho, P. Loiko, X. Mateos, U. Griebner, and V. Petrov, Opt. Lett. **42**, 3076 (2017).
493. C. Huo, Z. Wang, X. Li, and H. Zeng, Chin. J. Laser. **44**, 0703008 (2017).
494. Y. Ye, Z. J. Wong, X. Lu, X. Ni, H. Zhu, X. Chen, Y. Wang, and X. Zhang, Nat. Photon. **9**, 733 (2015).
495. J. C. Reed, A. Y. Zhu, H. Zhu, F. Yi, and E. Cubukcu, Nano Lett. **15**, 1967 (2015).
496. J. Lu, X. Zou, C. Li, W. Li, Z. Liu, Y. Liu, and Y. Leng, Chin. Opt. Lett. **15**, 041401 (2017).
497. R. Mary, G. Brown, S. J. Beecher, F. Torrisi, S. Milana, D. Popa, T. Hasan, Z. Sun, E. Lidorikis, S. Ohara, A. C. Ferrari, and A. K. Kar, Opt. Express **21**, 7943 (2013).
498. A. Choudhary, S. Dhingra, B. D'Urso, T. L. Parsonage, K. A. Sloyan, R. W. Eason, and D. P. Shepherd, Opt. Lett. **39**, 4325 (2014).
499. A. Choudhary, S. J. Beecher, S. Dhingra, B. D'Urso, T. L. Parsonage, J. A. Grant-Jacob, P. Hua, J. I. Mackenzie, R. W. Eason, and D. P. Shepherd, Opt. Lett. **40**, 1912 (2015).
500. H. Liu, C. Cheng, C. Romero, J. R. V. de Aldana, and F. Chen, Opt. Express **23**, 9730 (2015).
501. A. G. Okhrimchuk and P. A. Obraztsov, Sci. Rep. **5**, 11172 (2015).
502. Y. Ren, G. Brown, R. Mary, G. Demetriou, D. Popa, F. Torrisi, A. C. Ferrari, F. Chen, and A. K. Kar, IEEE J. Sel. Top. Quantum Electron. **21**, 395 (2015).
503. J. W. Kim, S. Young Choi, S. Aravazhi, M. Pollnau, U. Griebner, V. Petrov, S. Bae, K. J. Ahn, D. Yeom, and F. Rotermund, AIP Adv. **5**, 017110 (2015).
504. R. He, J. R. V. de Aldana, and F. Chen, Opt. Mater. **46**, 414 (2015).
505. F. Thorburn, A. Lancaster, S. McDaniel, G. Cook, and A. K. Kar, Opt. Express **25**, 26166 (2017).
506. Y. Tan, H. Zhang, C. Zhao, S. Akhmadaliev, S. Zhou, and F. Chen, Opt. Lett. **40**, 637 (2015).
507. C. Cheng, H. Liu, Y. Tan, J. R. V. de Aldana, and F. Chen, Opt. Express **24**, 10385 (2016).
508. L. Ma, Y. Tan, S. Wang, S. Akhmadaliev, S. Zhou, H. Yu, H. Zhang, and F. Chen, J. Lightwave Technol. **35**, 2642 (2017).
509. C. Cheng, Z. Li, N. Dong, J. Wang, and F. Chen, Opt. Express **25**, 6132 (2017).
510. C. Cheng, H. Liu, Z. Shang, W. Nie, Y. Tan, B. Rabes, J. Aldana, D. Jaque, and F. Chen, Opt. Mater. Express **6**, 367 (2016).
511. Y. Tan, Z. Guo, L. Ma, H. Zhang, S. Akhmadaliev, S. Zhou, and F. Chen, Opt. Express **24**, 2858 (2016).
512. Z. Li, C. Cheng, N. Dong, C. Romero, Q. Lu, J. Wang, J. Aldana, Y. Tan, and F. Chen, Photon. Res. **5**, 406 (2017).
513. K. S. Novoselov, A. Mishchenko, A. Carvalho, and A. H. Neto, Science **353**, aac9439 (2016).
514. Y. Liu, N. O. Weiss, X. Duan, H. C. Cheng, Y. Huang, and X. Duan, Nat. Rev. **42**, 1 (2016).
515. D. Deng, K. S. Novoselov, Q. Fu, N. Zheng, Z. Tian, and X. Bao, Nat. Nanotechnol. **11**, 218 (2016).
516. D. Pierucci, H. Henck, C. H. Naylor, H. Sediri, E. Lhuillier, A. Balan, J. E. Rault, Y. J. Dappe, F. Bertran, P. L. Fèvre, A. C. Johnson, and A. Ouerghi, Sci. Rep. **6**, 26656 (2016).
517. D. Jariwala, T. J. Marks, and M. C. Hersam, Nat. Mater. **16**, 170 (2016).
518. Z. Zhang, P. Chen, X. Duan, K. Zang, J. Luo, and X. Duan, Science **357**, 788 (2017).
519. H. Mu, Z. Wang, J. Yuan, S. Xiao, C. Chen, Y. Chen, J. Song, Y. Wang, Y. Xue, H. Zhang, and Q. Bao, ACS Photon. **2**, 832 (2015).
520. Z. Wang, H. Mu, C. Zhao, Q. Bao, and H. Zhang, Opt. Eng. **55**, 081314 (2016).
521. Z. Wang, H. Mu, J. Yuan, C. Zhao, Q. Bao, and H. Zhang, IEEE J. Sel. Top. Quantum Electron. **23**, 1 (2017).
522. H. Chen, J. Yin, J. Yang, X. Zhang, M. Liu, Z. Jiang, J. Wang, Z. Sun, T. Guo, W. Liu, and P. Yan, Opt. Lett. **42**, 4279 (2017).
523. S. Liu, Z. Li, Y. Ge, H. Wang, R. Yue, X. Jiang, J. Li, Q. Wen, and H. Zhang, Photon. Res. **5**, 662 (2017).
524. Y. Xu, Z. Wang, Z. Guo, H. Huang, Q. Xiao, H. Zhang, and X. F. Yu, Adv. Opt. Mater. **4**, 1223 (2016).
525. Z. Wang, Y. Xu, S. C. Dhanabalan, J. Sophia, C. Zhao, C. Xu, Y. Xiang, J. Li, and H. Zhang, IEEE Photon. J. **8**, 1 (2016).
526. Y. Xu, W. Wang, Y. Ge, H. Guo, X. Zhang, S. Chen, Y. Deng, Z. Lu, and H. Zhang, Adv. Funct. Mater. **27**, 1702437 (2017).
527. J. Du, M. Zhang, Z. Guo, J. Chen, X. Zhu, G. Hu, P. Peng, Z. Zheng, and H. Zhang, Sci. Rep. **7**, 42357 (2017).
528. M. Liu, X. F. Jiang, Y. R. Yan, X. D. Wang, A. P. Luo, W. C. Xu, and Z. C. Luo, Opt. Commun. **406**, 85 (2018).
529. L. Lu, X. Tang, R. Cao, L. Wu, Z. Li, G. Jing, B. Dong, S. Lu, Y. Li, Y. Xiang, J. Li, D. Fan, and H. Zhang, Adv. Opt. Mater. **5**, 1700301 (2017).
530. S. Liu, Q. Wang, K. Wang, Y. Yao, H. Zhang, T. Ren, Z. Yin, F. Du, B. Zhang, and J. He, Opt. Lett. **42**, 3972 (2017).
531. Y. W. Lee, C. M. Chen, C. W. Huang, S. K. Chen, and J. R. Jiang, Opt. Express **24**, 10675 (2016).
532. J. Li, H. Dong, B. Xu, S. Zhang, Z. Cai, J. Wang, and L. Zhang, Photon. Res. **5**, 457 (2017).
533. M. Pumera and Z. Sofer, Adv. Mater. **29**, 1605299 (2017).
534. S. C. Dhanabalan, B. Dhanabalan, J. S. Ponraj, Q. Bao, and H. Zhang, Adv. Opt. Mater. **5**, 1700257 (2017).
535. Y. I. Jhon, J. Koo, B. K. Yu, J. Lee, M. Seo, J. H. Lee, Y. Gogotsi, and Y. M. Jhon, Adv. Mater. **29**, 1702496 (2017).
536. K. Wei, S. Fan, Q. Chen, and X. Lai, Adv. Mater. **29**, 1700754 (2017).
537. S. Chen and G. Shi, Adv. Mater. **29**, 1605448 (2017).
538. B. Huang, J. Yi, G. Jiang, L. Miao, W. Hu, C. Zhao, and S. Wen, Opt. Mater. Express **7**, 1220 (2017).
539. J. Yi, L. Miao, J. Li, W. Hu, C. Zhao, and S. Wen, Opt. Mater. Express **7**, 3894 (2017).
540. J. Guo, H. Zhang, C. Zhang, Z. Li, Y. Sheng, C. Li, X. Bao, B. Man, Y. Jiao, and S. Jiang, Opt. Mater. Express **7**, 3494 (2017).
541. Q. Guo, Y. Cui, Y. Yao, Y. Ye, Y. Yang, X. Liu, S. Zhang, X. F. Liu, J. Qiu, and H. Hosono, Adv. Mater. **29**, 1700754 (2017).
542. J. Lee, B. K. Yu, Y. I. Jhon, J. Koo, S. J. Kim, Y. M. Jhon, and J. H. Lee, Adv. Opt. Mater. **5**, 1700096 (2017).
543. X. Jiang, S. Li, W. Liang, S. Luo, Z. He, Y. Ge, H. Wang, R. Cao, F. Zhang, Q. Wen, J. Li, Q. Bao, D. Fan, and H. Zhang, Laser Photon. Rev. 1700229 (2017).
544. Y. Song, Z. Liang, X. Jiang, Y. Chen, Z. Li, L. Lu, Y. Ge, K. Wang, J. Zheng, S. Lu, J. Ji, and H. Zhang, 2D Mater. **4**, 045010 (2017).
545. Y. F. Song, H. Zhang, and D. Y. Tang, Opt. Express **20**, 27283 (2012).
546. Y. Meng, S. Zhang, X. Li, H. Li, J. Du, and Y. Hao, Opt. Express **20**, 6685 (2012).

547. X. L. Li, S. M. Zhang, Y. C. Meng, Y. P. Hao, H. F. Li, J. Du, and Z. J. Yang, Laser Phys. **22**, 774 (2012).
548. Y. F. Song, L. Li, H. Zhang, D. Y. Tang, and K. P. Loh, Opt. Express **21**, 10010 (2013).
549. L. Gui, X. Li, X. Xiao, H. Zhu, and C. Yang, IEEE Photon. Technol. Lett. **25**, 1184 (2013).
550. J. Zhao, P. Yan, and S. C. Ruan, Appl. Opt. **52**, 8465 (2013).
551. A. P. Luo, P. F. Zhu, H. Liu, X. W. Zheng, N. Zhao, M. Liu, H. Cui, Z. C. Luo, and W. C. Xu, Opt. Express **22**, 27019 (2014).
552. R. Y. Lin, Y. G. Wang, P. G. Yan, G. L. Zhang, J. Q. Zhao, H. Q. Li, S. S. Huang, G. Z. Cao, and J. A. Duan, IEEE Photon. J. **6**, 1 (2014).
553. J. Zhao, Y. Wang, S. Ruan, P. Yan, H. Zhang, Y. H. Tsang, J. H. Yang, and G. Huang, J. Opt. Soc. Am. B **31**, 716 (2014).
554. N. Zhao, Z. C. Luo, H. Liu, M. Liu, X. W. Zheng, L. Liu, J. H. Liao, X. D. Wang, A. P. Luo, and W. C. Xu, IEEE Photon. Technol. Lett. **26**, 2450 (2014).
555. B. C. Yao, Y. J. Rao, Z. N. Wang, Y. Wu, J. H. Zhou, H. Wu, M. Q. Fan, X. L. Cao, W. L. Zhang, Y. F. Chen, Y. R. Li, D. Churkin, S. Turitsyn, and C. W. Wong, Sci. Rep. **5**, 18526 (2015).
556. L. Gao, T. Zhu, K. S. Chiang, and W. Huang, IEEE Photon. Technol. Lett. **27**, 2535 (2015).
557. L. Gao, T. Zhu, M. Liu, and W. Huang, IEEE Photon. Technol. Lett. **27**, 38 (2015).
558. Y. F. Song, H. Zhang, L. M. Zhao, D. Y. Shen, and D. Y. Tang, Opt. Express **24**, 1814 (2016).
559. X. Zou, J. Qiu, X. Wang, Z. Ye, J. Shi, and J. Wu, Appl. Opt. **55**, 4323 (2016).
560. Z. R. Cai, M. Liu, S. Hu, J. Yao, A. P. Luo, Z. C. Luo, and W. C. Xu, IEEE J. Sel. Top. Quantum Electron. **23**, 20 (2017).
561. A. P. Luo, H. Liu, N. Zhao, X. W. Zheng, M. Liu, R. Tang, Z. C. Luo, and W. C. Xu, IEEE Photon. J. **6**, 1 (2014).
562. M. Liu, A. P. Luo, X. W. Zheng, N. Zhao, H. Liu, Z. C. Luo, W. C. Xu, Y. Chen, C. J. Zhao, and H. Zhang, J. Lightwave Technol. **33**, 2056 (2015).
563. M. Liu, Z. R. Cai, S. Hu, A. P. Luo, C. J. Zhao, H. Zhang, W. C. Xu, and Z. C. Luo, Opt. Lett. **40**, 4767 (2015).
564. B. Guo, Y. Yao, J. J. Xiao, R. L. Wang, and J. Y. Zhang, IEEE J. Sel. Top. Quantum Electron. **22**, 8 (2016).
565. B. Guo, Y. Yao, J. Tian, Y. Zhao, S. Liu, M. Li, and M. Quan, IEEE Photon. Technol. Lett. **27**, 701 (2015).
566. J. Liu, X. Li, S. Zhang, H. Zhang, P. Yan, M. Han, Z. Pang, and Z. Yang, Sci. Rep. **6**, 29128 (2016).
567. Y. Meng, G. Semaan, M. Salhi, A. Niang, K. Guesmi, Z. C. Luo, and F. Sanchez, Opt. Express **23**, 23053 (2015).
568. Y. Chen, M. Wu, P. Tang, S. Chen, J. Du, G. Jiang, C. Zhao, H. Zhang, and S. Wen, Laser Phys. Lett. **11**, 055101 (2014).
569. K. X. Li, Y. R. Song, J. R. Tian, H. Y. Guoyu, and R. Q. Xu, IEEE Photon. J. **9**, 1 (2017).
570. W. Liu, L. Pang, H. Han, W. Tian, H. Chen, M. Lei, P. Yan, and Z. Wei, Opt. Express **23**, 26023 (2015).
571. A. P. Luo, M. Liu, X. D. Wang, Q. Y. Ning, W. C. Xu, and Z. C. Luo, Photon. Res. **3**, A69 (2015).
572. Y. Wang, D. Mao, X. Gan, L. Han, C. Ma, T. Xi, Y. Zhang, W. Shang, S. Hua, and J. Zhao, Opt. Express **23**, 205 (2015).
573. B. Guo, Q. Lyu, Y. Yao, and P. Wang, Opt. Mater. Express **6**, 2475 (2016).
574. W. Liu, L. Pang, H. Han, Z. Shen, M. Lei, H. Teng, and Z. Wei, Photon. Res **4**, 111 (2016).
575. S. Wang, H. Yu, and H. Zhang, Photon. Res. **3**, A10 (2015).
576. S. Chen, L. Miao, X. Chen, Y. Chen, C. Zhao, S. Datta, Y. Li, Q. Bao, H. Zhang, Y. Liu, S. Wen, and D. Fan, Adv. Opt. Mater. **3**, 1769 (2015).
577. P. Y. Ma, B. J. Shastri, T. F. de Lima, A. N. Tait, M. A. Nahmias, and P. R. Prucnal, Opt. Express **25**, 33504 (2017).
578. F. Wang, Chin. Phys. B **26**, 034202 (2017).
579. K. Wu, C. Guo, H. Wang, X. Zhang, J. Wang, and J. Chen, Opt. Express **25**, 17639 (2017).
580. J. Zheng, Z. Yang, C. Si, Z. Liang, X. Chen, R. Cao, Z. Guo, K. Wang, Y. Zhang, J. Ji, M. Zhang, D. Fan, and H. Zhang, ACS Photon. **4**, 1466 (2017).
581. J. Zheng, X. Tang, Z. Yang, Z. Liang, Y. Chen, K. Wang, Y. Song, Y. Zhang, J. Ji, Y. Liu, D. Fan, and H. Zhang, Adv. Opt. Mater. **5**, 1700026 (2017).
582. L. Lu, W. Wang, L. Wu, X. Jiang, Y. Xiang, J. Li, D. Fan, and H. Zhang, ACS Photon. **4**, 2852 (2017).
583. L. Wu, Z. Xie, L. Lu, J. Zhao, Y. Wang, X. Jiang, Y. Ge, F. Zhang, S. Lu, Z. Guo, J. Liu, Y. Xiang, S. Xu, J. Li, D. Fan, and J. Liu, Adv. Opt. Mater. **6**, 1700985 (2018).
584. Y. Ge, Z. Zhu, Y. Xu, Y. Chen, S. Chen, Z. Liang, Y. Song, Y. Zou, H. Zeng, S. Xu, H. Zhang, and D. Fan, Adv. Opt. Mater. 1701166 (2017).
585. B. Yao, Y. Liu, S. W. Huang, C. Choi, Z. Xie, J. F. Flores, Y. Wu, M. Yu, D. L. Kwong, Y. Huang, Y. Rao, X. Duan, and C. W. Wong, Nat. Photon. **12**, 22 (2018).
586. V. Sorianello, M. Midrio, G. Contestabile, I. Asselberghs, J. Van Campenhout, C. Huyghebaert, I. Goykhman, A. K. Ott, A. C. Ferrari, and M. Romagnoli, Nat. Photon. **12**, 40 (2018).